**Title**
THE OLE OF ENERGY EXCHANGE IN VIBRATIONAL DEPHASING PROCESSES IN LIQUIDS AND SOLIDS



**Author**
Marks, S.

**Publication Date**
1981-08-01

# Lawrence Berkeley Laboratory
UNIVERSITY OF CALIFORNIA



## Materials & Molecular Research Division

# THE ROLE OF ENERGY EXCHANGE IN VIBRATIONAL DEPHASING PROCESSES IN LIQUIDS AND SOLIDS

Steven Marks
(Ph.D. thesis)

August 1981





Prepared for the U.S. Department of Energy under Contract W-7405-ENG-48

LBL-13124

# THE ROLE OF ENERGY EXCHANGE IN VIBRATIONAL DEPHASING PROCESSES IN LIQUIDS AND SOLIDS

Steven Marks
(Ph.D. thesis)
Lawrence Berkeley Laboratory
University of California
Berkeley, CA 94720

August 1981

This work was supported in part by a grant from the National Science Foundation and by the Director, Office of Energy Research, Office of Basic Energy Sciences, Chemical Sciences Division of the U.S. Department of Energy under Contract Number W-7405-ENG-48.

# The Role of Energy Exchange in Vibrational Dephasing Processes in Liquids and Solids

By

Steven Marks

B.S. (Indiana University) 1977

DISSERTATION

Submitted in partial satisfaction of the requirements for the degree of

DOCTOR OF PHILOSOPHY

in

Chemistry

in the

GRADUATE DIVISION

OF THE

UNIVERSITY OF CALIFORNIA, BERKELEY

Approved: .. 7/28/81
Date

.. Alcov 8/3/81

..... 8/3/81

.....

# THE ROLE OF ENERGY EXCHANGE IN VIBRATIONAL DEPHASING PROCESSES IN LIQUIDS AND SOLIDS

Steven Marks

## ABSTRACT

Three theories which claim relevance to the dephasing of molecular vibrations in condensed phase matter are presented. All of these theories predict (in certain limiting cases) that the widths and shifts of molecular vibrations will obey an Arrhenius temperature dependence. The basic tenants of the theories are detailed so that the differences between them may be used in an experiment to distinguish between them. One model, based on intermolecular energy exchange of low-frequency modes, results in dephasing the high-frequency modes when anharmonic coupling is present. A computer analysis of temperature dependent experimental lineshapes can result in the extraction of various parameters such as the anharmonic shifts and the exchange rates.

It is shown that, in order to properly assess the relative validity of the three models, other evidence must be obtained such as the spectral parameters of the low-frequency modes, the combination bands, and the isotopic dilution behavior. This evidence is presented for $d_{14}$-durene (perduetero-1,2,4,5-tetramethylbenzene) and compared to previous data obtained on pure $h_{14}$-durene. An extension of the (HSC) intermolecular energy exchange model which allows for the possibility of partial delocalization of the low-frequency modes gives an adequate description of the experimental evidence. Isotopic dilution experiments, in particular, have resulted in a detailed picture of the energy transfer dynamics of the low-frequency modes.

A section in which some spontaneous Raman spectra support a model of inhomogeneous broadening in liquids based on results of picosecond stimulated Raman spectroscopy is presented. The model is that a distribution of environmental sites is created by a distribution in the local density and thus creates inhomogeneous broadening.

DEDICATION

*I dedicate this to my mother who was not able to complete college but worked to ensure that her children could.*

"And I am for encouraging the progress of science in all its branches; and not for raising a hue and cry against the sacred name of philosophy; for awing the human mind by stories of raw-head and bloody bones to a distrust of its own vision, and to repose implicitly on that of others; to go backwards instead of forwards to look for improvement; to believe that government, religion, morality, and every other science were in the highest perfection in ages of darkest ignorance, and that nothing can ever be devised more perfect than what was established by our forefathers."

Thomas Jefferson
from letter to Elbridge Gerry, 1799

# ACKNOWLEDGMENT

Science to me is at least as much of a human endeavor, involving the interactions of the individual contributor with other individuals and aggregates of individuals, as it is a purely logical affair which relates quantum mechanical particles and their interactions. In that spirit, I would like to express my appreciation to a cross-section of individuals and aggregates thereof who have helped me and this work.

First and foremost, I am indebted to Charles Harris, my research director. The very first day I talked to him, he stated to me that "the important thing in science is the question- learn not to ask how you should answer a question, but to learn what the question that should be asked is." Four years have faded the exact words, but that is the essence of the quote. His careful balance between guidance and independence pays heed to the true meaning of an educational institution- the education of its students. The financial support he provided is very much appreciated.

Our department is one that I am very proud to have been associated with. This is a very stimulating place to work and learn; our research group is not an exception. Two former members of our group who were with us until the "Mafia" transferred them, Alan Campion and Tony "Vito" Gallo, were very likeable and knowledgeable and willing to share that knowledge. I hope to maintain my friendship with Jim Chao.

My sister, Marilynn Quick, who will soon obtain her Ph.D. could always be counted on to give "quick" and timely advice and encouragement. My aunt, Mary Schaub, was always willing to provide her hexagonal house near Glen Ellen as a welcome retreat. I am grateful for the help that all the members of my family provided to me and I hope to be able to reciprocate.

Gloria Pelatowski transformed crude sketches into professional drawings. Cordelle Yoder did an excellent and patient job typing this manuscript. Hillario Bercila, a good friend, proofed this work.

This work was supported in part by a grant from the National Science Foundation and by the director, Office of Energy Research, Office of Basic Energy Sciences, Chemical Sciences Division of the U. S. Department of Energy under Contract Number W-7405-ENG-48.

TABLE OF CONTENTS

# Chapter I

## INTRODUCTION

The elucidation of structural and dynamical properties of condensed phase matter is a primary goal of physical chemistry. One major focus of recent activity is concerned with vibrational relaxation times. While experimental insight into the magnitudes of these times may come from a variety of spectroscopic techniques, our laboratory has been concerned with picosecond and spontaneous Raman lineshape measurements. Theoretical insight is obtained by comparing the predicted results of a model to the results obtained experimentally; and thereby either accepting, rejecting, or modifying the model. Utilizing the theoretical insight obtained this way allows the use of lineshape data to characterize and quantify the interactions between a vibrating molecule and its environment. In turn, the use of a vibrating molecule as a probe in this manner allows more fundamental questions to be addressed such as the effect the interactions have on molecular discreteness or "gas-like" properties of the constituent molecules in condensed phase.

A Raman lineshape (within a certain degree of approximation) can be deconvoluted into a homogeneous portion and an inhomogeneous portion. The inhomogeneous portion arises from a quasistatic environmental distribution which causes molecules subjected to differing environmental interactions to vibrate at differing frequencies. The homogeneous portion of the lineshape is caused by dynamical processes which cause loss of phase coherence, i.e., dephasing of the vibration.

Vibrational dephasing is easily envisioned, as on Figure 1, in terms of an ensemble of molecular oscillators. Consider this ensemble

Figure 1. This shows the various processes which lead to the dephasing of a vibration in a molecular ensemble. $T_1$ is a population relaxation. $T_2^*$ processes lead to a direct randomization of the phase. The simple lineshape relation is only applicable for the case of exponential decay of the phase coherence (see text).

# VIBRATIONAL DEPHASING

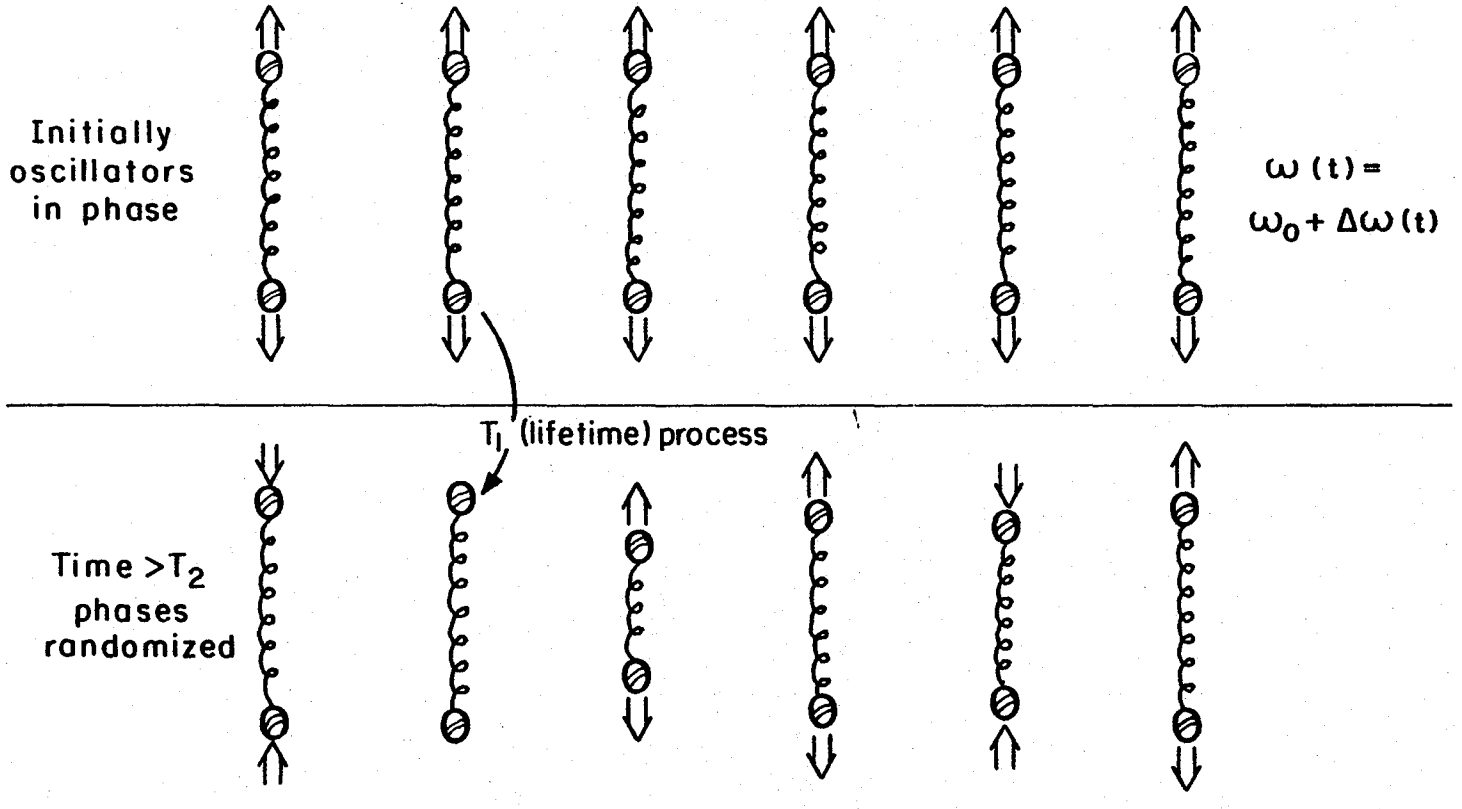


$$\text{FWHM } (cm^{-1}) = \frac{1}{2\pi c\, T_2\,(psec)}$$

XBL 816-5934

prepared to an initial state in which all the oscillators have not only been excited to the same excited state but have also all been imparted the same phase. Thus, initially the motion of a given molecule represents the motion of the ensemble average. This would be true for all times if it were not for various processes which disrupt the phase. There are two contributions which determine the time evolution of dephasing, hence the homogeneous lineshape: 1) energy relaxation or a $T_1$ process, 2) pure dephasing or a $T_2^*$ process. Recent picosecond stimulated Raman scattering experiments have shown the importance of both of these contributions.[1,2] A $T_1$ process leads to a loss in the ensemble average of the phase, because a molecule which has relaxed is no longer in the excited state- therefore it is no longer in the excited state with a definite phase relationship. A $T_2^*$ process leads to a randomization of the phase without a commensurate population relaxation. There is a common theme to all $T_2^*$ processes; namely, a stochastic time-dependent modulation of the frequency associated with a molecular vibration. Because the oscillators are vibrating at a given moment with differing frequencies they are acquiring a differing increment to their phase such that:

$$\frac{d\phi_i(t)}{dt} = \omega_i(t) \tag{1}$$

where $\phi_i$ is the phase of the $i^{th}$ member of the ensemble and $\omega_i$ is the instantaneous vibrational frequency of the same molecule. Thus $T_2^*$ processes lead to a randomization or 'dephasing' of the initially prepared state.

As described here, if $T_1$ and $T_2^*$ are processes which take place independent of each other with exponential decay time constants $T_1$ and

$T_2^*$ respectively, then the overall dephasing time $T_2$ satisfies:[3]

$$1/T_2 = 1/T_1 + 1/T_2^* \tag{2}$$

In that simple case the resulting lineshape function can easily be derived using the techniques outlined in Chapter II:

$$I(\omega) \sim \frac{I(\omega_o)}{1+(T_2)^2(\omega-\omega_o)^2} \tag{3}$$

This is a simple Lorentzian lineshape of full width at half maximum (FWHM) in $cm^{-1}$ of $1/2\pi cT_2$(psec). Models which predict a more complicated form for the time dependence of the dephasing necessarily predict a more complicated lineshape function.

This thesis is organized in the following way. Chapter II discusses three different theories which in a phenomenological manner predict a form for the homogeneous portion of the temperature dependent spontaneous Raman spectra of molecular solids and liquids. The predicted results are very similar; namely an Arrhenius shift and broadening of the various stretching bands. However, the underlying physical assumptions and mechanisms differ among the three theories. A discussion of how the three theories can be experimentally differentiated is also included. Chapter III presents experimental results on the durene (1,2,4,5 tetramethylbenzene) system for both isotopically pure and mixed $h_{14}$ and $d_{14}$ durene, as well as an interpretation in terms of the three above theories. Chapter IV presents some results obtained using molecular vibrations as a probe of structure and dynamical information but in the context of liquids and inhomogeneous broadening. Chapter V concludes this work and points out the author's assessment of where future effort should be directed.

# Chapter II

## THREE THEORIES OF VIBRATIONAL DEPHASING

### A. Raman Scattering Considerations

As mentioned in the previous chapter there are many different theories put forth to explain dephasing of molecular vibrations in molecular solids. The purpose of this chapter is to outline three of the more prominent of those theories which relate to the observed temperature dependent broadening and shifts seen in polyatomic systems (such as the durene system to be discussed extensively in Chapter III). Other theories such as the binary collision model[4] or the hydrodynamic model[5] based on intermolecular dephasing are more applicable to smaller molecules such as diatomics and are not concerned with an important mechanism in larger systems based on intramolecular dephasing.

Because the experimental probe is the lineshape function of spontaneous Raman spectroscopy, it is worth while spending some time on that:[6,7]

$$I(\omega) \sim \int_{-\infty}^{\infty} \exp(-i\omega t)\langle[\vec{\varepsilon}_s \cdot \overleftrightarrow{\alpha}(0) \cdot \varepsilon_I][\vec{\varepsilon}_s \cdot \overleftrightarrow{\alpha}(t) \cdot \vec{\varepsilon}_I]\rangle_{or} \times \langle Q(o)Q(t)\rangle_{vib}\, dt \quad (4)$$

Note that the usual assumption of independence of orientational (or) and vibrational (vib) relaxation has been made which results in their separation in the polarizability autocorrelation function. The intensity at a frequency Stokes' shifted by an amount is proportional to the amplitude of the same frequency component of autocorrelation function and are the polarization vectors of the electric field of the Stokes and incident light. $\alpha(t)$ is the Raman tensor for the vibrational transition of interest and $Q(t)$ is the normal coordinate associated with that

same vibration. <> represents ensemble averages, that is:

$$\langle X \rangle = \sum_i \rho_i \langle i|X|i\rangle. \tag{5}$$

Since the three theories of this chapter deal with the vibrational autocorrelation function, this brings up the natural question of the effect of the orientational autocorrelation function on the observed spectra. If that effect is not negligible then it must also be accounted for as a dephasing mechanism, making the task of using the Raman spectra as a probe of molecular interactions more difficult. Fortunately, in the system chosen as a critical test of the three theories, durene, the argument in favor of neglecting the orientational contribution runs as follows.[7] The elements of the Raman tensor can be decomposed into spherical and anisotropic parts:

$$\alpha_{ij}(t) = \alpha\delta_{ij} + \beta_{ij}(t) \tag{6}$$

where $\beta$ is traceless and $\alpha$ is independent of time because there is no orientational dependence associated with this quantity. The intensities of Raman scattering where the Stokes radiation is polarized parallel or perpendicular to the incident radiation ($I_\parallel$ or $I_\perp$) is:

$$I_\parallel(\omega) = A(\omega_l - \Omega_v)^4 \int_{-\infty}^{\infty} \langle(\alpha)^2 + \frac{2}{15}[\vec{\beta}(0)\cdot\vec{\beta}(t)]\rangle \times \langle Q(0)Q(t)\rangle\, e^{i\omega t}\, dt \tag{7}$$

$$I_\perp(\omega) = A(\omega_l - \Omega_v)^4 \int_{-\infty}^{\infty} \langle 1/10 T_r[\vec{\beta}(0)\cdot\vec{\beta}(t)]\rangle \times \langle Q(0)Q(t)\rangle_{vib}\, e^{i\omega t}\, dt. \tag{8}$$

Thus the quantity which eliminates the orientational contribution is:

$$\hat{I}_{vib}(\omega) = I_\parallel(\omega) - \frac{4}{3} I_\perp(\omega) \sim \int_{-\infty}^{\infty} \langle Q(0)Q(t)\rangle\, e^{i\omega t}, \tag{9}$$

a quantity which depends just upon the correlation function for the vibration.

The author determined that for solid durene at room temperature (where the orientational contribution should be the greatest for the experiments described in Chapter III) the perpendicularly polarized spectrum of each of the C-D stretching bands was at most 8 to 10% of the intensity associated with the same band's parallel component, and that about 3% of that is probably due to depolarization by the pyrex sample holder. Also within the experimental uncertainty, the peak position and width were the same; thus subtraction as indicated by Eqn. (9) yields no change in the lineshape function. So the observed lineshape corresponds directly to $I_{vib}(\omega)$ and information is obtained which directly relates to the vibrational contribution to the polarizability autocorrelation function. There are two reasons why the orientational part would not enter in. First, the molecule is in a solid and does not experience a significant amount of rotational freedom. This might be expected since the melting point of durene[8] is 79.2°C and the highest experimental temperature is 23°C. Secondly, the anisotropic part of the Raman tensor, $\beta$, might be small. $\beta$ is zero for a vibration which is totally symmetric in the following point groups: T, $T_d$, $T_h$, O, $O_h$. For example, consider Figure 2 in which particular Raman active modes in durene experience very small change of polarizability with various changes of orientation.

Since the molecular system which is studied only has a significant contribution to the vibrational lineshape based on the dephasing of the vibration, the rest of this chapter as well as the following chapter will be concerned with vibrational dephasing, particularly as it relates to microscopic structure and dynamics.

Figure 2. Shows that in the case of a molecule with sufficient symmetry (in this case durene possessing $D_{2h}$ point group symmetry-assuming that the methyls are freely rotating) that changes in orientation (librations) can have a very small effect on Raman scattering. Thus the Raman spectra associated with the vibrations arises from the vibrational autocorrelation function.

# ORIENTATION EFFECTS ON VIBRATIONS IN DURENE

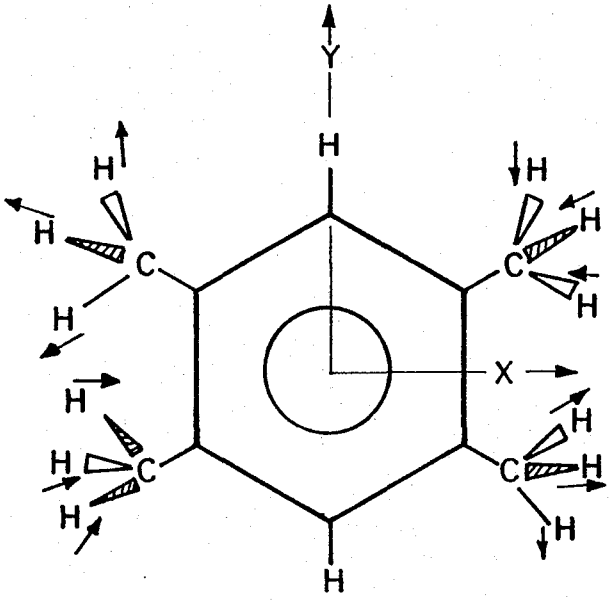


$B_{1g}$ $CH_3$ Symmetric C-H Stretch

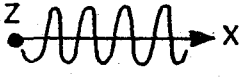


The XZ scattering tensor is unaffected by rotations on Z axis but is slightly affected by rotations on either X or Y.

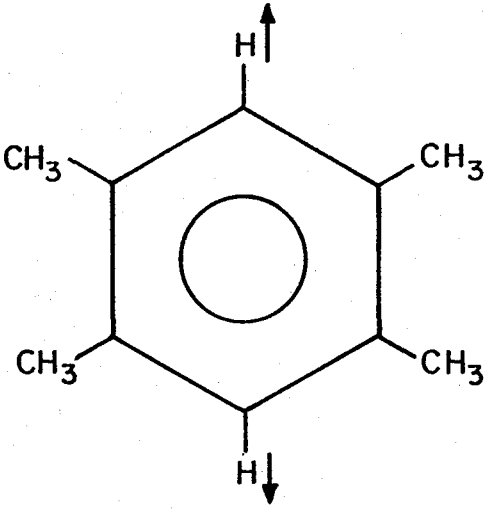


$A_g$ Aromatic C-H Stretch

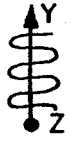


The YZ tensor is unaffected by rotations on Y axis but is severely affected by rotation on either X or Y.

XBL 817-6041

B. Intermolecular Energy Exchange Theory (HSC Theory)

The model of vibrational dephasing theory based upon the exchange theory of Anderson[10] was developed in our laboratory by Harris, Shelby, and Cornelius[13,14] (hereafter referred to as HSC). Exchange theory is a general phenomena which can be applied to a whole range of spectroscopic problems. Swift and Connick[15] applied the theory to the study of ligand exchange kinetics by Nuclear Magnetic Resonance lineshapes. Strauss applied the theory to rotational motion in solid state organic hydrocarbon chains.[16] Besides vibrational dephasing theory, Harris et al. applied exchange theory to the study of the dephasing of triplet excitons through anharmonic coupling to optical phonons.[17,18]

For every specific application of exchange theory, there exists a common idea; namely, a system which is in a particular state can scatter out of that state and at a later time return to the original state retaining some correlation to the phase the system would have had if the scattering events would not have taken place. This correlation is called phase memory and results in a narrowing of the lineshape and longer dephasing times than that which would have resulted if there were no phase memory (as would be the case if the scattering event randomized the phase). There are two main approaches to exchange theory; first it may be derived using Anderson's exchange theory,[9,10] secondly, the derivation may be based on reservoir theory.[11,12] In either case the initial assumptions are the same as well as the final resulting lineshape. The outline of the derivation of HSC exchange theory below is based on reservoir theory.

Consider a mode, A, which to zeroth order has a Hamiltonian (harmonic approximation) which can be written as follows:

$$H_A = \hbar\omega_A(a^\dagger a + \tfrac{1}{2}). \tag{10}$$

This will result in the following set of eigenvalues for the energy:

$$E_A = \hbar\omega_A(n + \tfrac{1}{2}); \text{ where } n = 0,1,\ldots \tag{11}$$

In most of the cases to be considered $\hbar\omega_A >> kT$ and mode A will be probed at the fundamental frequency only; thus A is considered to be a two level system ($n_A = 0,1$). In a similar manner the zeroth order Hamiltonian for the B modes is:

$$H_B = \sum_j \hbar\omega_j(b_j^\dagger b_j + \tfrac{1}{2}). \tag{12}$$

The B modes are those modes which interact strongly with mode A to cause a change in the frequency of mode A depending on the number of quanta in a B mode. This interaction or coupling is a result of those terms in the anharmonic potential which involve the coordinates of both mode A and a B mode:

$$V_{anh} = V(a^\dagger, a, b_j^\dagger, b_j). \tag{13}$$

If the Hamiltonian were composed of simply $H_A$, $H_B$, and $V_{anh}$, the system would be statical. Figure 3 illustrates this situation for the case of one B mode.

Energy exchange comes about by considering the effect all the other modes, both intermolecular and intramolecular, not yet considered (the Reservoir) have on the B modes. The zeroth order Hamiltonian for the reservoir is written:

$$H_R = \sum_r \hbar\omega_r(\beta_r^\dagger \beta_r + \tfrac{1}{2}) \tag{14}$$

coupling to the B modes takes place by the socalled "motional" Hamiltonian, $H_I$:

Figure 3. This shows the effect of anharmonic coupling between modes. The harmonic approximation allows the reproduction of the entire energy level spectrum of a molecule based on the values of the energies associated with each state. Real systems have a variety of anharmonicities. Figure 3 treats each mode as being harmonic

$$(\Delta E(n_A,n_B,n_C\text{--};\ n_Z \rightarrow n_{Z+1}) = \Delta E(n_A,n_B,n_C\text{--};\ n_{Z+1} \rightarrow n_{Z+2}))$$

but allows anharmonic coupling between modes

$$(\Delta E(n_A \rightarrow n_{A+1},\ n_B) \neq \Delta E(n_A \rightarrow n_{A+1},\ n_{B+1})).$$

# EFFECT OF ANHARMONIC COUPLING ON VIBRATIONAL ENERGY LEVELS

HARMONIC APPROXIMATION-
DECOUPLED OSCILLATORS

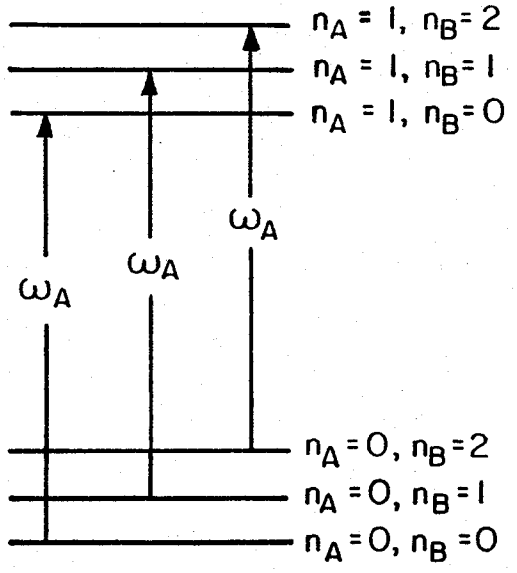


$$\mathcal{H}_0 = H_A + H_B$$
$$= \hbar\omega_A (n_A + 1/2) + \hbar\omega_B (n_B + 1/2)$$

INCLUDING
ANHARMONIC COUPLING
BETWEEN MODES

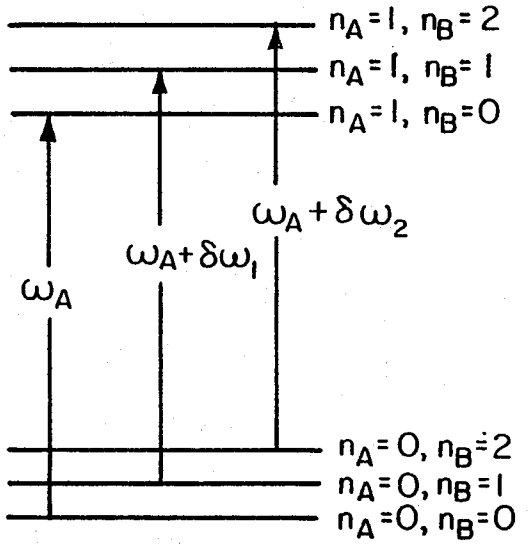


$$\mathcal{H} = \mathcal{H}_0 + H_{A\text{-}B}(n_A, n_B)$$

XBL 816-5931

$$H_I = \sum_{j,r} \hbar g_{j,r} (b_j \beta_r^\dagger + \beta_r b_j^\dagger). \tag{15}$$

The effect of the motional Hamiltonian is to preserve the total number of excitations in both the B and reservoir modes, but to allow the exchange of energy between them. Figure 4 summarizes this situation.

The method of solution parallels that of reference 19. The combined density matrix for the A and B modes and reservoir is:

$$\rho_{AB\text{-}Res}(t) = \rho_{AB}(t) \otimes \rho_{Res}(t). \tag{16}$$

Note that it is an "outer product" of both density matrices. By tracing over the reservoir states, a reduced density matrix is formed:

$$\rho_{AB,Red} = Tr_R \, \rho_{AB\text{-}Res}. \tag{17}$$

The equation of motion for the reduced density matrix is:

$$\dot{\rho}_{AB,Red} = (-i/h) \, Tr_{Res}([\mathcal{H}, \rho_{AB\text{-}Res}]). \tag{18}$$

Note that this would be the usual equation of motion for a density matrix except the tracing operation is performed outside of the commutator and not directly on $\rho_{AB\text{-}Res}$.

The first assumption that is used at this point is that the reservoir is in equilibrium and so much larger than the B modes that absorbing a quantum of energy from a B mode does not affect the equilibrium thermal distribution in the reservoir; i.e., $\rho_{Res}$ is a time independent constant. This results in the following equation of motion for the reduced density matrix in the interaction representation (see Ref. 12 and 19 for derivation):

Figure 4. This shows schematically the reservoir approach to exchange theory. The mode of interest, A, is anharmonically coupled to the exchanging modes, B. This coupling manifests itself through a frequency change in A which depends on the population level in B. The reservoir modes, R, induce population fluctuations in B; therefore frequency fluctuations in A arise.

# RESERVOIR APPROACH TO EXCHANGE THEORY

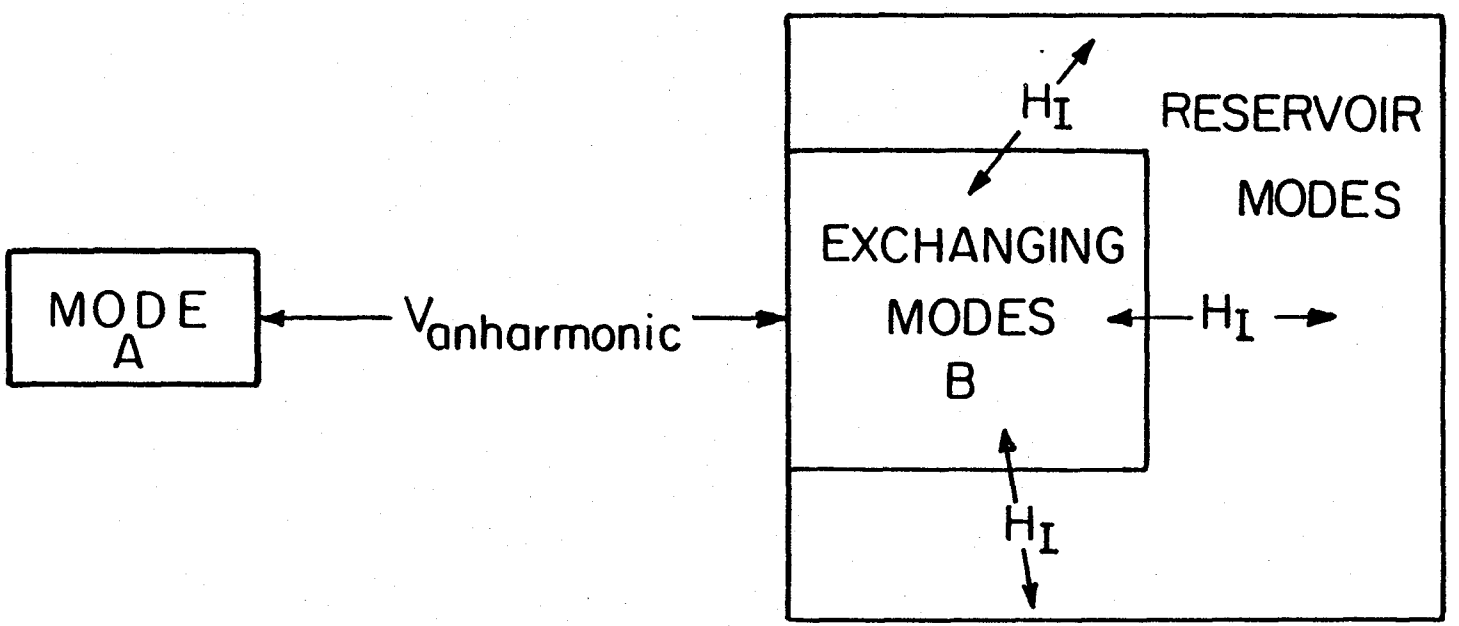


XBL816-5933

$$\dot{\rho}^{int}_{AB,red} = -1/\hbar^2 \int_0^t dt' \, Tr_{Res}[H_I^{int}(t) \, H_I^{int}(t') \, \rho^{int}_{AB,red}(t')$$

$$\circledast \rho^{int}_{Res} - H_I^{int}(t) \, \rho^{int}_{AB,red}(t') \circledast \rho_I^{int}(0) \, H_I^{int}(t')]$$

$$+ \text{Hermitian adjoint.} \qquad (19)$$

$H_I^{int}(t)$ is the motional Hamiltonian in the interaction representation:

$$H_I^{int}(t) = \sum_{j,r} \hbar g_{j,r}\{b_j \beta_r^\dagger \exp[-i(\omega_j-\omega_r)t] + \beta_r b_j^\dagger \exp[-i(\omega_r-\omega_j)t]\}. \qquad (20)$$

$\rho^{int}_{Res}$ is also in the interaction representation.

The second approximation needed to get a handle on the solution of the density matrix is the Markoff approximation. In this context, this approximation is that the interactions between the reservoir and the molecule ($H_I(t)$) fluctuate rapidly compared to a change in $\dot{\rho}_{AB}$; so the term $H_I^{int}(t) \, H_I^{int}(t')$ in Eqn. 19 can be replaced with a $\delta$-function. Then by replacing the sum over reservoir states with an integral and a density of states function, $D(\omega)$, and transforming to the Schroedinger picture, the equation of motion is obtained:

$$\dot{\rho}_{AB,red} = (-i/\hbar)[H_{AB},\rho_{AB,red}] - \frac{1}{2}\sum_j \gamma_j\{[b_j b_j^\dagger \, \rho_{AB,red}$$

$$- b_j^\dagger \, \rho_{AB,red} \, b_j] \, \bar{n}(\omega_j)$$

$$- [b_j \, \rho_{AB,red} \, b_j^\dagger - \rho_{AB,red} \, b_j^\dagger b_j](\bar{n}(\omega_j)+1)$$

$$+ \text{H.a.}\} = L\rho_{AB,red}. \qquad (21)$$

In this expression $\bar{n}(\omega_j) = 1/(\exp(\hbar\omega_j/kT)-1)$ which is the thermal average for the number of reservoir excitations at $\omega_j, \gamma_j = 2\pi\hbar^2 |gjk(\omega_k=\omega_j)|^2 D(\Omega_j)$

which is a "golden rule" expression for coupling the bath (k) to the B mode (j), and $L$ is the Louisville operator.

This is a general theory which can describe a variety of problems in the context of coupling to a reservoir which is appropriate to condensed matter systems. The selective coupling case for HSC theory is depicted on Figure 5, where we are studying a high frequency mode A coupled selectively to a lower frequency mode B. For this to be an appropriate model, the energy scale relative to the highest experimental temperature should be: $kT \lesssim \hbar\omega_B << \hbar\omega_A$. If we call (for reasons which will soon be obvious) $\gamma_j \bar{n}(\Omega_j) = W_+$ and $\gamma_j(\bar{n}(\Omega_B)+1) = W_-$ then Eqn. (21) becomes:

$$\dot{\rho}_{AB,red} = (-i/\hbar)[H_{AB},\rho_{AB,red}]$$
$$- \frac{1}{2} W_+[bb^\dagger\rho_{AB,red} - b^\dagger\rho_{AB,red}b]$$
$$- W_-[b\rho_{AB,red}b^\dagger - \rho_{AB,red}b^\dagger b] + H.a\} \qquad (22)$$

The reduced Hamiltonian, $H_{AB}$, in this simple four level scheme becomes $H_{AB} = \hbar\omega_o a^\dagger a + \hbar\omega_b b^\dagger b + \delta\omega a^\dagger a b^\dagger b$. The states will be represented as $|n_A,n_B>$ where $n_A,n_B = 0,1$. There are 16 elements of the reduced density matrix of the form:

$$\rho_{AB,red}^{n_An_B;n_A'n_B'} = <n_A'n_B'|\rho_{AB,red}|n_An_B>;$$

however, as will be detailed below there is only a need for two elements, $\rho_{AB,red}^{00,10}$ and $\rho_{AB,red}^{01,11}$. "Sandwiching" Eqn. 22 by $<10|$ and $|00>$ yields:

Figure 5. Schematic representation of the selective coupling case for HSC exchange theory. In this case, a vibrational mode of higher frequency (A) is anharmonically coupled to only one lower frequency mode (B) resulting in the anharmonic shoft. Changes in the state of mode B will be manifested as a modulation in the resonance frequency of mode A. Note that $W_{-}$ is the inverse of the lifetime associated with mode B.

# VIBRATIONAL ENERGY EXCHANGE BETWEEN ANHARMONICALLY COUPLED STATES

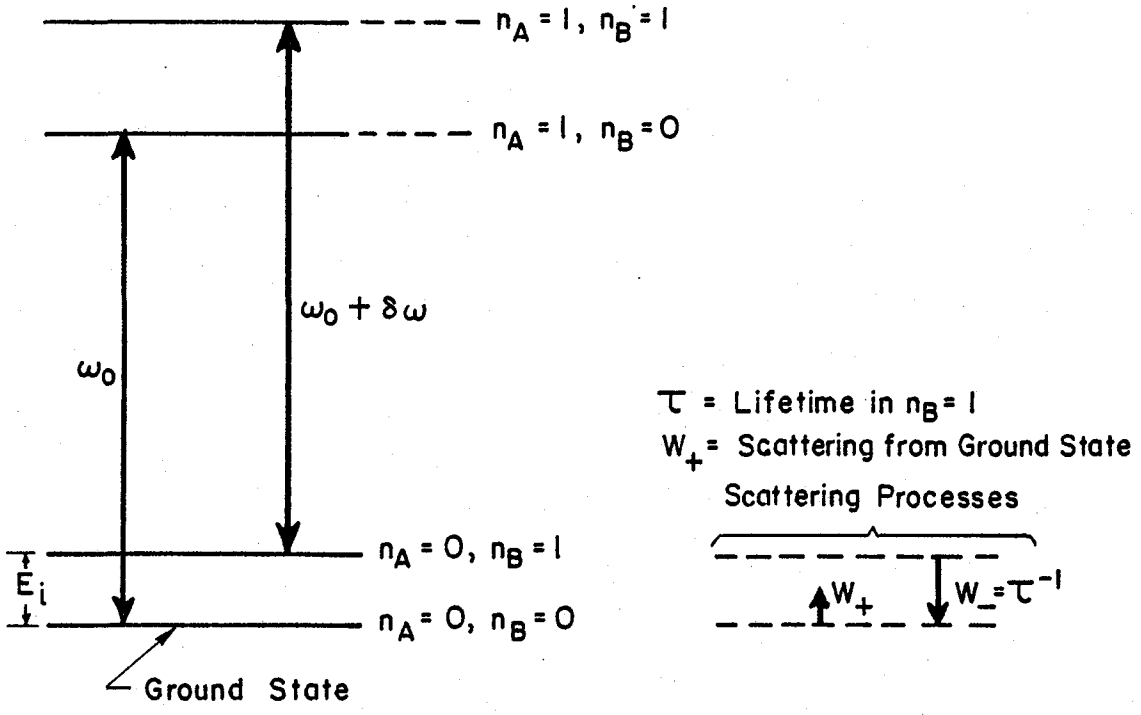


XBL 794-6107

$$\langle 10|\dot{\rho}_{AB,red}|00\rangle = \dot{\rho}^{00,10}_{AB,red} =$$

$$\langle 10|-i[\omega_o a^\dagger a\rho_{AB,red} + \overline{W_B b^\dagger b\rho_{AB,red}} + \overline{\delta\omega a^\dagger a b^\dagger b\rho_{AB,red}}$$

$$- \underline{\rho_{AB,red}\omega_o a^\dagger a} - \overline{\rho_{AB,red}\omega_B b^\dagger b} - \underline{\overline{\rho_{AB,red}\,\delta\omega a^\dagger a b^\dagger b}}]|00\rangle$$

$$- \frac{1}{2}\{W_+\langle 10|[bb^\dagger\rho_{AB,red} - \overline{b^\dagger\rho_{AB,red}b}]|00\rangle$$

$$- W_-\langle 10|[b\rho_{AB,red}\,b^\dagger - \overline{\rho_{AB,red}\,b^\dagger b}]|00\rangle + H.a\}. \qquad (23)$$

The expressions which are $\overline{\text{overlined}}$ go to zero because $\langle 10|b^\dagger$ or $b|00\rangle = 0$ in a similar manner the underlined expressions vanish since $a|00\rangle$ is zero. Further manipulation yields:

$$\dot{\rho}^{00,10}_{AB,red} = -i\omega_o\,\rho^{00,10}_{AB,red} - W_+\,\rho^{00,10}_{AB,red} + W_-\,\rho^{01,11}_{AB,red}. \qquad (24)$$

In an analogous way, the following expression can be obtained:

$$\dot{\rho}^{01,11}_{AB,red} = -i(\omega_o + \delta\omega)\,\rho^{01,11}_{AB,red} - W_-\rho^{01,11}_{AB,red} + W_+\rho^{00,10}_{AB,red}. \qquad (25)$$

Note that Eqns. (24) and (25) represent a closed system of mathematically coupled differential equations; that is, these equations involve only the two density matrix elements of interest. Also, detailed balancing[20] is satisfied by the exchanging rates such that

$$|\rho^{00,10}_{AB,red}|/|\rho^{01,11}_{AB,red}| = W_+/W_-. \qquad (26)$$

The exchanging rates can assume a more general role than what was assigned to them for solving the HSC model. For instance, in the presence of a photon field resonant with the B mode, additional rates in the form of Einstein's A and B coefficients[21] must be included in addition to the thermal relaxation processes accounted for by the W's. Ultimately the form for the motional Hamiltonian, $H_I$, determines the form for $W_+$ and $W_-$.

It is instructive at this point to consider limiting cases of Eqns. (24) and (25). First, this gives physical insight into the problem; and second, it points out the need for an additional factor. Both limits are based on the relative magnitudes of the anharmonic shift to the exchange rates. The first limit is that of "fast exchange", characterized by $W_+ > W_- >> |\delta\omega|$. Mathematically this is accounted for by ignoring $\delta\omega$ in Eqn. (25), which introduces an error on the order of $\delta\omega/(\delta\omega + W_-)$. Then Eqns. (24) and (25) may be added to each other to result in:

$$(\dot{\rho}^{00,10}_{AB,red} + \dot{\rho}^{01,11}_{AB,red}) = (-i\omega_o)(\rho^{00,10}_{AB,red} + \rho^{01,11}_{AB,red}). \tag{27}$$

The solution of Eqn. (27) is simply

$$(\rho^{00,10}_{AB,red} + \rho^{01,11}_{AB,red})(t) \sim e^{-i\omega_o t}. \tag{28}$$

This results in a single resonance at $\omega_o$ (a more complete derivation puts the resonance at $\omega_o + \frac{\delta\omega}{2}\ \frac{W_+}{W_-}$). The "slow exchange" regime is the other limiting case. Here $|\delta\omega| >> W_+ > W_-$. To zeroth order, the W's can be neglected; this uncouples the two transitions. Thus in this case, two resonances result; one at $\omega_o$ and the other at $\omega_o + \delta\omega$. Note that as modeled here, in either the slow or fast exchange regime the resonances are characterized by zero width, that is no intrinsic dephasing processes have been included besides the exchange mechanism. A phenomenological dephasing rate, $T_2$, may be added to Eqns. (24) and (25) to include these other dephasing mechanisms:

$$\dot{\rho}^{00,10}_{AB,red} = (-i\omega_o - 1/T_2)\ \rho^{00,10}_{AB,red} - W_+\ \rho^{00,10}_{AB,red} + W_-\ \rho^{01,11}_{AB,red} \tag{29}$$

$$\dot{\rho}^{01,11}_{AB,red} = (-i(\omega_o+\delta\omega) - 1/T_2)\ \rho^{00,10}_{AB,red} - W_-\ \rho^{01,11}_{AB,red} + W_+\ \rho^{00,10}_{AB,red}. \tag{30}$$

This makes the density matrix equations of motion formally analogous to the Bloch equations[22] for the magnetization in magnetic resonance. One essential point of this derivation is that there is no intrinsic dephasing associated with mode A when mode B experiences a state fluctuation other than the modulation of the frequency of mode A; the frequency of A adiabatically tracks the changes in B with a preservation of the phase.

As the discussion in Section A indicated, we need the vibrational autocorrelation function to calculate the Raman lineshape function. For the HSC selective coupling case this is

$$\langle Q(t)Q(0)\rangle \sim \rho^{00,10}_{AB,red} + \rho^{01,11}_{AB,red}. \tag{31}$$

Equations (29) and (30) may be put into matrix form:

$$\dot{\underset{\sim}{P}}^{01}_{AB,red}(t) \equiv \begin{bmatrix} \dot{\rho}^{00,10}_{AB,red}(t) \\ \dot{\rho}^{00,11}_{AB,red}(t) \end{bmatrix} = \begin{bmatrix} (-i\omega_o - 1/T_2 - W_+) & W_- \\ W_+ & (-i(\omega_o+\delta\omega) - 1/T_2 - W_-) \end{bmatrix}$$

$$\times \begin{bmatrix} \dot{\rho}^{00,10}_{AB,red}(t) \\ \rho^{01,11}_{AB,red}(t) \end{bmatrix} \equiv (-i\underset{\approx}{\omega}_v + \underset{\approx}{\pi})\ \underset{\sim}{P}^{01}_{AB,red}(t) \tag{32}$$

where $i\underset{\approx}{\omega}_v$ is the diagonal matrix of vibrational frequencies and $\underset{\approx}{\pi}$ contains rates for dephasing or transition between the frequencies. This can be solved by standard techniques:[23]

$$\frac{\langle Q(t)Q(0)\rangle}{\langle Q(0)Q(0)\rangle} = [11] \cdot \begin{bmatrix} \rho^{00,10}_{AB,red}(t) \\ -\rho^{01,11}_{AB,red}(t) \end{bmatrix} = \underset{\sim}{1} \cdot \exp[t(-i\underset{\approx}{\omega}_v + \underset{\approx}{\pi})] \cdot \underset{\sim}{P}^{01}_{AB,red}(0). \tag{33}$$

Substituting into Equation (9) gives,

$$I(\omega) \sim \int_{-\infty}^{\infty} dt\ \exp(i\omega t)\{\underset{\sim}{1}\cdot\exp[t(-i\underset{\approx}{\omega}_v+\underset{\approx}{\pi})]\cdot\underset{\sim}{P}^{01}_{AB,red}(0)\}. \tag{34}$$

The solution is[23]

$$I(\omega)\sim\{\mathrm{Re}\ \underset{\sim}{1}\cdot\underset{\approx}{A}^{-1}\cdot\underset{\sim}{P}^{01}_{AB,red}(0)\} \tag{35}$$

where $\underset{\approx}{A} = i(\omega\underset{\approx}{I}-\underset{\approx}{\omega}_v)+\underset{\approx}{\pi}$. The analytical solution of this is given by

$$I(\omega) = \frac{\begin{array}{l}\{W_+W_-(\delta\omega)^2+T_2'^{-1}[(W_++W_-)^3 + W_-(\delta\omega/2-\omega')^2 + W_+(\delta\omega/2+\omega')^2] \\ + 2T_2'^{-2}(W_++W_-)^2 + T_2'^{-3}(W_++W_-)\}/(W_++W_-)\end{array}}{\begin{array}{l}\{[(\delta\omega/2)^2-\omega'^2 + T_2'^{-2} + T_2'^{-1}(W_++W_-)]^2 + [W_-(\delta\omega/2+\omega') \\ - W_+(\delta\omega/2-\omega') + 2\omega'/T_2']^2\}\end{array}} \tag{36}$$

where $\omega' = \omega-\omega_o-\delta\omega/2$. In the limit that $W_+$, $W_- \to 0$ such that $(W_+/W_-) \to 1$ (no exchange) this reduces to two Lorentzian lineshapes each of full width $1/T_2'$; one centered at $\omega = \omega_o$, the other at $\omega = \omega_o + \delta\omega$. When $T_2'^{-1} \to 0$ (no residual dephasing besides the exchange process) Eqn. (36) reduces to:

$$I(\omega) = \frac{W_+(\delta\omega/2)^2/(1+W_+/W_-)}{[\omega'^2-(\delta\omega/2)^2]^2 + [W_-(\omega'+\delta\omega/2) + W_+(\omega'-\delta\omega/2)]^2}\ . \tag{37}$$

Just as we considered the limiting cases of fast or slow exchange from Equations (24) and (25), the same information can easily be obtained from Equation (37). It is useful to consider another limit of Equation (37), the low temperature approximation. In this case $\frac{\delta\omega}{W_+} < 1$, $\frac{W_+}{W_-} < 1$, and $\delta\omega/W_- \lesssim 1$; there should be one peak near $\omega_o$ and another (which is much smaller) near $\omega_o + \delta\omega$. For the purposes of finding the behavior of the lineshape near $\omega_o$ ($\omega' = -\delta\omega/2$) those factors which go as $(\omega'-\delta\omega/2)$ which vary slowly about $\omega_o$, may be set to $-\delta\omega$. We obtain the following result:

$$I(\omega) = \frac{W_+ \tau^2 (\delta\omega)^2 / [D(1 + W_+ \tau)]}{(\omega - \omega_o - W_+ \tau \delta\omega / D)^2 + W_+^2 [(\delta\omega)^2 \tau^2]^2 / D^2} \tag{38}$$

where $\tau = (W_-)^{-1}$ and $D = 1 + (\delta\omega)^2 \tau^2$. This results in an effective frequency

$$\omega_{eff} = \omega_o + W_+ \, \delta\omega\tau / (1 + (\delta\omega)^2 \tau^2) \tag{39}$$

as well as an effective relaxation rate

$$(T_2^{eff})^{-1} = W_+ (\delta\omega)^2 \tau^2 / (1 + (\delta\omega)^2 \tau^2) \tag{40}$$

Because Equations (38-40) represent a Lorentzian lineshape, the residual dephasing processes may be incorporated by simply convoluting this lineshape with the residual lineshape. Since the convolution of a Lorentzian with a Lorentzian is a Lorentzian possessing a width which is simply the sum of the initial widths, we have (low temperature approximation):

$$I(\omega) = I(\omega_o) / (1 - (\omega - \omega_{eff})^2 (T_2^{eff})^2) \tag{41}$$

$$\omega_{eff} = \omega_o + \frac{\delta\omega [\exp(-E_i / kT)]}{1 + (\delta\omega)^2 \tau^2} \tag{42}$$

$$(T_2^{eff})^{-1} = (T_2')^{-1} + \frac{\delta\omega^2 \tau}{1 + (\delta\omega)^2 \tau^2} [\exp(-E_i / kT)] \tag{43}$$

where the following relationship has been used (see Fig. 5 and Eqn. 26):

$$W_+ = W_- \exp(-E_i / kT) = 1/\tau \exp(-E_i / kT). \tag{44}$$

The aspects of Equations (42) and (43) which should be noted are: 1) Both the peak position as well as the shift due to exchange display the same temperature factor, $\exp(-E_i/kT)$, with the same Arrhenius

activation energy, $E_i$. 2) $E_i$ corresponds to the energy of a low frequency mode which the vibration is coupled to (Fig. 5). 3) Though it could display a temperature behavior on its own, $\tau$ is assumed to be a temperature independent constant. This assumption can be checked by dividing the temperature dependent width by the temperature dependent part of the peak position (the second terms in Eqns. (43) and (42) to obtain a temperature-independent unitless quantity, $\delta\omega\tau$). If this is indeed a constant over the temperature range of interest, then the theory may be applied. Also the value of this quantity gives a quantitative measure of the regime of exchange: 1) Slow exchange is characterized by $|\delta\omega\tau| >> 1$, here the broadening predominates the shift - a result which might be expected, since the influence of the small $|01> \rightarrow |11>$ transition is to create a "hot band". 2) Rapid exchange is when $|\delta\omega\tau| << 1$. Here the two transitions are said to be exchange averaged or narrowed; resulting in a shift but a small broadening. 3) When the broadening and shift are comparable ($|\delta\omega\tau| \sim 1$) then the transition is in the intermediate exchange regime. It is this latter case which will provide the most definite experimental evidence of HSC exchange, because the shift and broadening independently provide evidence (e.g., same activation energy) for the model.

The HSC selectively coupled model requires a fit of five parameters ($\delta\omega$, $\tau$, $E_i$, $\omega_o$, and $(T_2')^{-1}$) to the temperature dependent Raman lineshape. This theory will be discussed in greater detail in Section E,particularly how it relates to other theories which give similar expressions for the low temperature asymptopic limit (Eqns. (41-43)). Chapter III presents experimental evidence.

C. Interacting Fundamentals (AO Theory)

Abbott and Oxtoby proposed an alternative model[24] (hereafter referred to as AO) which yields a temperature dependent lineshape which is similar in form to the HSC model (Eqns. (41, 42, and 43) but having a strikingly different interpretation. The purpose of this section as well as the following one is to show two differing models of vibrational dephasing which have claimed applicability to results obtained on $h_{14}$-durene.[25] A discussion of the experimental differentiation of these three models is in Section E. Experimental results and interpretation is the subject of Chapter III.

The physical basis for the AO exchange model is displayed on Figure 6. As in the case of the HSC model, only the selective coupling case will be considered. In that case, as illustrated on Figure 6, two normal modes (e.g., two different C-H stretches on a molecule) are coupled together by a low frequency mode:

$$V_c = F_{AB}(t)\ Q_A Q_B + F_{iiAB}(t)\ Q_i^2 Q_A Q_B \tag{44}$$

where A and B represent two different fundamentals and i represents a low frequency mode. The approach is also based on reservoir theory. It is worth going into the formalism in some detail, particularly since certain dropped terms are retained by Wertheimer (Sec. D). As in the last section, the Hamiltonian is divided in parts related to the vibration, the bath, and coupling between the bath and the vibration:

$$H = H_v + H_b + V_c \tag{45}$$

In a similar fashion the density matrix is written as

$$\rho = \rho_b \rho_b \rho_c \tag{46}$$

Figure 6. The selective coupling case for interacting fundamentals (AO theory). When two closely spaced fundamentals are coupled together by a low frequency mode, then dephasing can result.

# INTERACTING FUNDAMENTALS

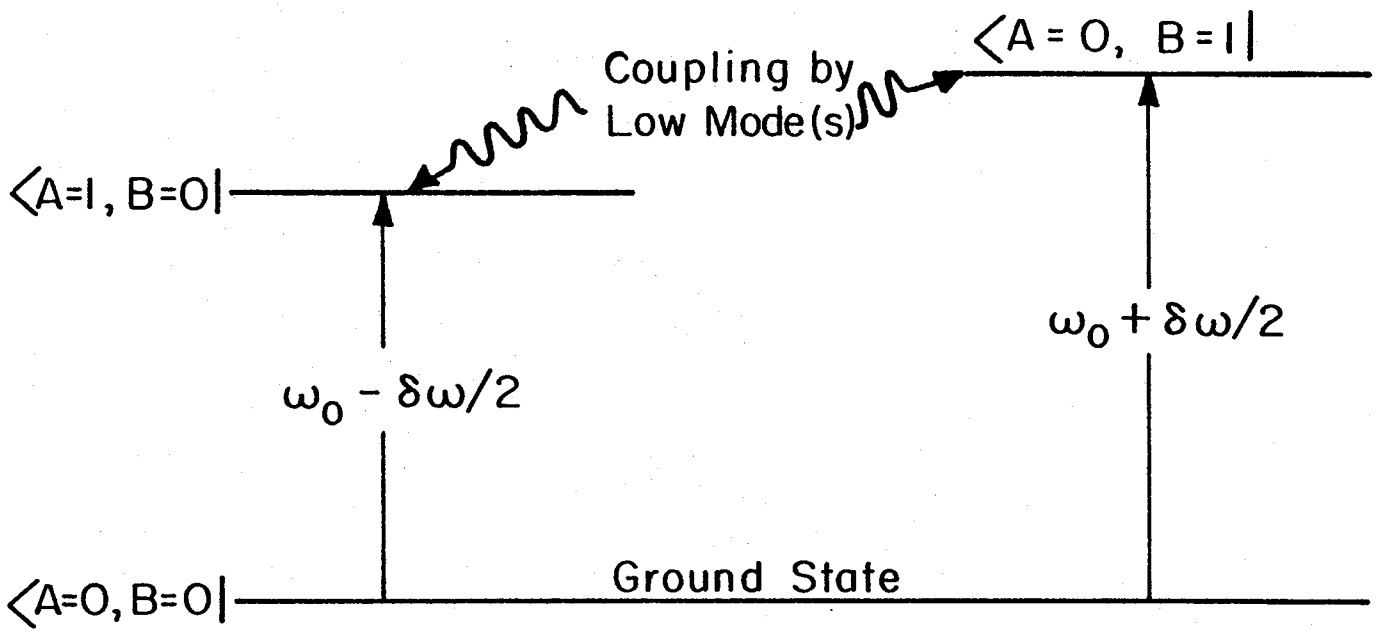


$$V_{coupling} = F_{ABLL}(t)\, \underbrace{Q^2_{low}}_{\text{Statistically Weighted}}\, Q_A\, Q_B$$

XBL 7911-7282

The molecular polarizability autocorrelation function, in the Heisenberg representation is given by

$$\langle\alpha\alpha(t)\rangle = \mathrm{Tr}[\rho\alpha \exp(iHt)\alpha \exp(-iHt)], \tag{47}$$

where the trace is over bath coordinates. Expanding Equation (47) yields

$$\langle\alpha\alpha(t)\rangle = \sum_{i,j,k,l} \langle\rho_v^i\rho_c^i \langle i|\alpha|j\rangle\langle j|\exp(iHt)|k\rangle \langle k|\alpha|l\rangle\langle l|\exp(-iHt)|i\rangle\rangle_b \tag{48}$$

where $\langle\rangle_b$ is an average over the bath states and i, j, k, l are vibrational eigenstates. Making the standard assumption that initially there is no coupling between the bath and system (i.e., $\rho_c^i = 1$);[26] and factoring out the molecular polarizabilities (which do not depend on the bath) results in

$$\langle\alpha\alpha(t)\rangle = \sum_{i,j,k,l} \rho_v^i \alpha_{ij}\alpha_{kl}\langle\langle j|\exp(iHt)|k\rangle \langle l|\exp(-iHt)|i\rangle\rangle_b \tag{49}$$

This may be rewritten as

$$\langle\alpha\alpha(t)\rangle = \sum_{i,j,k,l} \rho_v^i\alpha_{ij}\alpha_{kl}\langle j|G_{kl}(t)|i\rangle \tag{50}$$

where

$$G_{kl}(t) = \langle C_k^\dagger(t)\ C_l(t)\rangle_b \tag{51}$$

and where

$$|k\rangle = C_k^\dagger \text{ and } \langle l| = C_l.$$

$G_{kl}(t)$ is the socalled "superoperator" which operates in the vibrational degrees of freedom. Note that at $t = 0$ the only matrix element of $G_{kl}$ which is nonzero is the kl element. The coupling between the system and bath causes the other elements to assume nonzero values at later times. The approach of Kubo[27] in the interaction representation is used to obtain an equation of motion

$$\exp(iLt) = \exp_0[i \int_0^t dt_1 \bar{V}^x(t_1)] \exp(iL_o t) \tag{52}$$

where for an arbitrary operator X

$$L_o X = [H_v + H_b, X] \tag{53}$$

and

$$\bar{V}^x(t_1)\ X = [\exp(iL_o t_1)V, X] \tag{54}$$

and $\exp_0$ is a time ordered exponential. Following the approach of Nitzan and Silbey[28] we utilize

$$G(t) = \exp(iLt)G(t=0) \tag{55}$$

or

$$\frac{d}{dt} G_{kl}(t) = \langle \exp_0[i \int_0^t dt_1 V^x(t_1)] \rangle_b \left[\frac{d}{dt} e^{iL_o t}\right]_b G_{kl}(t)$$

$$+ \langle \frac{d}{dt} \exp_0[i \int_0^t dt_1 V^x(t_1)] \rangle_b e^{iL_o t} G_{kl}(t)$$

$$= i\omega_{kl} G_{kl}(t) + \frac{d}{dt} \langle \exp_0[i \int_0^t dt_1 V^x(t_1)] \rangle e^{iL_o t} G_{kl}(t=0) \tag{56}$$

where $\exp_0$ is a time ordered exponential.

Nitzan and Silbey[28] showed that the cumulant expansion[27] of the bath averaged quantities are:

$$\langle \exp_0[i \int_0^t V^x(t_1)dt_1]\rangle_b = \exp_0[\sum_{n=1}^{\infty} \int_0^t dt_1 \frac{K_n^x(t_1)}{n!}] \tag{57}$$

and

$$\frac{d}{dt}[\exp_0 \int_0^t dt_1 \sum_n \frac{K_n^x(t_1)}{n!}] = \exp_0[\int_0^t dt_1 \sum_n \frac{K_n^x(t_1)}{n!}] \times [\sum_n \frac{1}{n!} K_n^x(t_1)] \tag{58}$$

here $K_n^x$, n 1,2,3,... are the cumulants.[27,29] The value of $K_1^x(t)$ is given by $\langle i\bar{V}^x(t_1)\rangle_b$ which without loss of generality may be set to zero by simply adding $\langle \bar{V}^x(t_1)\rangle_b$ to the zeroth order vibrational Hamiltonian. By taking the cumulant expansion to just second order, justified by treating the bath as a Gaussian process or by assuming that V is small enough for perturbation theory to be valid, the equation of motion becomes

$$\frac{d}{dt} G_{kl}(t) = i\omega_{kl} G_{kl}(t) - \int_0^t dt_1 \{e^{i\omega_{kl}t} \langle \bar{V}^x(t)\bar{V}^x(t_1)\rangle_b C_k C_1\}. \tag{59}$$

After manipulation of the potential correlation function by taking matrix elements Equation (59) becomes

$$\begin{aligned}\frac{d}{dt} G_{kl}(t) = {} & i\omega_{kl} G_{kl}(t) \\ & - \sum_{i,j} \int_0^t d\tau \{e^{i\omega_{ki}\tau} \langle V_{ji}(\tau)\, V_{ik}(0)\rangle G_{jl}(t) \\ & - e^{i\omega_{ki}\tau} \langle V_{ik}(0)\, V_{lj}(\tau)\rangle G_{ij}(t) \\ & - e^{i\omega_{jl}\tau} \langle V_{ik}(\tau)\, V_{lj}(0)\rangle G_{ij}(t) \\ & + e^{i\omega_{jl}\tau} \langle V_{lj}(0)\, V_{ji}(\tau)\, G_{ki}(t)\}\end{aligned} \tag{60}$$

Recall that the only assumptions used in deriving Equation (60) are: 1) molecular chaos ($\rho = \rho_v \rho_b$), and 2) there is either "special" (Gaussian or weak) processes such that the cumulant expansion of V may be truncated after second order. Therefore, once the Hamiltonian describing the system, bath, and system-bath coupling have to be decided on, then the coefficients which go into Equation (60) may be determined. Note that this yields a system of coupled differential equations which in principle may be solved for the $G_{kl}(t)$'s; then by utilizing these values in Equation (48) the molecular polarizability autocorrelation function may be determined which is the Fourier transformation of the lineshape function (Sec. II.A).

Abbott and Oxtoby applied this formalism to the HSC selective coupling model (Sec. B) and achieved the same results (Eqn. (36)). It is instructive to briefly outline some points of that derivation, particularly since an assumption made by the HSC model as well as Abbott and Oxtoby which is challenged by Wertheimer (Sec. D) is most clearly seen in that context. Returning to the HSC model and renaming the states on Figure 5: 0,0 becomes 0; 0,1 becomes 1; 1,0 becomes 2; and 1,1 becomes 3- an application of Equation (50) yields:

$$\begin{aligned} \langle \alpha\alpha(t) \rangle = {} & \rho_0 \alpha_{02} \alpha_{20} \langle 2 | G_{20}(t) | 0 \rangle \\ & + \rho_0 \alpha_{02} \alpha_{31} \langle 2 | G_{31}(t) | 0 \rangle \\ & + \rho_1 \alpha_{13} \alpha_{20} \langle 3 | G_{20}(t) | 1 \rangle \\ & + \rho_1 \alpha_{13} \alpha_{31} \langle 3 | G_{31}(t) | 1 \rangle . \end{aligned} \tag{61}$$

The first and last terms of this expression correspond to the fundamental and hot band lineshapes; if there were only these terms, then as assumed in the HSC model the two lineshapes are simply additive. The effect of

the middle terms is to provide a correction to the spectrum due to interference effects. Wertheimer[30] is concerned with this effect which he calls Dynamic Coupling (DC) and is the subject of Section D. Dynamic Coupling becomes more important when the anharmonic shift is small and there is appreciable overlap between the fundamental and its hot band as well as an energy exchange mechanism. Abbott and Oxtoby made the same assumptions as in the HSC case: 1) neglect of Dynamic Coupling; 2) lifetime coupling between levels 0 and 1 and between 2 and 3 only; 3) that coupling is independent of the excitation of the high frequency mode (i.e., $V_{01} = V_{23}$); 4) the Raman cross section of the high frequency mode is independent of the number of quanta in the low frequency mode (i.e., $\alpha_{02} = \alpha_{13}$); 5) the intrinsic dephasing width of the high frequency mode is independent of the state of the low frequency mode (i.e., $D_{31}$ $D_{20}$); 6) $\delta\omega << \omega_{10} \approx \omega_{32}$; and 7) the Markov approximation may be invoked (bath relaxation is fast compared to vibrational relaxation). Application of the Nitzen-Silbey techniques yield the same results as the derivation in Section B, namely Equation (36).

Thus this technique is equivalent to the reservoir approach of Section B, Anderson's result (Ref. 10, Eqn. (49) and Ref. 9), as well as the modified Bloch equations. The Nitzen-Silbey approach is more compatible with incorporation of the quantum interference effects which lead to Dynamic Coupling (Sec. D).

This formalism was applied also to the interacting fundaments or AO model. This is illustrated in Figure 6. It is useful to rename the three states which comprise the <u>system</u>: namely (A = 0, B = 0) becomes 0; (1,0) becomes state 1; and (0,1) becomes 2. The <u>bath</u> now includes the low-frequency mode(s) coupled to the fundamentals as discussed below.

The molecular polarizability autocorrelation function is easily obtained from Equation (49),

$$\begin{aligned}\langle\alpha\alpha(t)\rangle = |\alpha_{01}|^2 \ &\langle 1|G_{10}(t)|0\rangle \\ + \alpha_{01}\alpha_{20} \ &\langle 1|G_{20}(t)|0\rangle \\ + \alpha_{02}\alpha_{10} \ &\langle 2|G_{10}(t)|0\rangle \\ + |\alpha_{02}|^2 \ &\langle 2|G_{20}(t)|0\rangle. \end{aligned} \tag{62}$$

Again cross correlation quantum interference effects are represented by the middle terms which will be retained for now. Again, assuming that the only exchange-like effect is between levels 1 and 2 yields the following equation of motion for the superoperators:

$$\frac{d}{dt}\begin{pmatrix} G_{10}(t) \\ G_{20}(t) \end{pmatrix} \quad \frac{d}{dt}\underset{\sim}{G}(t) = \underset{\approx}{\underset{\approx}{A}}\underset{\sim}{G}(t), \tag{63}$$

where the A matrix becomes after applying the Markov approximation.

$$\underset{\approx}{\underset{\approx}{A}} = \begin{pmatrix} -(D_{01} + \Gamma_{12}) & B_{12} \\ B_{21} & -(D_{02} + \Gamma_{21}) \end{pmatrix} \tag{64}$$

where the relaxation rate is given by

$$\Gamma_{ij} = \int_0^\infty dt \ \exp(i\omega_{ji}t) \ \langle V_{ij}(t) \ V_{ji}(0)\rangle \tag{65}$$

and the off diagonal cross correlation terms by

$$\begin{aligned} B_{ij} = &- \int_0^\infty dt \ \langle V_{ji}(t)[V_{ii}(0) - V_{00}(0)] \\ &- \int_0^\infty dt \ e^{i\omega_{ij}t} \ \langle V_{jj}(t) \ V_{ji}(0) \\ &- V_{ji}(0) \ V_{00}(t)\rangle. \end{aligned} \tag{66}$$

These terms also lead to effects which prevent the lineshape from simply being the sum of the two fundamentals. This, as in the case of the molecular polarizability, is most important when the bands overlap. Thus the case of interacting (but sufficiently well separated) fundamentals is given by dropping the B terms in the A matrix and dropping those dynamic coupling like terms in Equation (62). This results in the ability to separate the 0-1 and 0-2 lineshapes. The lineshape associated with the 0-1 transition is

$$I_{01} \sim |\alpha_{01}|^2 \, \mathrm{Re}\{i[\omega-(\omega_0 - \tfrac{\delta\omega}{2}) + \beta_{12}] + (D_{01} + \gamma_{12})\}^{-1} \qquad (67)$$

where $\gamma_{12}$ (the additional linewidth) and $\beta_{12}$ (the shift) are real and imaginary components of the relaxation between the fundamentals, $\Gamma_{12}$ given by

$$\Gamma_{12} = \int_0^\infty dt \; e^{i(\delta\omega)t} \; \langle V_{12}(t_1) \; V_{21}(0)\rangle. \qquad (68)$$

Equations (67) and (68) have an interesting interpretation. Note that it is only that frequency component of the potential autocorrelation which occurs at the zero temperature splitting frequency ($\delta\omega$) of the two fundamentals which is responsible for shifting and broadening the lineshapes of those fundamentals. Since "noise" usually has a frequency spectrum which peaks about $\omega = 0$[30] then it would appear that the fundamentals have to be closely spaced for the AO mechanism to play an important role. More will be said about this point below.

In parallel with the selective coupling HSC model, the introduction of selective coupling in the AO model is the adoption of a potential of the form of Equation (44) where only one low frequency mode is used to couple the interacting fundamentals. Note also that this potential

involves terms which are very nearly energy conserving; as an example the last expression in Equation (44) can be written in terms of creation and annihilation operators:

$$Q_i^2 Q_A Q_B = a_i a_i^\dagger a_A a_B^\dagger + a_i a_i^\dagger a_A^\dagger a_B + a_i^\dagger a_i a_A a_B^\dagger + a_i^\dagger a_i a_A^\dagger a_B \tag{69}$$

where the energy mismatch is on the order of $\delta\omega$, and terms having a much larger mismatch (such as $a_i^\dagger a_i^\dagger a_A a_B$) have been eliminated. By a similar analysis, a term in the perturbative potential, $Q_i Q_1 Q_2$, has been dropped because there are no energy conserving terms.

With the potential of Equation (44) chosen, Equation (68) assumes the form

$$\begin{aligned}\Gamma_{12} = |q_{10}|^2 |q_{20}|^2 [&\int_0^\infty dt_1\, e^{i\delta\omega t_1} \langle F_{12}(t_1) F_{12}\rangle \\ &+ \langle q_i^2\rangle \int_0^\infty dt_1\, e^{i\delta\omega t_1} \langle F_{12}(t_1) F_{ii12} + F_{ii12}(t_1) F_{12}\rangle \\ &+ \langle q_i^4\rangle \int_0^\infty dt_1\, e^{i\delta\omega t_1} \langle F_{ii12}(t_1) F_{ii12}\rangle ].\end{aligned} \tag{70}$$

Assuming a temperature range such that only the ground and first excited states of the low frequency mode, i, need be considered results in

$$\langle q_i^2\rangle,\ \langle q_i^4\rangle \propto \exp(-E_i/kT). \tag{71}$$

Also if it is the case that all the correlation functions in Equation (70) decay exponentially with a time constant $\tau$, then Equation (70) may be rewritten as

$$\Gamma_{12} = [B + A \exp(-\hbar\omega_i/kT)] \int_0^\infty dt_1 \, e^{i\delta\omega t_1} e^{-t_1/\tau}$$

$$= [B + A \exp(-\hbar\omega_i/kT)] \frac{\tau + i\delta\omega\tau^2}{1+\delta\omega^2\tau^2}$$

with

$$B = |q_{10}|^2 |q_{20}|^2 \langle F_{12}^2 \rangle$$

and

$$A = |q_{10}|^2 |q_{20}|^2 \{2\langle q_i^2 \rangle \langle F_{12} F_{ii12} \rangle + \langle F_{ii12}^2 \rangle\}. \quad (72)$$

Substituting Equation (72) into Equation (67) yields the following parameters for the Lorentzian lineshape

$$\omega_A = (\omega_0 - \frac{\delta\omega}{2}) + B \left(\frac{\delta\omega\tau^2}{1+\delta\omega^2\tau^2}\right) + A \exp\left(-\frac{\hbar\omega_i}{kT}\right)\left(\frac{\delta\omega\tau^2}{1+\delta\omega^2\tau^2}\right) \quad (73)$$

$$\text{Width (HWHM)} = D_{01} + B\left(\frac{\tau}{1+\delta\omega^2\tau^2}\right) + A \exp\left(-\frac{\hbar\omega_i}{kT}\right)\left(\frac{\tau}{1+\delta\omega^2\tau^2}\right) \quad (74)$$

Note the formal similarity to the HSC model, Equations (42) and (43). In both cases (in the low temperature limit), the broadening and shift display an "Arrhenius" behavior with the same activation energy - this energy corresponds to the energy of a low frequency mode.

A complete comparison of these theories will be the subject of Section E. The salient predictions of this theory are: for the selectively coupled AO model as represented on Figure 6 the two fundamentals should shift toward each other with increasing temperature with the same activation energy; if there is an isolated peak if should not experience an appreciable shift or broadening; and the parameters $\delta\omega$ and $\tau$ which have a different interpretation than in the HSC model cannot be extracted separately but only there product, $\delta\omega\tau$.

D. Dynamic Coupling (DC Theory)

Wertheimer,[31-37] in a recent series of papers has developed a very thorough theory relating dynamical processes in condensed phase to the resulting lineshape function for molecular vibrations. The purpose of this section is to focus on that aspect of his theory called dynamic coupling (hereafter referred to as DC) which predicts under special circumstances a temperature dependent lineshape function similar in form to that predicted by both the HSC model of Section B and the AO model of Section C; namely, the shift and width obeying an Arrhenius behavior with an activation energy corresponding to the energy associated with a low frequency mode. Wertheimer's theory is general enough to include both the AO and HSC theories as restricted cases. Three conditions must be met for dynamic coupling (DC) to play a significant role; 1) the high frequency modes (whether they are a fundamental and its hot band in HSC theory or two "distinct" fundamentals in AO theory) must overlap, 2) the high frequency modes must have an "excitonic dispersive shift", $\delta\nu$, which is resonance with the static splitting, $\delta\omega$, 3) there should be an exchange interaction between the high modes with a characteristic time $\tau$ which is in intermediate exchange ($|\delta\omega\tau| \sim 1$).

The first condition above, overlap, manifests its affect on the lineshape through off-diagonal terms of the transition correlation matrix (TCM) which has the following form:

$$C_{ab}(t) = \langle\{\sigma_a^\dagger(t),\ \sigma_b(0)\}\rangle,$$

$$\sigma_a = N^{-\frac{1}{2}} \sum_i \sigma_{k\lambda}^i,\ \sigma_b = N^{-\frac{1}{2}} \sum_i \sigma^i{}_{\mu\nu}$$

$$\sigma_{k\lambda}^i = \langle a_k^{i\dagger} a_\lambda^i \rangle \qquad (75)$$

where a corresponds to the $\lambda \rightarrow k$ transition and b to the $\nu \rightarrow \mu$ transition. The sum is over all molecules i. If there are N transitions of interest (fundamentals, hotbands, etc.) then the TCM is an N x N matrix. The spectral function for Raman transitions is written in terms of the LaPlace transformation of the TCM and the polarizabilities

$$I(\omega) = \mathrm{Re} \sum_{a,b} \alpha_a^* C_{ab}(\omega) \alpha_b \tag{76}$$

where

$$\alpha_a^i = \alpha_{k\lambda}^i = \langle k,i|\alpha|\lambda,i\rangle. \tag{77}$$

This formalism is somewhat unusual for most spectroscopists. Instead of considering the self-correlation part of the TCM ($C_{ii}$) as sufficient to determine the lineshape, here the off-diagonal terms are also considered. Off-diagonal terms can arise from correlations between different transitions, either the same band on different molecules (intermolecular correlations) or correlations between different bands. The origin of the cross correlations arises since an externally induced ($\beta \rightarrow \alpha$) transition causes a phase coherence or phase-correlation in the appropriate oscillator, $\sigma_{\alpha\beta}^i$. This phase correlation is lost in a time scale $T_2$ (the dephasing time). If there exists mutual coupling between the various other oscillators of the system and $\sigma_{\alpha\beta}^i$, then they can be coherently driven for the dephasing time. This results in the transfer of vibrational energy and phase memory between oscillators.

Two conditions must be met in order to have this energy and phase transfer take place and have a significant effect on the lineshape. If it does the two (or more) modes are said to be dynamically coupled together. The first condition is that the energy transfer must take place

within the dephasing time. The second condition is that the frequency difference between the two oscillators satisfies $|\omega_{\alpha\beta} - \omega_{\gamma\delta}|^{-1} > T_2$, that is the time it takes the two oscillators to run out of phase is greater than the dephasing time (the oscillators overlap to zeroth order). Both of these conditions can be met in the HSC exchange model of hotbands being exchanged when the anharmonic shifts are small. Thus HSC theory appears as the large anharmonic shift asymptotic limit of the DC theory.

Using the technique of Mori the TCM can be evaluated (Ref. 38,39)

$$\underset{\approx}{C}(\omega) = i[\omega \underset{\approx}{1} - \underset{\approx}{L}(\omega)]^{-1} \underset{\approx}{C}^{o}$$

$$\underset{\approx}{L}(\omega) = \underset{\approx}{\Omega} - i\underset{\approx}{R}(\omega)$$

$$\underset{\approx}{C}^{o} = \underset{\approx}{C}(t = 0). \tag{78}$$

As in the case of the two previous models, the Hamiltonian may be decomposed into sub-Hamiltonians and coupling between the sub-Hamiltonians

$$H = H_0 + \delta H \tag{79}$$

where

$$H_0 = H_v + \bar{H}_{pot} + H_R \tag{80}$$

Here $H_V$ is the energy operator of just the molecular vibrations

$$H_V = \sum_i \sum_\alpha \varepsilon_\alpha \sigma^i_{\alpha\alpha} \tag{81}$$

Wertheimer makes the point that the $\varepsilon_\alpha$ are weakly temperature dependent because the basis set is chosen in a manner which minimizes the off diagonal averages in terms of $\delta H$:

$$\langle\sigma_{\alpha y}\rangle - \langle\sigma_{\alpha y}\rangle_0 = \text{Order } (\delta H)^2 \tag{82}$$

where

$$\langle \sigma_{\alpha y} \rangle_0 = \delta_{\alpha y} \exp(-\beta\varepsilon_\alpha)/\sum_n \exp(-\beta\varepsilon_n)$$

$$\equiv \delta_{\alpha y} \bar{\sigma}_\alpha \tag{83}$$

$\delta_{\alpha y}$ is explained below. $\langle\rangle$ and $\langle\rangle_0$ represent canonical averages related to H and $H_o$ respectively. Wertheimer has shown (Ref. 31, 36) that this procedure also minimizes $\delta H$. $H_R$ is the energy operator for the phonon and libron states of the solid. $\delta H$, which should be small after this procedure, describes the coupling between oscillators as well as the coupling between the oscillators and the bath. Wertheimer has also shown (Ref. 31,36) that even though the individual Hamiltonians display a temperature dependence, the total Hamiltonian (Eqn. (79)) is temperature independent.

$H_V$, the molecular vibrational operator, is such that the various vibrations are decoupled. The interactions between molecules which affect the potential energy are denoted as

$$\mathcal{H}^{ij}_{pot} = \sum_{\alpha\beta\gamma\delta} \phi^{ij}_{\alpha\beta\gamma\delta} \sigma^{i}_{\alpha\beta} \sigma^{j}_{\gamma\delta} \tag{84}$$

where $\phi$, the vibrational matrix elements, represent a change in the potential energy which takes place based on changes in the vibrational coordinate, orientation, and position due to changes in the vibrational state. Thus the effect of the average value of the potential energy, $\bar{H}_{pot}$, in Equation (80) depends on the average of the vibrational subsystem

$$\bar{H}_{pot} = 1/2 \sum_{ij}{}' \bar{\phi}^{ij} \tag{85}$$

$$\bar{\phi}^{ij} = \sum_{\alpha\beta} \phi^{ij}_{\alpha\alpha\beta\beta}\, \bar{\sigma}_\alpha \bar{\sigma}_\beta \tag{86}$$

where $\sigma_\alpha$, the thermal averages have been defined in Equation (83). Note that $\bar{H}_{pot}$ is a static average, where molecule i remains in the $\alpha$ vibrational state and molecule j stays in the $\beta$ state is the form of all the elements in the average. Thus far this theory is only a very formal way of expressing a general theory of vibrational structure (anharmonicities) and dynamics and can represent either the HSC or AO theories. What makes this different is the various cross-correlation terms which are formally represented and are assumed to be non zero. These terms are contained in the coupling Hamiltonian

$$\delta H = \delta H_{pot} - \delta H_{vib} = 1/2 \sum_{ij}{}' \sum_{\alpha\beta\gamma\delta} [\delta\phi^{ij}_{\alpha\beta\gamma\delta}\, \sigma^{i}_{\alpha\beta}\, \sigma^{i}_{\gamma\delta} - \delta_{\gamma\delta} \langle \delta\phi^{ij}_{\alpha\beta\gamma\gamma} \rangle\, \sigma^{i}_{\alpha\beta}\, \bar{\sigma}_\gamma]. \tag{87}$$

The coupling potentials here represent an energy correlation between states:

$$\delta\phi^{ij}_{\alpha\beta\gamma\delta} = \langle \alpha,i|\gamma,j\| \delta\phi^{ij} \|\delta,j|\beta,i\rangle = \phi^{ij}_{\alpha\beta\gamma\delta} - \delta_{\alpha\beta}\delta_{\gamma\delta}\, \bar{\phi}^{ij} \tag{88}$$

where $\bar{\phi}^{ij}$ is the vibrational (uncorrelated) average. Table 1 and Figure 7 show various processes which lead to interference terms for vibrational dephasing. The solution of the time variation of dynamical variables can be obtained within the framework of Zwanzig-Mori formalism.[31,38-41] Briefly, this involves operator techniques including the Louisville operator which propagates dynamical variables as

$$a_i(t+\tau) = \exp(iLt)\, a_i(\tau) \tag{89}$$

Table 1. Types of Processes which Lead to Dephasing of a Well Separated (no hot Bands, nor 'Accidentally' Nearly Degenerate States) State $\alpha$ on Molecule i. The Dephasing Occurs Either Directly (Pure Dephasing or Population Relaxation of State $\alpha$) or by Other Mechanisms Including Interference Terms in the Transition Correlation Matrix (TCM). For Two Vibron Processes see Wertheimer (Ref. 31).

| Class of Process | Mechanism | | Molecular Transitions | Coupling Potential |
|---|---|---|---|---|
| Zero vibron | Pure dephasing | a | $\|\alpha,i\|\beta,j\rangle \rightarrow \|\alpha,i\|\beta,j\rangle$ | $\delta\phi^{ij}_{\alpha\alpha\beta\beta}$ |
| | Resonance transfer | b | $\|\alpha,i\|\beta,j\rangle \rightarrow \|\beta,i\|\alpha,j\rangle$ | $\delta\phi_{\beta\alpha\alpha\beta}$ |
| One vibron | Intramolecular decay | c | $\|\alpha,i\|\beta,j\rangle \rightarrow \|\alpha,i\|\gamma,j\rangle$ | $\delta\phi_{\alpha\alpha\gamma\beta}$ |
| | | d | $\|\alpha,i\|\beta,j\rangle \rightarrow \|\gamma,i\|\beta,j\rangle$ | $\partial\phi_{\gamma\alpha\beta\beta}$ |
| | One vibron transfer | e | $\|\alpha,i\|\beta,j\rangle \rightarrow \|\gamma,i\|\alpha,j\rangle$ | $\delta\phi_{\gamma\alpha\alpha\beta}$ |
| | | f | $\|\alpha,i\|\beta,j\rangle \rightarrow \|\beta,i\|\gamma,j\rangle$ | $\delta\phi_{\beta\alpha\gamma\beta}$ |

Figure 7. Shows some of the processes discussed in Table 1 and the text. If there is sufficient intermolecular coupling the various processes all contribute to the collective $0 \rightarrow \alpha$ transition.

SOME RELAXATION MECHANISMS WHICH CONTRIBUTE TO INTERFERENCE TERMS IN DEPHASING $O \rightarrow \alpha$ TRANSITION

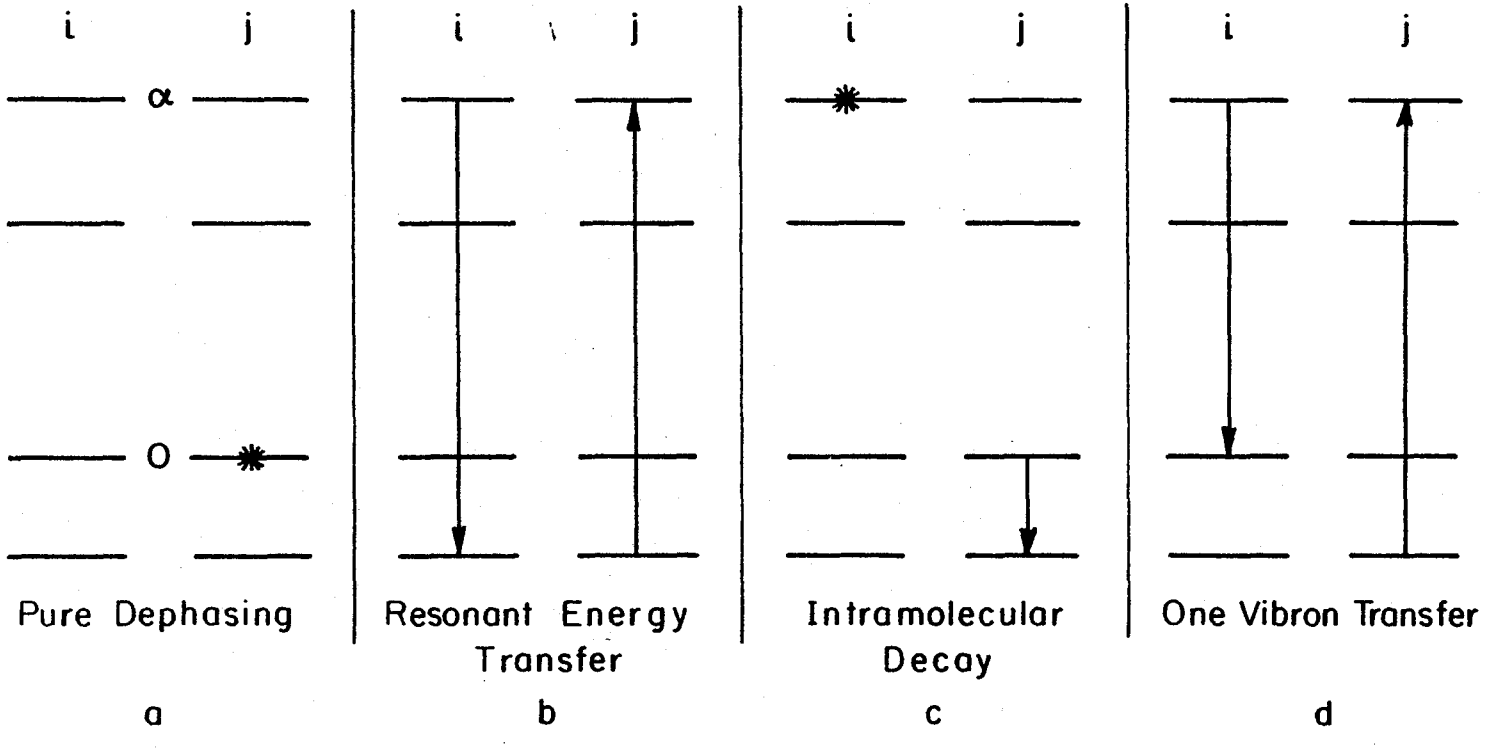


XBL 816-5935

and the projection operator P which projects a function into a subspace spanned by the socalled primary variables {b}

$$P = \sum_i |b_i)(b_i|b_i)^{-1}(b_1| . \tag{90}$$

The set $\{b_i\}$ is a subset of interest of all the dynamical variables $\{a_i\}$ and can without loss of generality be assumed to be orthogonal, $(b_i|b_j) = \delta_{ij}(b_i|b_i)$. Q defined by Q = 1-P is the projection operator complementary to P (spans the space orthogonal to $\{b_i\}$). The scalar product is defined as an anticommutator

$$(a_i|a_j) = 1/2 \langle\{a_i^\dagger, a_j\}\rangle. \tag{91}$$

Wertheimer (Ref. 31) showed that after tedious algebra that the Zwanzig-Mori representation of the TCM is

$$\sum_j [-i\omega\ \delta_{ij} + i\Omega_{ij} + K_{ij}(\omega)]\ C_{jk}(\omega) = \delta_{ik} C_{ii}(t=0) \tag{92}$$

where the frequency matrix $\Omega$ and the relaxation matrix R are given by

$$\Omega_{ij} = (b_i|Lb_j)(b_j|b_j)^{-1} \tag{93}$$

$$K_{ij}(Z) = (QLb_i|i\{Z-QLQ\}^{-1} QLb_j)(b_j|b_j)^{-1}. \tag{94}$$

One useful analysis is a small coupling limit. By that it is meant that the quantities in Equation (87) satisfy

$$(\delta H_{pot}),\ (\delta H_{vib}) << Nk_B T. \tag{95}$$

In this limit Wertheimer arrived at a perturbation scheme which among other requirements included changing the projection operators:

$$Q_o = 1-P_o,\ P_oA \equiv \sum_i b_i(b_i|A)_o(b_i|b_i)_o^{-1} \tag{96}$$

where the subscript 'o' represents the quantity assuming the value it would possess in the absence of coupling. The equation of motion in the weak coupling limit becomes

$$\sum_j[-i\omega\delta_{ij} + i\Omega_{ij}^{(0)} + K_{ij}^{(0)}(\omega)]\ C_{jk}(\omega) = \delta_{ik}C_{ii}^{(0)}(t=0) \tag{97}$$

with

$$C_{ij}^{(0)}(t=0) = \delta_{ij}(b_i|b_i)_o\ \{1 + 0(\frac{\delta H}{k_BT})\} \tag{98}$$

and the frequency matrix

$$\Omega_{ij}^{(0)} = (b_i|Lb_j)_o(b_j|b_j)_o^{-1}\ \{1 + 0(\frac{\delta H}{k_BT})\} \tag{99}$$

and the relaxation matrix

$$K_{ij}^{o}(t) = (Q_oLb_i|i\{t - Q_oL_oQ_o\}^{-1}\ \ Q_oLb_j)_o$$
$$(b_i|b_j)_o^{-1}\ \{1 + 0(\frac{\delta H}{k_BT})\}. \tag{100}$$

To illustrate these ideas on a system of interest, consider an <u>isolated doublet</u> of overlapping modes. In this case, application of Equation (78) yields

$$\underset{\approx}{C}(\omega) = \frac{i}{\det\underset{\approx}{A}(\omega)}\ \underset{\approx}{A}^{-1}(\omega)\ \underset{\approx}{C}(t=0) \tag{101a}$$

with

$$\underset{\approx}{A} = \begin{pmatrix} A_{11}(\omega) & A_{12}(\omega) \\ A_{21}(\omega) & A_{22}(\omega) \end{pmatrix} = \begin{pmatrix} \omega - \Omega_{22} + iR_{22}(\omega) & \Omega_{12} - iR_{12}(\omega) \\ \Omega_{21} - iR_{21}(\omega) & \omega - \Omega_{11} + iR_{11}(\omega) \end{pmatrix} \tag{101b}$$

If as in the case of HSC theory our doublet consists of a fundamental transition and what Wertheimer calls its associated upper stage transition ($0 \rightarrow \nu$ and $\nu' \rightarrow \nu' + \nu$), then interferences between processes which are quasi-elastic ($|\nu,0> \rightarrow |0,\nu>$) and two vibron conversion ($|\nu + \nu'|0> \rightarrow$ $\rightarrow |\nu|\nu'>$ and $|\nu + \nu'|0> \rightarrow |\nu'|\nu>$) result in finite terms for the off-diagonal expressions in Equation (101b). HSC exchange theory deals with off-diagonal terms which result from conversion of the low frequency mode ($|\nu> \leftrightarrow |0>$), and the spectrum was calculated using the self correlation part not the collective part as in Equation (76).

Because some of the energy redistribution schemes (one vibron, etc.) impart nonzero off-diagonal values to the L matrix of Equation (78), inversion of the $(\omega \underset{\approx}{I}-\underset{\approx}{L})$ is somewhat difficult. There is a prescription which is equivalent to Rayleigh-Schroedinger perturbation theory which assumes that the off-diagonal elements of L are small in comparison to differences in the matrix elements, i.e., $|L_{ab}L_{ba}|^{\frac{1}{2}} << |L_{aa}-L_{bb}|$. To second order in the off-diagonal terms we have

$$C_{ab}(\omega) = i\bar{\sigma}_a/(\omega-Z_a) \qquad \text{for } a = b$$

$$= \frac{iL_{ab}\,\bar{\sigma}_b}{(L_{aa}-L_{bb})}\left[\frac{1}{(\omega-Z_a)} - \frac{1}{(\omega-Z_b)}\right] \text{ for } a \neq b \qquad (102)$$

where the pole functions are

$$Z_a = L_{aa} + \sum_{b\neq a} \frac{L_{ab}L_{ba}}{(L_{aa}-L_{bb})} \qquad (103)$$

Substituting Equation (103) into Equation (76) yields the contribution to the Raman spectrum from the $a^{th}$ transition

$$\hat{I}_a(\omega) = \mathrm{Re}\{A_a(\omega)/[\omega-Z_a(\omega)]\} \qquad (104a)$$

where

$$A_a(\omega) = i\alpha_a^* \bar{\sigma}_a \alpha_a + i \sum_{b \neq a} \frac{(\alpha_a^* L_{ab} \bar{\sigma}_b \alpha_b + \alpha_b^* L_{ba} \bar{\sigma}_a \alpha_a)}{(L_{aa} - L_{bb})} \tag{104b}$$

The total spectrum is obtained by:

$$\hat{I}(\omega) = \sum_a \hat{I}_a(\omega) \tag{105}$$

Now the various interferences are contained in the second term on the right hand side of Equation (104b).

Wertheimer introduces what he calls the quasi-Markovian approximation, namely that the amplitude and pole functions in Equation (104) may be approximated by complex constants for each transition a, $A_a(\omega_a)$ and $Z_a(\omega_a)$. The spectral function for transition a becomes

$$I_a(\omega) = A_a'' D_a''(\omega) + A_a' D_a'(\omega) \tag{106}$$

The superscripts' and " represent respectively either the real or imaginary part of the amplitude A, or dispersive or absorptive part of pole $Z_a(\omega_a)$. The parameters $\omega_a^{eff} = \text{Re } Z_a(\omega_a)$ and $\Gamma_a^{eff} = \text{Im} Z_a(\omega_a)$ are the effective transition frequency and the effective dephasing rate for the best Lorentzian approximation to mode a:

$$D_a''(\omega) = \Gamma_a^{eff} / [(\omega - \omega_a^{eff})^2 + (\Gamma_a^{eff})^2] \tag{107a}$$

$$D_a'(\omega) = (\omega - \omega_a^{eff}) / [(\omega - \omega_a^{eff})^2 + (\Gamma_a^{eff})^2]. \tag{107b}$$

Thus the quantity $A_a'/A_a''$ is a measure of the asymmetry associated with the transition.

Thus far this theory is very general and exchange theory has not even been incorporated for the high frequency transitions. In order to include exchange in such a way that contact can be made to experiments various approximations must be made. It is the goal here to show 1) what approximations need to be made to recover the HSC exchange theory, then 2) what the effect of various generalizations that Wertheimer suggests have, with the focus on how they may be experimentally tested.

Only the following types of hot band transitions will be considered as being coupled to the fundamental transition ($0 \rightarrow \mu$): $\nu \rightarrow \mu + \bar{\nu}$, $2\bar{\nu} \rightarrow \mu + 2\bar{\nu}$ and $\bar{\nu} + \bar{\lambda} \rightarrow \mu + \bar{\nu} + \bar{\lambda}$. The anharmonic shifts for these hot bands are given by:

$$\Delta\omega_{\bar{\nu}} = \omega_{\mu+\bar{\nu},\bar{\nu}} - \omega_{\mu,o}$$

$$\Delta\omega_{2\bar{\nu}} = \omega_{\mu+2\bar{\nu},2\bar{\nu}} - \omega_{\mu,o}$$

$$\Delta\omega_{\bar{\nu}+\bar{\lambda}} = \omega_{\mu+\bar{\nu}+\bar{\lambda},\bar{\nu}+\bar{\lambda}} - \omega_{\mu,o} \qquad (108)$$

The assumptions used to constrict the theory to this point include: 1) the neglect of thermal population in a low frequency mode in a quantum number greater than two, 2) the neglect of any other dynamic coupling process to other modes such as a combination band, 3) the low frequency mode is considered to be harmonic as far as the transition matrix elements are concerned (quasi-harmonic approximation, 4) besides the process $\bar{\nu} \rightarrow 0$ other depopulation processes which have a mismatch frequency greater than the Debye cutoff are neglected, 5) in the relaxation matrix, R, mismatch frequencies on the order of $\delta\Omega_{ab}$ or of the anharmonicities are neglected, 6) as discussed before, the relaxation

matrix is evaluated in the quasi-Markovian limit, and 7) coupling potentials of the type $\delta\phi_{\alpha+\lambda,\beta+\lambda,\gamma+\nu,\delta+\nu}$ are approximated by $\delta\phi_{\alpha\beta\gamma\delta}$.

Within the context of these seven approximations the frequency matrix elements (Eqn. (78)) becomes

$$\begin{aligned}\Omega_{oo} &= \omega_o + \bar{\sigma}_o \delta\Omega \\ \Omega_{\nu\nu} &= \omega_o + \Delta\omega_\nu + \bar{\sigma}_\nu \delta\Omega \\ \Omega_{o\nu} &= (\bar{\sigma}_o/\bar{\sigma}_\nu)\ \Omega_{\nu o} = \bar{\sigma}_o \delta\Omega \end{aligned} \tag{109}$$

where $\nu = \bar{\nu}$, $2\bar{\nu}$ or $\bar{\nu} + \bar{\lambda}$ and $\omega_o = \omega_{\mu o}$.

The frequency shift is given by

$$\delta\Omega = \sum_{j\neq i} \langle T^{ij}_{\mu\mu} \rangle_o, \tag{110}$$

and results from exciton (resonant) transfer processes of the $\mu$ transition; i.e., of the type $|\nu + \mu|\lambda\rangle \leftrightarrow |\nu|\lambda + \mu\rangle$. The reason there is only a single $\delta\Omega$ results from the fact that approximation 7) is adopted.

The frequency matrix is more complicated, but in the context of the seven above named approximations its elements assume the values

$$R_{\nu\nu} = R_s + \bar{\sigma}_\nu R_D + \sum_{\bar{n}} (\sigma_{\bar{n}}/\bar{\sigma}_o)\ [R^I_{o\bar{n}} + R^T_{\bar{n}}] + \Delta R_\nu \tag{111}$$

for $\nu = 0,\ \bar{\nu},\ 2\bar{\nu},\ \bar{\nu} + \bar{\lambda}$

where $\Delta R_\nu = 0$, for $\nu = 0$

$$\begin{aligned} &= R^I_{o\bar{\nu}} + R_{\bar{\nu}} + R^T_{\bar{\nu}} + R^A_{\bar{\nu}}, \text{ for } \nu = \bar{\nu},\ 2\bar{\nu} \\ &= R^I_{o\bar{\nu}} + R^I_{o\bar{\lambda}} + R^I_{\bar{\nu}} + R^I_{\bar{\lambda}} + R^T_{\bar{\nu}} \\ &= R^A_{\bar{\nu}+\bar{\lambda}}, \text{ for } \nu = \bar{\nu} + \bar{\lambda} \end{aligned} \tag{112}$$

$$R_{o\nu} = \bar{\sigma}_o R_D - R^I_{o\bar{\nu}} - R^T_{\bar{\nu}} \quad \text{for} \quad \nu = \bar{\nu}$$

$$= \bar{\sigma}_o R_D, \text{ for } \bar{\nu} = 2\bar{\nu},\ \bar{\nu} + \bar{\lambda}. \tag{113}$$

The interested reader can read Reference (33), the Appendix and Reference (35), Sections 3 and 4 for details on the relaxation matrix elements. Here I shall confine myself to some brief comments. $R_S$ is the relaxation kernel of the self-correlation function, which is appropriate for the study of an isolated transition. Various interference terms from having closely spaced transitions result in $R_D$ which contributes to both diagonal and off-diagonal terms in the relaxation matrix. The remaining terms which are superscripted in Equations (111-3) (e.g., $R^I_o\nu$) result from energy redistribution processes where the 'I' represents intramolecular decay and the 'T' stands for intermolecular redistribution processes; the 'A' corresponds to intramolecular processes that have not been included in 'I' such as decay to an overtone or another high frequency mode. Figure 8 shows some of these processes and their grouping into active or passive exchange mechanisms. To anticipate a discussion below, the active (passive) mechanisms affect the off-diagonal (diagonal) elements of L and will be represented by $X_\nu$ ($Y_\nu$).

The pole function, $Z_0$, for the $0 \rightarrow \mu$ transition which determines the spectral properties (Eqns. (102-5)) is given by

$$Z_0 = Z_{iso} + \sum_\nu a_\nu\, \delta Z_\nu$$

$$a_\nu(T) = \exp(-\frac{E_{\nu o}}{k_B T})$$

$$\nu = \bar{\nu},\ 2\bar{\nu},\ \bar{\nu} + \bar{\lambda}. \tag{114}$$

$Z_{iso}$ is the pole of the isolated $0 \rightarrow \mu$ transition where the effects of the neighboring hotbands have not been considered, and is given by

Figure 8. This shows some of the individual transitions which in the limit of small anharmonicities contribute to the collective transition of the mode μ. Two classes of exchange mechanisms contribute to the dynamic coupling of the transitions, and can result from intermolecular energy transfer or intramolecular decay.

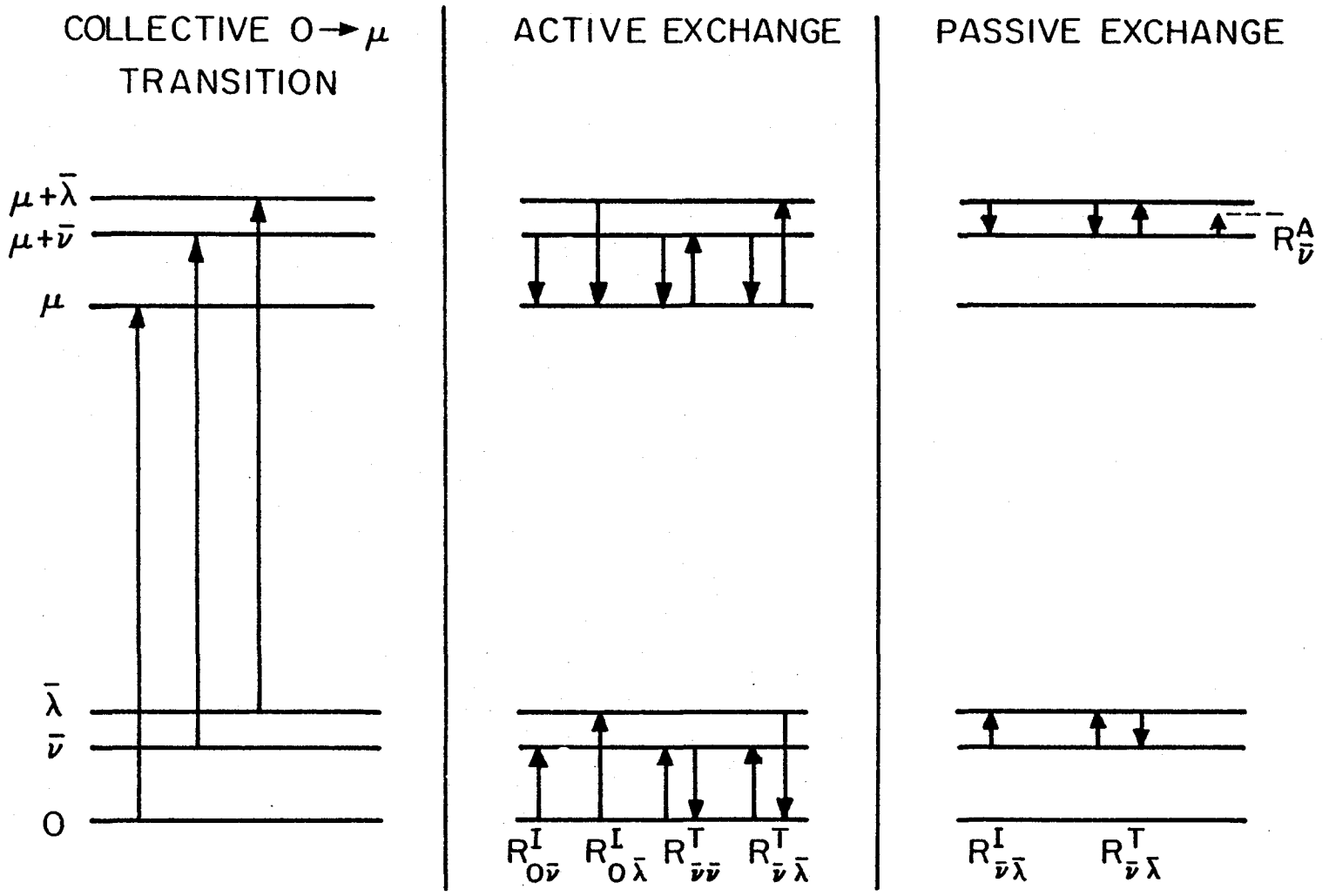
COLLECTIVE O→μ TRANSITION
ACTIVE EXCHANGE
PASSIVE EXCHANGE
μ+λ̄
μ+ν̄
μ
λ̄
ν̄
O
R^A_ν̄
R^I_Oν̄
R^I_Oλ̄
R^T_ν̄ν̄
R^T_ν̄λ̄
R^I_ν̄λ̄
R^T_ν̄λ̄

X BL 816 - 5936

$$Z_{iso} = \omega_o + \delta\Omega - iR. \tag{115}$$

The exchange parameters are given by

$$\delta Z_\nu = X_\nu Y_\nu / [X_\nu - Y_\nu] \tag{116}$$

where $X_\nu$ and $Y_\nu$ denote

$$\begin{aligned}
X_\nu &= \bar{\sigma}_o(\delta\Omega - iR_D) + iR^I_{o\nu} + iR^T_{\bar{\nu}} \quad \text{for } \nu = \bar{\nu} \\
&= \sigma_o(\delta\Omega - iR_D) \quad \text{for } \nu = 2\bar{\nu},\ \bar{\nu} + \bar{\lambda} \\
Y_\nu &= \Delta\omega_{\bar{\nu}} + \bar{\sigma}_{\bar{\nu}}(\delta\Omega - iR_D) - i(R^I_{\bar{\nu}} + R^A_{\bar{\nu}}) \text{ for } \nu = \bar{\nu} \\
&= \Delta\omega_{2\bar{\nu}} + \bar{\sigma}_{2\bar{\nu}}(\delta\Omega - iR_D) - i\Delta R_{2\bar{\nu}} \quad \text{for } \nu = 2\bar{\nu} \\
&= \Delta\omega_{\bar{\nu}+\bar{\lambda}} + \bar{\sigma}_{\bar{\nu}+\lambda}(\delta\Omega - iR_D) - i\Delta R_{\bar{\nu}+\bar{\lambda}} \quad \text{for } \nu = \bar{\nu} + \bar{\lambda}.
\end{aligned} \tag{117}$$

This mathematics yields the complex amplitude which should be substituted into Equation (106) to give the spectral function

$$A = i\bar{\sigma}_o|\alpha_o|^2\left(1 + 2\sum_{\bar{\nu},2\bar{\nu},\bar{\nu}+\bar{\lambda}} \frac{\bar{\sigma}_\nu X_\nu}{[X_\nu - Y_\nu]}\right) \tag{118}$$

The imaginary component of the amplitude which leads to a shift as well as an asymmetric lineshape, and additional broadening mechanisms are contained in the exchange terms.

Thus far the theory with the seven approximations as mentioned above gives rise to the following results. The lineshape function of the $0 \rightarrow \mu$ transition is affected by dynamic coupling to the hot bands $\nu \rightarrow \nu + \mu$ in an additive manner by the exchange term $a_\nu\ \delta Z_\nu$, which has the Arrhenius prefactor $a_\nu = \exp(-\hbar\omega_{\nu o}/k_B T)$.

To recover the selective coupling case for the HSC exchange theory, the following assumptions need to be made. First, as before it is assumed that there is only one hotband, characterized by a significant anharmonic shift, $\Delta\omega$, which affects the lineshape function. Secondly, the excitonic frequency shift, $\delta\Omega$, of the high frequency mode is neglected. Thirdly, if the anharmonic shift is sufficiently large then the interference term $R_D$ can be ignored. Fourthly, the intramolecular decay rates $R^I_{\bar{\nu}}$ $R^A_{\bar{\nu}}$ are set to zero. Thus the HSC approximations made thus far imply that Equation (117) becomes

$$X_\nu = i(R^I_{o\nu} + R^T_\nu)$$

$$Y_\nu = \Delta\omega. \tag{119}$$

The Markov approximation consists of $R_S = Re(R_S) = :(T_2')^{-1}$ and $R^I_{o\nu} + R^T_\nu = \tau^{-1}$. This yields exactly the same results as HSC theory which is Equations (41-43).

Wertheimer questions the validity of these approximations in Reference 35, and extends the HSC theory as follows. Approximations one and two (selectivity and small frequency shifts due to excitonic effects) are retained. The next three approximations are re-examined. This results in the quantities $X_\nu$ and $Y_\nu$ in Equation (119) becoming complex quantities instead of pure imaginary or pure real quantities respectively. $X_\nu$ can acquire a real component through what is called the dispersive shift of the low frequency mode $\delta\nu = Re(iR^I_{o\nu})$. In a similar manner the accounting of the decay terms gives an imaginary component to Y. Thus Equation (119) becomes

$$X = i/\tau + \delta\nu$$

$$Y = \Delta\omega + iY''. \tag{120}$$

Thus $\delta Z$ (Eqn. 116) becomes

$$\delta Z = \frac{(\delta_\nu + i/\tau)(\Delta\omega_\nu + iY''_\nu)}{(\delta_\nu - \Delta\omega_\nu) + i(1/\tau - Y'')} \tag{121}$$

Wertheimer now makes a questionable assumption. $R^I_{o\nu}$ is considered usually to be a real quantity, however, he wants to consider the following limit

$$\partial\nu =: \mathrm{Re}(iR^I_{o\nu}) > 1/\tau = \mathrm{Im}(iR^I_{o\nu} + iR^T_{\bar{\nu}}). \tag{122}$$

In this limit the exchange term is approximately

$$\delta Z = \frac{\delta_\nu \Delta\omega_\nu [(\delta_\nu - \Delta\omega) - i(1/\tau - Y'')]}{[(\delta_\nu - \Delta\omega)^2 + (1/\tau - Y'')^2]} \tag{123}$$

This yields the following values for the shift and width.

$$\text{shift} = \exp(-E_\nu/k_B T) \frac{\delta_\nu \Delta\omega_\nu (\delta_\nu - \Delta\omega)}{[(\delta_\nu - \Delta\omega)^2 + (1/\tau - Y'')^2]} \tag{124}$$

$$\text{width} = \exp(-E_\nu/k_B T) \frac{\delta_\nu \Delta\omega (1/\tau - Y'')}{[(\delta_\nu - \Delta\omega)^2 + 1/\tau - Y'')^2]} \tag{125}$$

The following points should be noted. 1) If the only temperature dependence is contained in the Arrhenius prefactor then this bears formal similarity to the HSC theory (Eqns. (42-43)) and the AO theory (Eqns. (73-74)); namely, the shift and broadening displaying the same "activation energy" which corresponds to the energy associated with a low frequency mode. 2) The maximum enhancements of the shift and broadening occurs when $\delta_\nu \lambda \Delta\omega$ (this could be the mechanism which causes selectivity) and when $1/\tau \approx Y''$ such that $|(\delta_\nu - \Delta\omega)/(1/\tau - Y'')| \sim 1$, which also represents

intermediate exchange. 3) The shift is either positive or negative depending on whether the dispersive shift is greater or smaller than the anharmonic shift. 4) $\delta\nu$ is a temperature dependent quantity, going as $1/k_BT$ at room temperature (Ref. 37).

## E. The Experimental Differentiation of Vibrational Dephasing Theories in Solids

In the three preceding sections, three different theories of vibrational dephasing applicable to polyatomic molecular solids were presented. Section B dealt with the HSC intermolecular energy exchange theory which (in the low-temperature selective coupling limit) resulted in an Arrhenius behavior for both the shift and broadening of a high frequency molecular vibration with an activation energy corresponding to the energy associated with a quantum of energy of the low-frequency mode it is coupled to (Eqns. 42-43). In a similar manner, both the AO-interacting fundamentals model (Eqns. 73-74) and the alternative model proposed as a special limiting case of the DC theory in which the 'dispersive shift' of the low frequency mode as well as the intramolecular decay of the low frequency mode are considered (Eqns. 124-125) results in a similar Arrhenius behavior. It should be emphasized that these theories are based on very different physical mechanisms and therefore accord a very different interpretation of the quantities which multiply the temperature dependent Arrhenius function. So as it stands, the observation of an Arrhenius behavior for the frequency shift and broadening of a high frequency vibration gives hope equally to the validity of these three theories (or perhaps others not yet proposed). Table 2 points out the meaning of some of the parameters which appear in the theories for a quick comparison. Note that a major difference

Table 2. Vibrational Dephasing Models (Selective Coupling Limit)

| | HSC | AO | DC |
|---|---|---|---|
| Temperature Dependence | Width $\alpha \exp(-\beta \omega)$. Shift $\alpha \exp(-\beta \omega)$. $\omega$ is frequency of the coupled low-frequency mode. | Same as HSC. | Very complicated, but approximately exponential as in HSC. |
| Coupling | Results from anharmonic shift; dominant term is of the general form $Q_A^2 Q_L^2$; suggests steric interaction. | Results from anharmonic term of form $Q_L^2 Q_A Q_B$; represents exchange between modes A and B induced by the low-frequency mode. | Results from accidental near-equality of dispersive shift and anharmonic shift. |
| Frequency Shift $\delta\omega$ | $\delta\omega$ is anharmonic shift of combination level; may be of either sign. | $\delta\omega$ is spacing between two adjacent fundamentals; they must shift together with increasing temperature. | Results from difference between dispersive and anharmonic shifts; may have either sign. |
| Time Parameter $\tau$ | $\tau$ is resident lifetime on a single molecule of a low-frequency vibrational excitation. | $\tau$ is bath correlation time for anharmonic force constant $F_{LLAB}$. | Decay rates for exciton transfer processes are included; '$\tau$' assumes complex values. |

between the theories is concerned with the meaning of '$\tau$'; in HSC theory all that is required of $\tau$ is that it represents the inverse of the rate (Markoff approximation) of decay from a given molecule-so both intramolecular decay as well as resonant energy transfer is included. Another major difference between the models is the mechanism for coupling. An analysis based on perturbation theory suggests that within the framework of the HSC model the dominant anharmonic term is $Q_L^2 Q_A^2$ -a quantity which can be interpreted as the root mean square overlap or a steric interaction between the modes. In the AO model the coupling results when there exists a fluctuating force which couples the low mode to the two fundamentals such as $Q_L^2 Q_A Q_B$, which as Equation (69) indicates induce an exchange of the excitation between the two modes A and B. The mechanism of coupling in the DC theory is based on an accidental near degeneracy between the anharmonic shift, $\delta\omega$, and the dispersive shift, $\delta\nu$.

Figure 9 shows the qualitative differences which are expected in the various theories. Note that a major difference between the HSC theory and the AO theory is concerned with adjacent peaks; in the HSC case peaks can shift and broaden independent of each other, in the AO case the peaks shift toward each other with increasing temperature.

In order to quantitatively assess the relative validity of these theories a more detailed study than simply obtaining and analyzing the temperature-dependent spectra associated with the vibrations of a molecular crystal. The reason being that all the theories predict essentially the same temperature behavior; however, there are slight differences such as whether the shift divided by the broadening is a temperature independent quantity. Figure 10 indicates the other spectral

Figure 9. The three models of vibrational dephasing discussed in the text are illustrated with respect to their qualitative differences that can arise as a function of temperature.

# A COMPARISON OF VIBRATIONAL DEPHASING MODELS

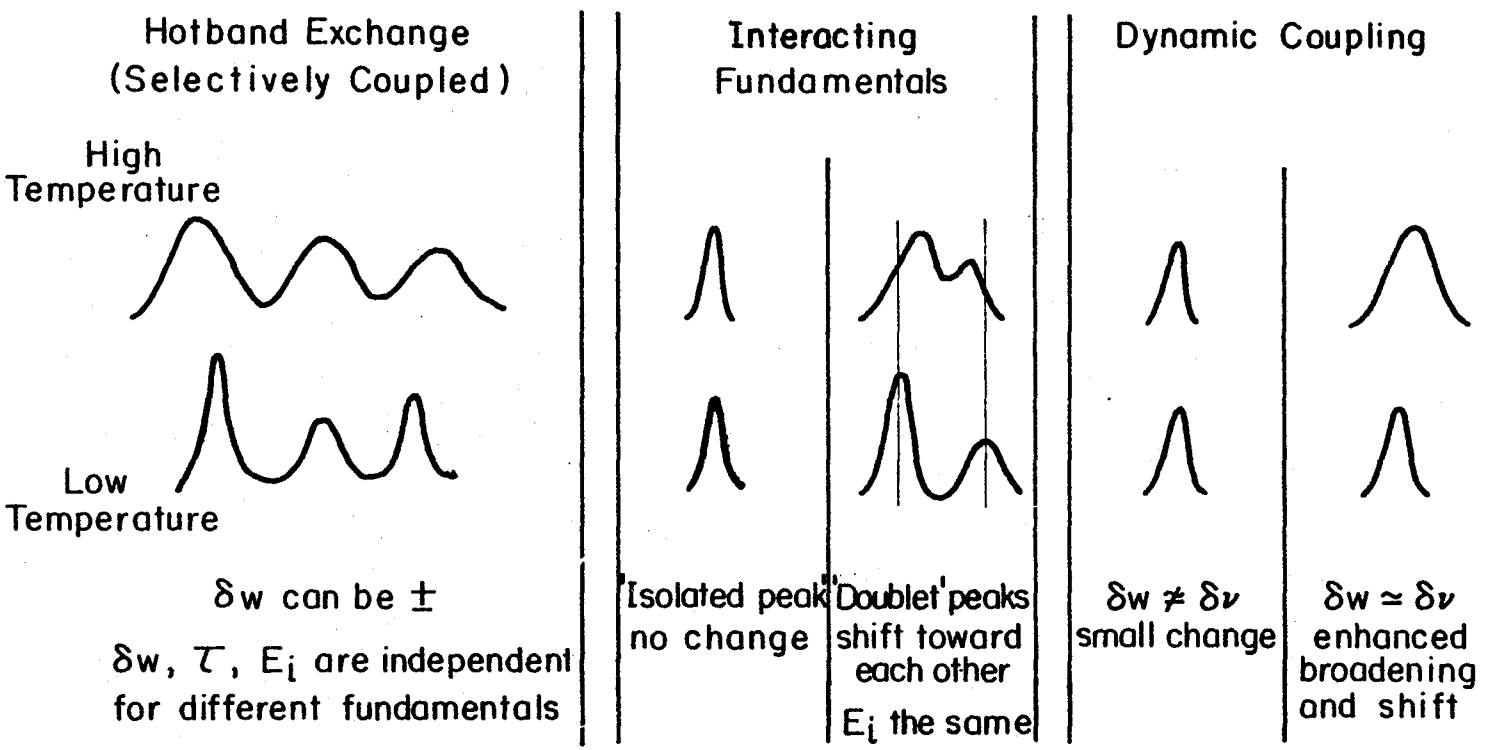


XBL7912-5479

Figure 10. This indicates the relevant spectral regions of a molecular solid. The fundamental region is studied to extract out the parameters which govern the exchange process. The predicted energy of a low-frequency mode should match an energy of a mode in the low-frequency region. A main differentiation between the theories occurs for the predicted existence and position of the combination bands.

# SPECTROSCOPY OF ANHARMONICALLY COUPLED VIBRATIONAL OSCILLATORS

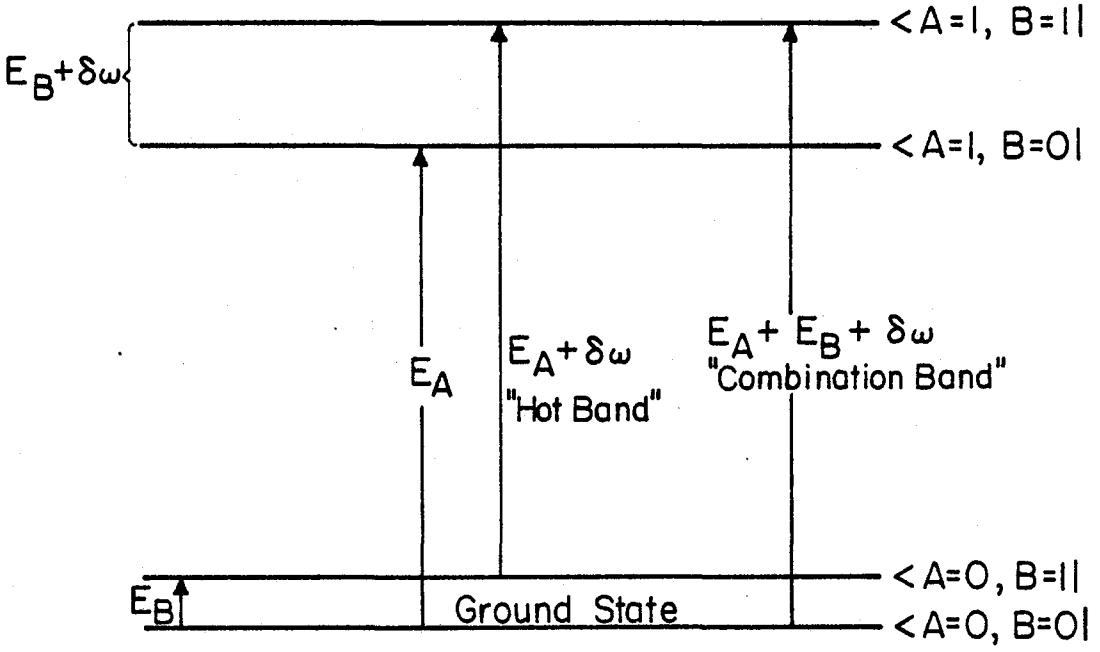


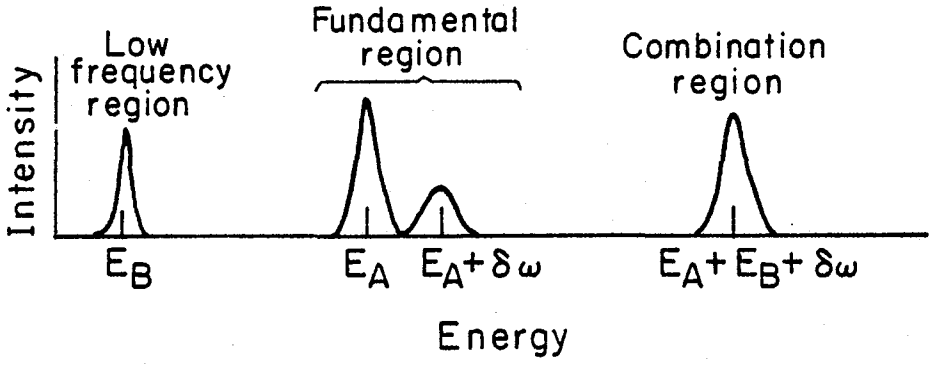


XBL7912-5467

regions where useful information may also be found. First, all three models (in their selective coupling limit) predict the positions of the low-frequency mode. Only HSC theory gives an upper bound on its linewidth. We shall see that the interpretation (in HSC theory) of $\tau$ is that of the residence lifetime, the shortest lifetime of the low-frequency excitation should be $\tau$. If it can travel from molecule to molecule with some retention of phase memory then its dephasing time will be longer than the residence lifetime, $\tau$. By comparing the lifetime extracted from exchange theory to that obtained by a direct analysis of the low-frequency mode, additional dynamical information should be gained.

Figure 10 also indicates the possibility of observing combination bands. Since in the HSC theory there exists a strong anharmonic coupling between the high and low frequency modes which manifests itself through the anharmonic shift $\delta\omega$, some oscillator strength should be given to the simultaneous transition of the low and high frequency modes. This transition should occur at the sum of the energies of the low-frequency mode and the high frequency mode plus the anharmonic shift. Thus the appearance of these peaks at approximately the predicted positions is collaborative evidence for the HSC theory and the DC theory. The anharmonic shifts for DC theory should be about 6 to +10 $cm^{-1}$[35], whereas the anharmonic shifts for HSC theory are the extracted values and can be either positive or negative. Therefore, if HSC theory predicts a negative anharmonic shift and a combination band is observed which definitely is positioned at less than the sum of the high and low-frequency modes the HSC theory has gained an excellent piece of collaborative evidence.

Another technique at our disposal involves isotopic dilution. That is, additional information can be obtained by analyzing the temperature dependent high-frequency spectrum as a function of isotopic composition. Table 3 summarizes the changes which are expected to occur in the various models. In the theory of interacting fundamentals (AO) virtually no change should be observed. The reason for this is that in the case of both the high and low-frequency modes being intramolecular and residing on the same molecule (an assumption adopted for now for all three models, but removed in a special case in the next chapter) the parameters experience negligible change. $\delta\omega$ which is the spacing between the two fundamentals which are interacting via the AO mechanism should be the same except for perhaps extremely small differences in the crystal shift (change in the frequency from gas phase transitions) in the different isotopic environments. Such differences were not observed for the $T = 0°K$ positions of the peaks of $d_{14}$-durene diluted in $h_{14}$-durene. The strength of the coupling, being an intramolecular mechanism does not change. The activation energy should stay the same because the energy of the low frequency mode is constant. Finally in the AO model the time parameter, $\tau$, should be roughly a constant with isotopic dilution because it arises from stochastic motions of the bath.

Some specific changes might arise in the HSC theory as a function of isotopic concentration and provide an important conformation as well as an opportunity to probe the vibrational dynamics in greater detail. Again in the case of intramolecular modes on the same molecule, the activation energy for the temperature dependence should remain the same as should the anharmonic frequency shift, $\delta\omega$. What can change is the residence lifetime, $\tau$. As will be detailed in the next chapter there are

Table 3. Variation of Parameters with Isotopic Dilution

| Parameter | HSC | AO | DC (If $\delta\Omega, R_D, R_\nu^T, R_\nu^A$ Significant) | DC (Alternative Theory) |
|---|---|---|---|---|
| $\delta\omega$ | No change | No change | Change upon shift to new resonance | No change |
| $E_i$ | No change | No change | Change upon shift to new resonance | No change |
| $\tau$ | No change- or increase | No change | Change upon shift to new resonance, also may lengthen | No change- or lengthening |

two contributions to the residence lifetime. First is decay into the lattice which is weakly dependent on isotopic concentration, the second mechanism is resonant energy transfer to the surrounding molecules which is highly dependent on the isotopic concentration. Thus we expect to see if the HSC model is valid as a predominant dephasing mechanism the parameters governing exchange remain constant with dilution- except for the time constant which should either remain the same or lengthen.

Isotopic dilution allows a test of specific areas of the dynamic coupling (DC) model. A significant value for any of the following parameters will cause changes in the observed temperature dependence of apparent '$\delta\omega$', and apparent '$\tau$': $\delta\Omega$(the excitonic shift associated with the high-frequency mode), a contribution to the collective mode interference relaxation matrix, $R_D$, due to interferences between resonant modes on neighboring molecules, and a contribution to the relaxation matrix due to intermolecular energy transfer ($R_\nu^T$ and appropriate terms in $R_\nu^A$). Thus a constancy in, for example, the activation energy can lead to the conclusion that those terms are unimportant and not required to describe the dynamical processes which affect the high-frequency vibration. Even though the important quantity $\delta\nu$ is given the name dispersive shift it is only weakly dependent on temperature. In a similar manner the anharmonic shift, $\delta\omega$, can be expected to remain a constant. An important parameter which can be expected to change is $\tau$, the time the low-frequency excitation resides on a given molecule. The reasons for the concentration dependence of $\tau$ are the same as in the HSC case but would manifest itself somewhat more complicatedly on the lineshape function than in that case. In the alternative model proposed by Wertheimer (Eqns. (124-5)) in which $\delta\Omega$, $R_D$, and $R^A$ is ignored but the excitonic dispersive shift of the low-frequency mode is significant,

the linewidth goes approximately as $1/\tau$. In the HSC case the linewidth goes approximately as $\tau$. Because of resonant energy transfer effects as our sample becomes progressively more dilute $\tau$ should lengthen, thus in the HSC case the linewidth broadening should be enhanced relative to the frequency shift, whereas in the DC case the broadening should be less.

Let us now consider what we expect to observe if the concentration and temperature dependent data is analyzed in terms of HSC exchange theory (Eqn. (36)) for the cases where the predominate mechanism is 1) HSC theory, 2) AO model, 3) DC model. In the HSC model $E_i$, and $\delta\omega$ should remain constant with dilution; but $\tau$ should remain the same or increase depending on the effect of intermolecular energy transfer. If the AO model is applicable and the data were to be analyzed in terms of HSC exchange theory then none of the (falsely) extracted parameters would be expected to change with dilution: $E_i$, '$\tau$', and '$\delta\omega$' (the quotes indicate a misinterpreted value). If the DC model with sufficiently large values of $\delta\Omega$, and intermolecular components of $R_D$ and $R^T$ is applicable the HSC model would extract out changing values for $E_i$, '$\delta\omega$' and '$\tau$' as the sample became more dilute. If $\delta\Omega$, $R_D$, and $R^T$ are neglected what HSC analysis would show is that $E_i$ would remain a constant, '$\delta\omega$' would be approximately a constant but <u>'$\tau$' would appear to remain the same or get shorter with dilution</u>. Thus the isotopic dilution data analyzed in terms of HSC theory provides a test of these three models. This is summarized in Table 4.

Table 5 summarizes the temperature dependence of the ratio of the temperature part of the broadening to the temperature dependent shift. Note that both the HSC model and the AO model predict a very weak dependence on the temperature. However, the DC model gives a strong

Table 4. Apparent Changes with Isotopic Dilution in Parameters of Various Dephasing Theories if Analyzed According to HSC Model

| Parameter | Theory HSC | Theory AO | DC with $R_D, \delta\Omega, \tau$ | DC Only Concentration Dependent $\tau$ |
|---|---|---|---|---|
| $E_i$ | Remain Constant | Remain Constant | Vary | Remain Constant |
| $\delta\omega$ | Remain Constant | Remain Constant | Vary | Remain Constant |
| $\tau$ | Stay the same or increase | Remain Constant | Vary | Stay the same or Decrease |

Table 5. Ratio of Temperature Dependent Broadening to Shift of the Various Dephasing Theories (Selectively Coupled) at a Given Concentration

| | HSC | AO | DC |
|---|---|---|---|
| Ratio | $\delta\omega\tau$ | $\frac{1}{\delta\omega\tau}$ | $\frac{(1/\tau-Y'')}{(\partial\nu-\Delta\omega)}$ |
| Interpretation | Anharmonic shift times residence lifetime | Inverse of splitting frequency times Bath Correlation time | Ratio of "enhancement" factors |
| Temperature Dependence | Weak-depends slight on $\tau$ | Weak-depends slight on $\tau$ | Strong-$\delta\nu$ goes as $k_BT$ at room temperature; weak dependence on $\tau$ |

temperature dependence because the shift is proportional to $(\delta\nu - \Delta\omega)$ and could conceivably start out negative and turn positive as $\delta\nu$ is proportional to $k_B T$ at room temperature.

# Chapter III

## RESULTS AND DISCUSSION ON THE DURENE SYSTEM

### A. Experimental

Durene (1,2,4,5 tetramethylbenzene) was the system chosen as a test of the various theories described in Chapter II. The reasons are partially historical. Robert Shelby and Paul Cornelius, in our research group, studied pure $h_{14}$-durene[13,14] and published their results. A major discrepancy appeared on the interpretation of $\tau$. The authors in developing the theory decided that it is the lifetime of low-frequency mode which is coupled to the high-frequency mode. Abbott and Oxtoby[24] pointed out that the $\tau$'s extracted by HSC theory are shorter than the lifetime of the low-frequency mode than that obtained by a direct spectroscopic analysis of the linewidth of the low-frequency mode. They then proposed an alternative model to HSC, namely the interaction fundamentals or AO model which was described in Chapter II, Section C. As Eqns. (73,74) point out because of the unknown value of A, it is impossible to separately extract out the values for $\delta\omega$ (the difference frequency between two fundamentals) and $\tau$ (the bath correlation time); however, the activation energy associated with the low-frequency mode may be obtained. In the fortunate case of an isolated doublet in which it is observed that the two fundamentals are shifting toward each other with an activation energy of a low-frequency mode, then the value of zero-temperature frequency splitting may be substituted in for $\delta\omega$. Since the ratio of the temperature dependent frequency shift to the temperature dependent broadening is $\delta\omega\tau$, the value of $\tau$, the bath correlation time, may be inferred. Thus in this fortunate case of an isolated doublet the

low-frequency mode which induces the coupling, and the bath correlation time can be extracted from the data as can the quantities A and B in Eqns. (73-74) which represent the magnitudes of the forces coupling the two modes together. However, to anticipate results in this present work, an isolated doublet obeying the predictions of the AO model was never seen and to the best knowledge of the author no other laboratory has of yet seen this experimental evidence. Also, see pages 125-128.

Another model which was advanced as an alternative to the HSC model is that proposed by Wertheimer and discussed in this work (Chapter III, Section D). It also gets around the problem of the HSC discrepancy with $\tau$ by introducing the excitonic dispersive shift, $\delta\nu$, and an imaginary component of some relaxation terms Y". This, as Eqns. (124-125) shows, causes an enhancement of the shift and broadening particularly when $\partial\nu$ and $\Delta\omega$ are almost (but not exactly) in resonance. Because of the additional number of parameters, the temperature dependent data will not suffice to allow a meaningful extraction of the parameters without independent supporting data such as anharmonicities or lifetimes.

The system which I chose to be a test of the relative test of the theories was $d_{14}$-durene. It is a solid which crystallizes nicely and has a Raman spectrum which is mainly polarized-thus as per the discussion of Chapter II, Section A the effects of orientation as opposed to vibration are neglected. The samples which I studied were of the following compositions: 100% $d_{14}$ durene, 50% $d_{14}$/50% $h_{14}$, 25% $d_{14}$/75% $h_{14}$, 10% $d_{14}$/90% $h_{14}$. They were prepared using zone-refined $h_{14}$-durene and, due to its expense, recrystallized $d_{14}$. The appropriate amount of material was weighed out to give a molar percent error of $\pm$1%, mixed and recrystallized from spectral grade hot methanol. The resulting material was

usually very polycrystalline which has the advantage of resulting in an orientationally averaged spectrum which is consistent from day to day and from sample to sample. The material was placed in a pyrex tube sealed at one end, subjected to five freeze/thaw cycles on a vacuum line, then sealed at the other. This capsule was placed in a copper holder where thermal contact was ensured by a combination of indium and vacuum grease. The samples were put in an Air products portable helium refrigerator/dewar in which the temperature could be varied from 10°K to room temperature and stabilized to within 1°K. The temperature was determined by a digital voltmeter which measured the potential between two Chromel verses Gold thermocouple junctions- one mounted inside a copper block where the copper sample holder is mounted on the other junction is the reference (ice water). This allowed a determination of the temperature to within 1°K except at the coldest temperature in which the error was 4°K. The same temperatures were used from sample to sample in order to avoid systematic errors: 10, 45, 90, 125, 150, 175, 225, 250, 275, and 298°K. Thus there is added confidence in trends with isotopic composition.

The parallel polarized component of the right angle Raman scattered light was collected using a Coherent CR2 Argon Ion Laser in conjunction with a Jobin-Yvon Ramanor H625 Raman spectrophotometer and Princeton Applied Research phototube. As mentioned in Section A of the last chapter, the ratio of perpendicularly polarized to the parallel polarized scattered light was at most 8 to 10%, where 3% is due to depolarization of the laser, depolarization by the pyrex and errors in the polarization filters. Because the spectra within the noise errors appeared to be the same whether it was polarized parallel or perpendicular as far as peak

position and full widths are concerned, it was decided that the parallel component would suffice as being the same as the isotropic spectra. Resolution was slightly better than 1.0 $cm^{-1}$ and adequate for this work. Two spectral regions were studied; the region of the C-D stretch and the low-frequency region from 50 to 300 $cm^{-1}$. In the work on pure $h_{14}$-durene which preceded me, the spectral regions were the C-H stretch and the low-frequency region. The region of the combination bands (Fig. 10) was attempted by Raman spectroscopy without success, but finally achieved by Fourier Transform Infrared Spectroscopy (FTIR). The Raman spectra were collected onto a strip chart recorder and then digitized using a Tektronics 4662 Digital Plotter in conjunction with a LSI-11 Minicomputer, typically collecting 20 points per lineshape. In the case of bands which overlapped by room temperature, a lineshape least squares analysis was done. The best fits to a Lorentzian full-width and position were obtained. These numbers were then input for a given peak at a given concentration for the entire temperature range into a least squares fitting routine which fit these values to the exchange parameters yielding the temperature dependent lineshape function which gives the best fits when the lineshape function is least squares fit to its best Lorentzian. This procedure is identical to that followed in the case of $h_{14}$-(durene), thus a meaningful comparison may be made between the results on $h_{14}$ and $d_{14}$. The extracted parameters are: $T_2'$, $\delta\omega$, $E_i$, $\omega_0$, and $\tau$, whose meanings have been described in Chapter II, Section B.

B. Pure Molecular Solids

In this section the results of an exchange analysis of the pure solids of $h_{14}$-durene which was done previously as well as my work on $d_{14}$-durene are presented. When appropriate the abbreviation $h_{14}$ ($d_{14}$)

in place of the more cumbersome $h_{14}$ ($d_{14}$)-durene will be adopted. Figure 11 shows the Raman spectrum of $d_{14}$-durene at three different temperatures. Note that the shifts and broadening are very real effects which are apparent to the naked eye. Thus an analysis in terms of the theories discussed in Chapter II can be undertaken. The spectrum of $h_{14}$ (not shown) also manifests a marked temperature dependence. It will be shown what can be learned in the case of these pure isotopic solids and why mixed solids are necessary to be studied.

An analysis based on computerized least squares fitting to the full lineshape of HSC theory (Eqn. (19)) according to the procedure outlined in the last section results in the values for the parameters given in Tables 6 and 7. As discussed in Chapter II the validity of some of these parameters depends in turn on the validity of the HSC mechanism, but an analysis based on the HSC model can be used to ascertain the applicability of the various models. All three models (in their selective coupling limits) predict that there should be a match between the HSC extracted "activation energies" and the energy associated with a low-frequency motion of the system. Note that for the two molecules, for 11 out of 12 cases there appears to be a good match with their energies of a low-frequency mode (in 2 out of those 11 cases the low-frequency mode appears to be the energy which corresponds to the energy of a Raman-inactive combination band of 116 $cm^{-1}$ torsion with an 83.5 $cm^{-1}$ libration[42]).

Another piece of information that we are able to learn from the isotopically pure sample is an example which is in serious disagreement with the AO theory. Figure 12 displays in greater detail two bands in the C-D stretching spectrum of $d_{14}$-durene (Fig. 11). Note that in direct contradiction to the predictions of AO theory these two modes shift apart

Figure 11. This indicates the striking shifts and broadening which occurs as the temperature is raised in the case of pure crystals of $d_{14}$-durene. Similar behavior has been seen in $h_{14}$-durene and in p-xylene. Typically ten temperatures were taken at a given concentration and the data was computer analyzed in terms of the HSC model.

RAMAN SPECTRA OF $d_{14}$-DURENE C-D STRETCH REGION

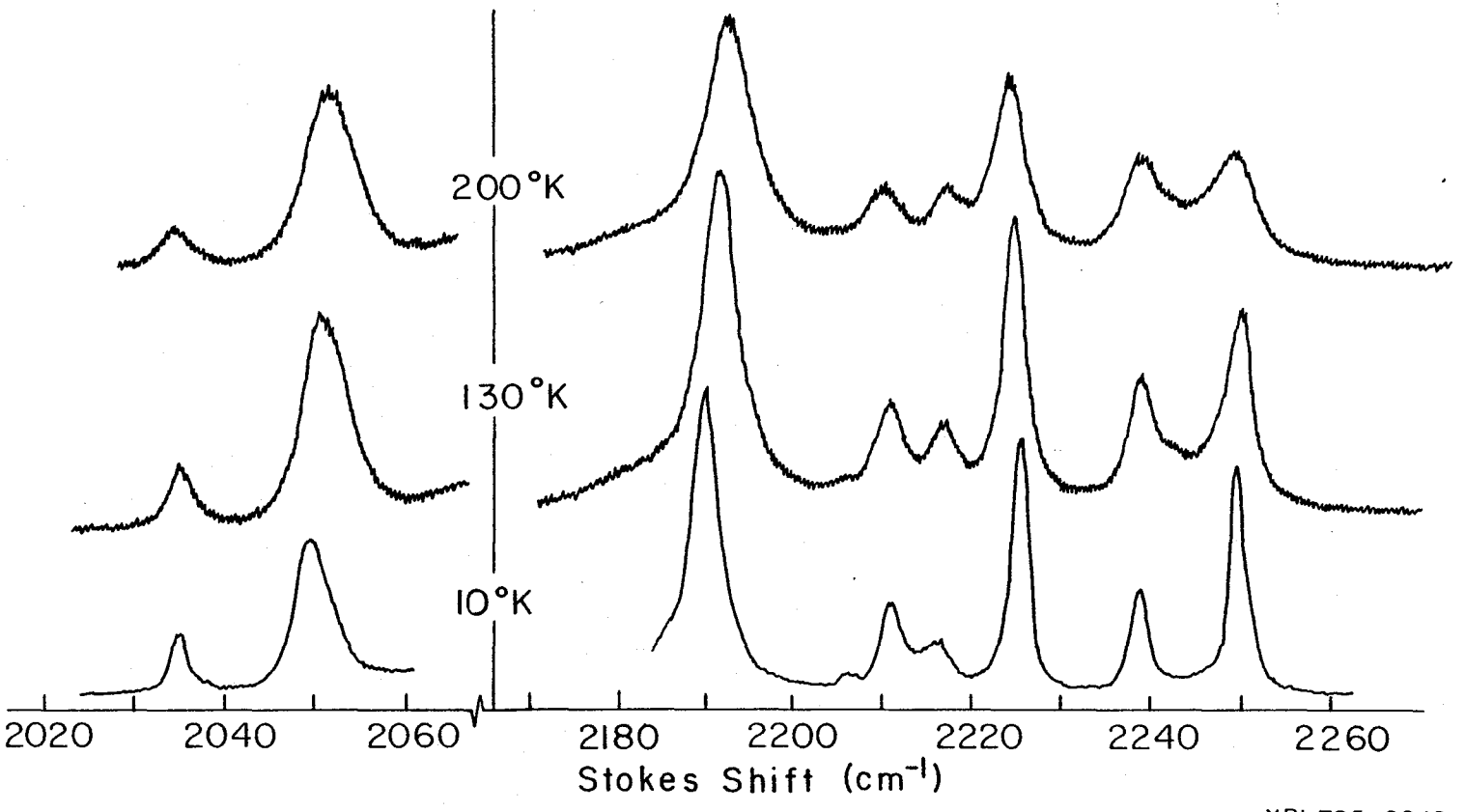


XBL795-6249

Table 6. Parameters Obtained from Least-squares Analysis of Temperature-dependent Lineshape Data for $h_{14}$-durene

| | Raman Active C-H Stretch | | Low Frequency Dephasing Channels | | | |
|---|---|---|---|---|---|---|
| | $\omega_o(cm^{-1})$ | Mode | Dephasing Mode | $\varepsilon_i(cm^{-1})$ | $\delta\omega(cm^{-1})$ | $\tau$(ps) |
| a | 2929.0 | $A_g$, $B_{1g}$ | $B_{3g}$ - Torsion | 194 ± 10 | +13.6 | 0.36 |
| b | 2957.7 | $A_g$, $B_{1g}$ | $A_g$ - Methyl Rock* | 229 ± 21 | + 10.5 | 0.86 |
| c | 2970.3 | | | 265 ± 06 | -24.2 | 0.19 |
| d | 2987.3 | $B_{2g}$, $B_{3g}$ | $B_{3g}$, $B_{2g}$ Out-of-plane Methyl Bend | 341 ± 13 | -20.6 | 0.25 |
| e | 3027.5 | $A_g$ | $B_{1g}$ - Methyl Rock* | 263 ± 19 | -21.2 | 0.36 |

* Symmetry of Methyl Rock deduced on the basis of comparison to analysis of data obtained on $d_{14}$-durene, see text for discussion.

Table 7. Exchange Parameters in $d_{14}$-durene

| $\omega_o(cm^{-1})$ | $E_i(cm^{-1})$ | Coupled low-frequency mode[e] | $\delta\omega(cm^{-1})$ | $\tau$(psec) | $\tau_{rel}$[a] | <n> |
|---|---|---|---|---|---|---|
| 2035.4 | 252 ± 10 | $B_{1g}$ methyl rock | -12.0 ± .5 | .66 ± .03 | 2.65 | 4.02 |
| 2049.9 | 190 ± 12 | Inactive combination band[b] | 8.8 ± .4 | .77 ± .06 | c | c |
| 2191.1 | 240 ± 20 | $A_g$ methyl rock | 19.5 ± 1.0 | .30 ± .06 | 2.65 | 8.83 |
| 2211.6 | 200 ± 10 | Inactive combination band[b] | -11.4 ± .6 | .45 ± .05 | c | c |
| 2225.9 | 240 ± 15 | $A_g$ methyl rock | -16.1 ± .7 | .36 ± .07 | 2.65 | 7.36 |
| 2250.1[d] | 105 ± 10 | | - 4.9 ± .3 | 3.1 ± .3 | 4.42 | 1.43 |
| 2238.9[d] | 90 ± 15 | | - 5.6 ± .2 | 4.3 ± .2 | 2.52 | 0.59 |

[a] Calculated from the observed FWHM of the low-frequency Raman spectrum, using $\tau = 1/\pi c(FWHM)$.

[b] A frequency of approximately 200 $cm^{-1}$ is expected from a combination of the torsional mode at 116 $cm^{-1}$ and a libration at 83.5 $cm^{-1}$.[42,43]

[c] The linewidth for the coupled, Raman-inactive combination band is not available.

[d] An additional source of error is present in these modes since the lineshapes overlap at higher temperatures.

[e] The low-frequency vibrational spectrum of $d_{14}$-durene consists of a methyl rock at 240 $cm^{-1}$, torsions at 116 $cm^{-1}$ and 140 $cm^{-1}$, and librations at 83.5 $cm^{-1}$ and 105 $cm^{-1}$.[42,43]

Figure 12. An "isolated doublet" which could serve as a test of the AO theory; contrary to the predictions of that theory the peaks shift away from each other as the temperature increases. The results indicated here are consistent with HSC theory and other corroborative evidence.

Raman Spectra of 'Isolated Pair' of Peaks
in $d_{14}$ - Durene

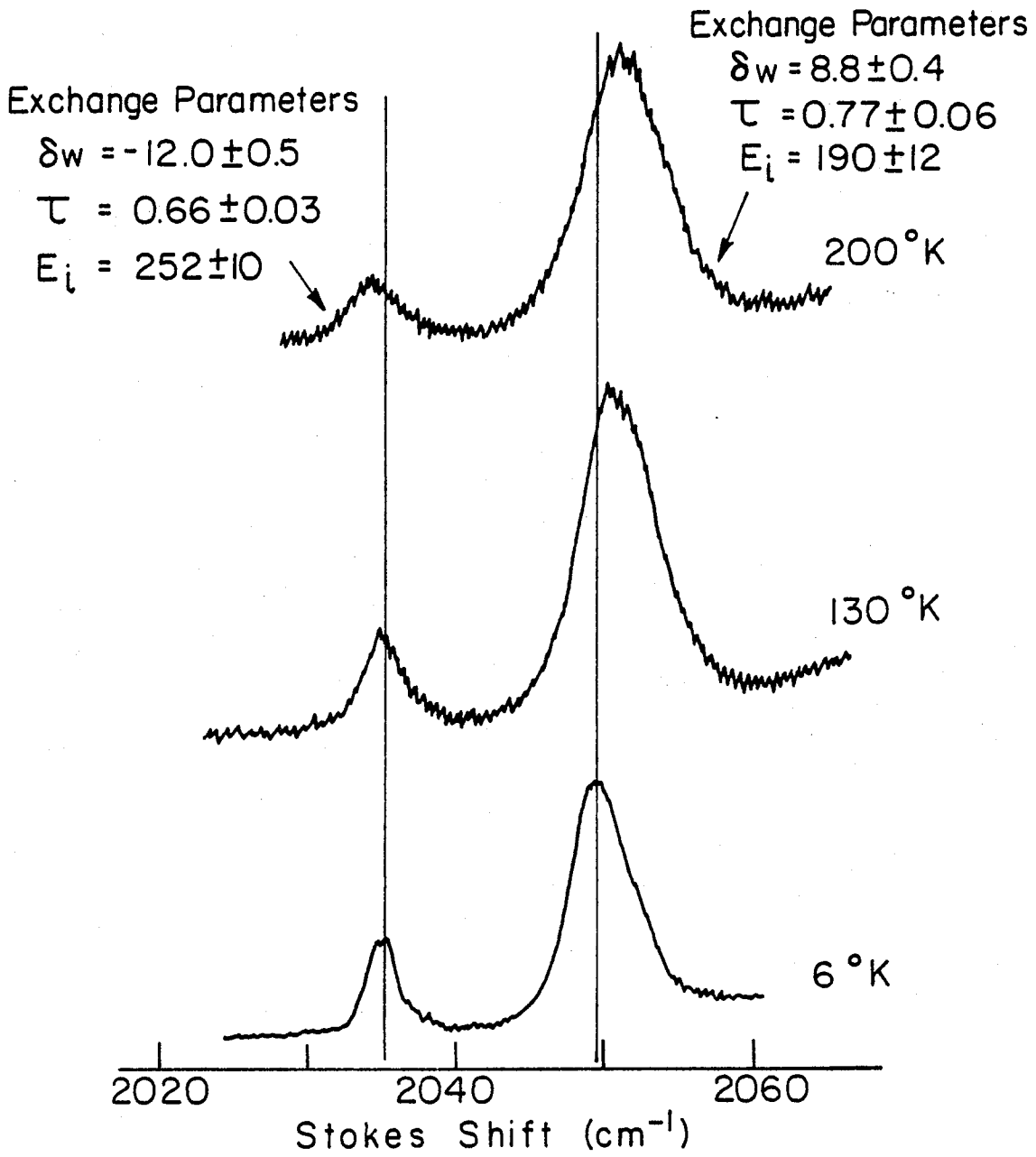


XBL7912-5432

from each other with increasing temperature. These peaks also meet the criterion for being "isolated". There are no other peaks within 800 $cm^{-1}$ on the low-frequency side in either the Raman or infrared spectrum, so that in particular the resonance at 2035 $cm^{-1}$ should shift toward higher frequencies in the AO model. However, it clearly shifts toward lower frequencies and does so with an excellent fit to the HSC model with an extracted value of the parameter of $E_i$ which corresponds to the $B_{1g}$ low-frequency methyl rock motion. Also as we shall see this mode satisfies the HSC model prediction of a temperature independent value of the ratio of the linebroadening to the line-shift, as well as excellent agreement with the FTIR predicted combination band and a very interesting isotopic dilution behavior which is consistent only with the HSC model. The other peak 2050 $cm^{-1}$ does have some other diffuse peaks about 50 $cm^{-1}$ higher in energy nearby in the Raman and one at 2060 $cm^{-1}$ in the infrared but the HSC model accounts for these peaks adequately. Given the form of the potential which in the AO model couples the two fundamentals together (Eqn. (44)) it becomes possible to couple an infrared mode to a Raman active mode. Note that durene possesses an inversion center consistent with the molecule having point group symmetry $D_{2h}$, assuming that the methyl groups have either arranged the protons in such a way to preserve the inversion center or that the methyl groups are structureless "atoms" (which would be the case if the methyl groups rotate on a time scale faster than the dephasing time of the C-D stretches). The crystal structure is such that the inversion center is maintained in the solid. Thus as Eqn. (44) indicates the AO potential is of the form:

$$V_c = F_{AB}(t)\, Q_A Q_B + F_{iiAB}(t)\, Q_i^2 Q_A Q_B \qquad (126)$$

where A and B represent the high-frequency modes coupled together and the low-frequency mode is i. $V_c$ should possess the symmetry of the system and in particular it should remain unchanged by the application of the inversion operation. Whether mode i is Raman or infrared active, $Q_i^2$ is totally symmetric. Assuming that one mode of A and B is Raman active and the other is infrared active, then the product $Q_A Q_B$ is antisymmetric with respect to the inversion center. Thus the part of the force which can couple a Raman to an infrared mode is the antisymmetric part of the F's. Given this molecular system and this form of the AO coupling potential and roughly equal magnitudes for the symmetric and antisymmetric parts of the stochastic force, F, then we conclude that the coupling of a Raman active transition should be with either Raman or infrared active transitions. Thus the peak at 2250 $cm^{-1}$ should be coupled to the peak at 2235 $cm^{-1}$ (Raman) or to the peak at 2260 $cm^{-1}$ (infrared) so nothing definite can be said concerning this peak in the context of the AO model. Other peaks suffer from this possibility of coupling to infrared modes.

As discussed in Chapter II, a quantity which is useful to monitor as a function of temperature is the ratio of the linebroadening to the frequency shift. This quantity assumes the value in HSC theory of $\delta\omega\tau$. Figures 13a and 13b display this for both forms of durene in their pure isotopic forms. In Figure 13b the peak at 2238.9 was not displayed because it behaves very similarly to the peak at 2250.1. Note that the ratio of the broadening to the shift is <u>not</u> a temperature independent constant for these two modes. This can be explained within the context of any of the three theories by relaxing the condition of selectivity in coupling - that is, the high-frequency stretch may be coupled to more than

Figures 13a and 13b. The ratio of the temperature dependent part of the line broadening to the temperature dependent part of the Raman shift is plotted verses temperature for $h_{14}$- and $d_{14}$-durene. HSC and AO theories predict that this ratio will be a constant in the selectively coupled limit.

RATIO OF THE TEMPERATURE DEPENDENT PORTION OF THE LINEWIDTH AND FREQUENCY SHIFT IN THE RAMAN TRANSITIONS OF TETRAMETHYLBENZENE (DURENE)

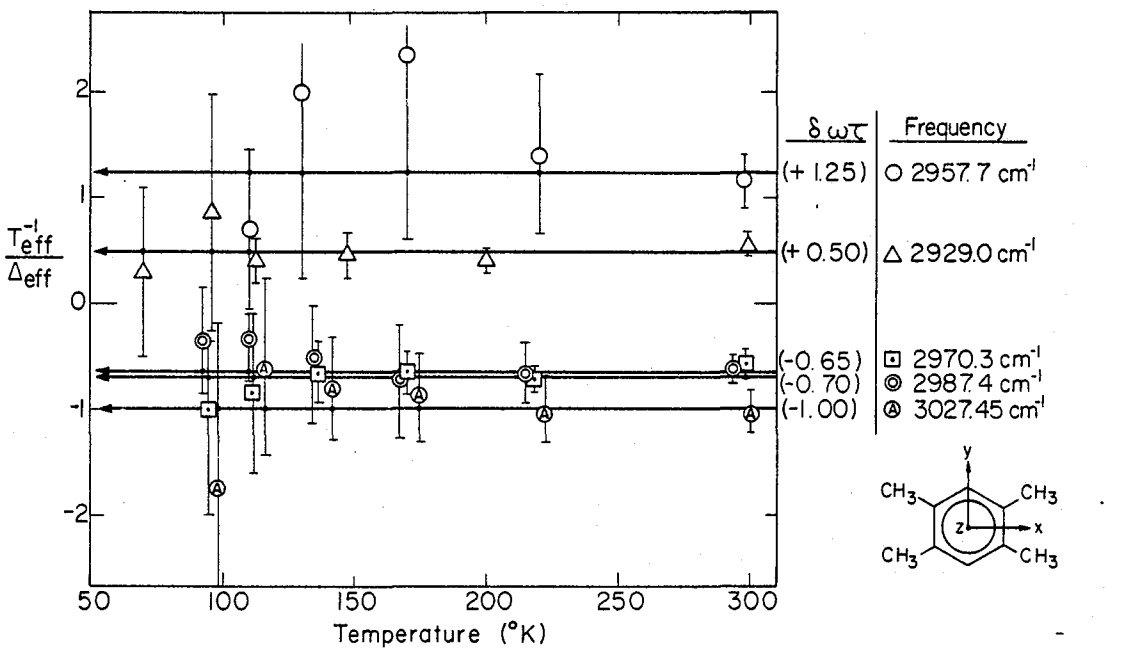


XBL777-5840A

RATIO OF THE TEMPERATURE DEPENDENT PART OF THE LINEWIDTH AND FREQUENCY SHIFT IN THE RAMAN TRANSITIONS OF d14-DURENE

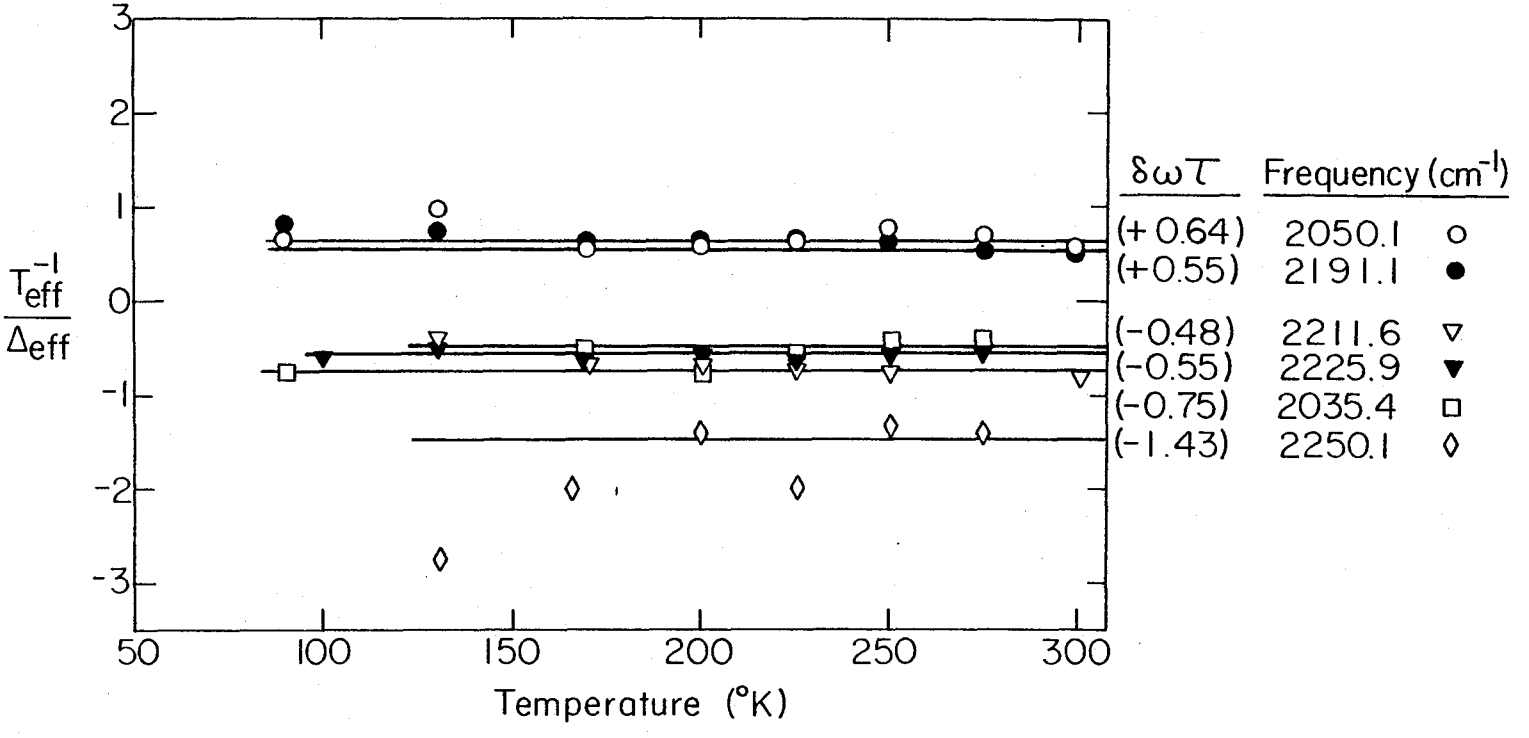


XBL7911-7281

one low frequency mode. A simple extension of HSC theory, for example, would result in the following form for the low-temperature limit for the lineshape function (see Appendix I)

$$\omega_{eff} = \omega_o + \frac{\delta\omega_1[\exp(-E_1/kT)]}{1+(\delta\omega_1)^2\tau_1^2} + \frac{\delta\omega_2[\exp(-E_2/kT)]}{1+(\delta\omega_2)^2\tau_2^2} \tag{127}$$

$$(T_{2eff})^{-1} = (T_2')^{-1} + \frac{(\delta\omega_1)^2\tau_1[\exp(-E_1/kT)]}{1+(\delta\omega_1)^2\tau_1^2} + \frac{(\delta\omega_2)^2\tau_2[\exp(-E_2/kT)]}{1+(\delta\omega_2)^2\tau_2^2} \tag{128}$$

This results in the following ratio of the broadening to the shift

$$\text{"}\delta\omega\tau\text{"} = \frac{\dfrac{(\delta\omega_1)^2\tau_1[\exp(-E_1/kT)]}{1+(\delta\omega_1)^2\tau_1^2} + \dfrac{(\delta\omega_2)^2\tau_2[\exp(-E_2/kT)]}{1+(\delta\omega_2)^2\tau_2^2}}{\dfrac{\delta\omega_1[\exp(-E_1/kT)]}{1+(\delta\omega_1)^2\tau_1^2} + \dfrac{\delta\omega_2[\exp(-E_2/kT)]}{1+(\delta\omega_2)^2\tau_2^2}} \tag{129}$$

Thus if the two low-frequency modes possess different energies, the broadening to the shift ratio will be a function of temperature except for very special values of $\delta\omega_1$, $\delta\omega_2$, $\tau_1$, and $\tau_2$ (such as $\delta\omega_1 = \delta\omega_2$ and $\tau_1 = \tau_2$). The case of similar activation energies is treated in Appendix I.

An intriguing explanation for the behavior of the peaks at 2238.9 and 2250.1 $cm^{-1}$ is that they do overlap at significant temperatures and perhaps some of the ideas of Wertheimer on collective transitions can be applied to these two modes such as the interference terms between the transitions.

Because none of the theories in their simplest form givesan adequate description of the behavior of these two resonances,attention will be focused on the other peaks.

As indicated on Figure 10 and Section E of the preceding chapter, a useful region of interest to study spectroscopically is the combination band. Since the energy of the high-frequency mode is known and the energy is the low-frequency mode and the anharmonic shift are extracted parameters the position of the combination band may be deduced. By means of Fourier Transform Infrared Spectroscopy (FTIR) this region of interest was seen in both $h_{14}$- and $d_{14}$-durene (Figs. 14a and 14b). The observation of the bands at approximately the predicted positions constitutes additional evidence in favor of either the HSC or DC models and is not expected on the basis of the AO model. Recall that the DC model predicts a small and positive anharmonic shift, so refinements on the position could help to distinguish between these two models. No prediction was made for the following modes: the overlapping bands in $d_{14}$ (2238.9 and 2250.1) discussed above, and the 2191.1 mode in $d_{14}$ which as we shall see in the following section appears to be a case of intermolecular coupling and is therefore not applicable to the environment which the infrared spectrum was taken (KBr).

There are some points which should be noted regarding these combination spectra. Because the exchange process "blurs" the levels, the position of the combination band is not simply predicted as Figure 10 would indicate. A matrix shift of the positions of the combination levels in $d_{14}$-durene is predicted because the spectrum was taken in KBr. The situation in $h_{14}$-durene is complicated by the presence of additional peaks, the origin of which is most likely due to an overtone of the C-C-H bend. Thus the evidence is less certain compared to $d_{14}$-durene which has a less crowded spectrum. Because of the match between the predicted and observed bands in $d_{14}$-durene, we feel that this is a major piece of evidence in favor of the HSC theory.

Figures 14a and 14b. The FTIR spectrum of $h_{14}$-durene (as either a thin film or in solution) and $d_{14}$-durene (in KBr). The predicted positions of the combination bands resulting from anharmonic coupling between a high-frequency stretch and a low-frequency mode based on HSC theory are indicated by arrows.

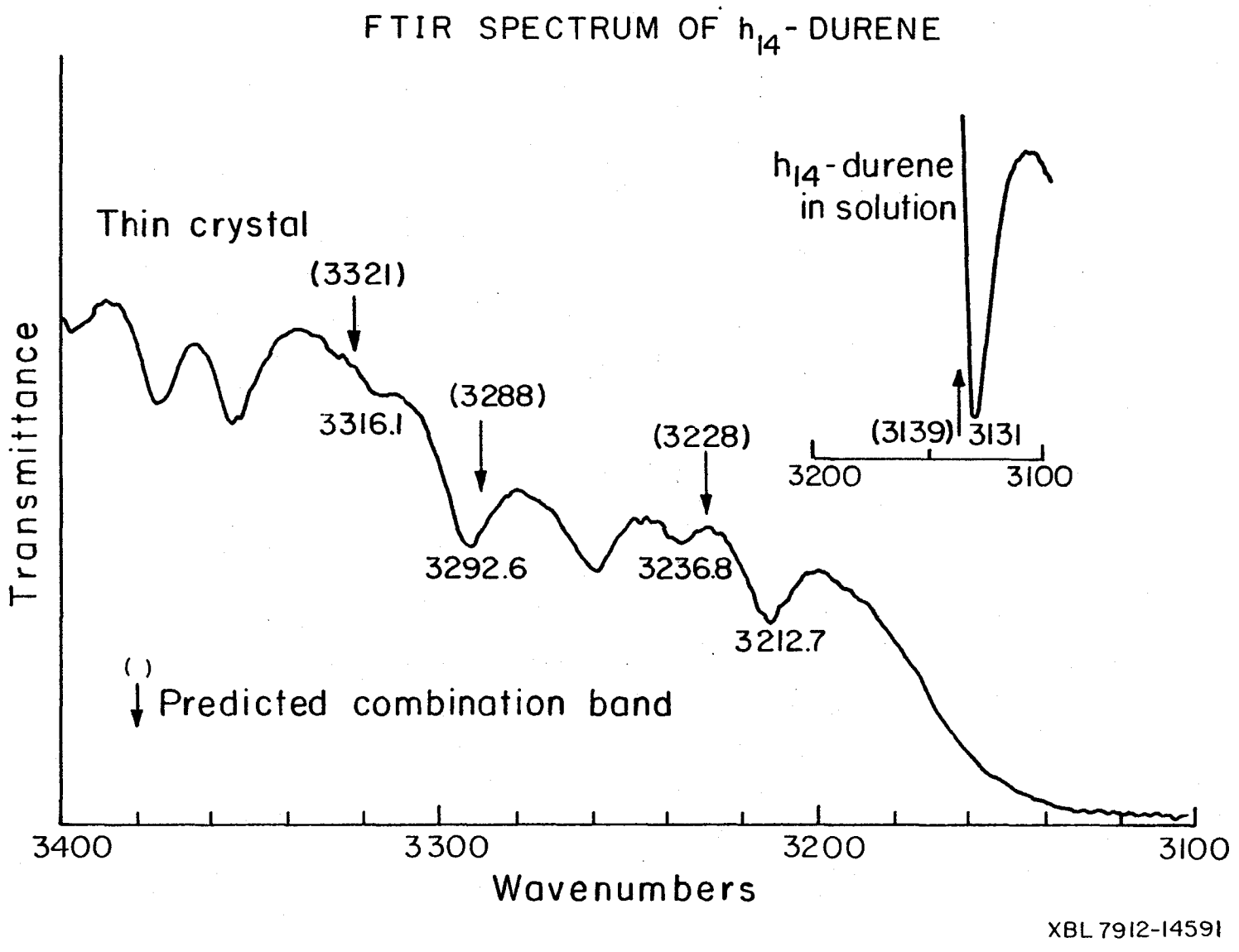
FTIR SPECTRUM OF $h_{14}$ - DURENE
Thin crystal
(3321)
3316.1
(3288)
3292.6
(3228)
3236.8
3212.7
$h_{14}$ - durene in solution
(3139)
3131
3200
3100
( )
Predicted combination band
Transmittance
3400
3300
3200
3100
Wavenumbers
XBL 7912-14591

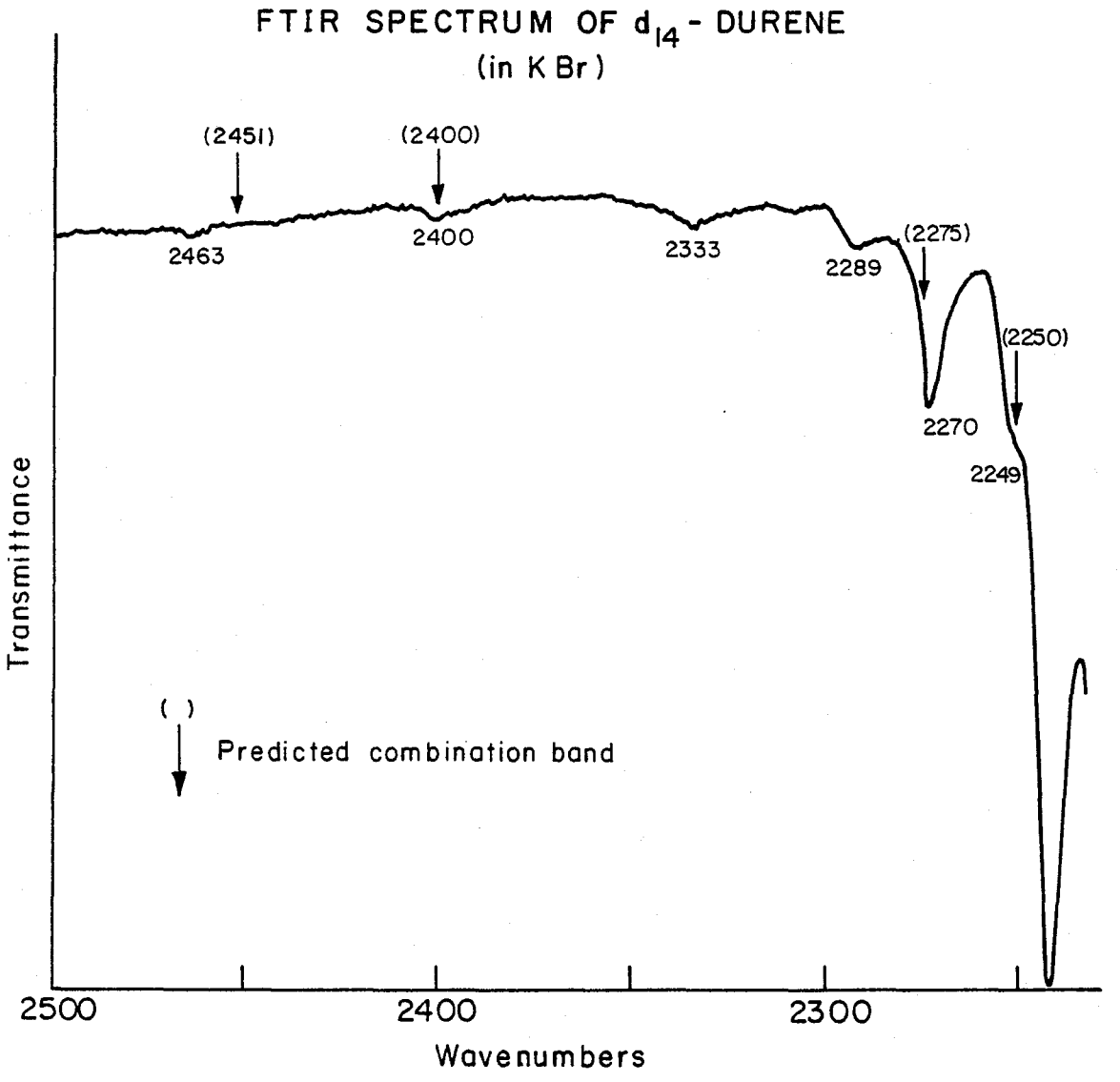


XBL 7912-14592

Let us examine in detail one particularly convincing case. Consider the 2225.9 $cm^{-1}$ mode in $d_{14}$-durene the data for which is displayed in Table 7. Let us predict a lower bound on the position of the combination level on the basis of Wertheimer's DC theory. Adding the base frequency 2225.9 to the smallest reasonable activation energy (240.0) to his predicted shift which should be at least +5 $cm^{-1}$ yields 2470.9 which exceeds the value of 2463.0 which is observed. By HSC analysis, using 241 $cm^{-1}$ as the activation energy and the anharmonic shift of -16.1 yields 2450.8 $cm^{-1}$ which is too small. By utilizing the correct value for the activation energy of 248 $cm^{-1}$ we obtain for the DC prediction 2479 $cm^{-1}$ and for the HSC prediction the value of 2458 $cm^{-1}$ which is closed to the observed value. The essential point which should be noted is that the only way to explain the position of the observed band is to envoke negative anharmonic shifts - which should not be in resonance with the positive dispersive shifts in DC theory and therefore not be able to give rise to the enhancement processes in DC theory. However, the value of the anharmonic shift is consistent with the prediction of HSC theory, in particular its sign is consistent.

An examination of Tables 6 and 7 reveal that in both forms of durene a predominant low-frequency dephasing mode is the in-plane methyl rock. Abbott and Oxtoby[24] pointed out that for $h_{14}$-durene that not only is the value of $\tau$ less than the spectroscopic lifetime based on linewidths but that also there is a discrepancy by a factor of two (.19 and .36 psec) between the two extracted values of $\tau$. Table 7 shows that there is a similar discrepancy in $d_{14}$-durene and also by a factor of two ((.30 and .36 psec) and .66 psec). Figure 15 shows the Raman spectra for the methyl rocking region for a mixed crystal of $h_{14}$- and $d_{14}$-durene. The

fact that it is a mixed crystal, for now, we can take as a convenience to display the spectra simultaneously for both forms of durene. Note that there is a second peak at higher frequencies than the predominate peak for both forms of durene at colder temperatures. This was the first time that peak was observed. Because of the fact that the $A_g$ methyl rock should have a greater Raman cross section than the $B_{1g}$ methyl rock, the assignments were easy and indicated on Figure 15. The fact that there are two different modes with two different lifetimes and temperature dependent properties implies that it is very consistent with the HSC-extracted values of $\tau$.

Figure 16 shows the general appearance of the two in-plane methyl rocks as well as the various C-H (D) stretches which are coupled to it in $h_{14}$ ($d_{14}$) - durene. This particular motion appears to interact with high-frequency modes through a steric interaction. Note that an activation of this mode is expected to affect the root mean squared overlap between adjacent methyl groups as well as the overlap between methyl groups and the aromatic proton. Depending on the change of overlap and whether the force is attractive or repulsive,the anharmonic shift may assume either sign.

Based on the data obtained thus far on the isotopically pure crystals we can state that at least for this system the evidence points toward the HSC model-but necessarily an extension of that model in which the possibility of coherent energy transfer for the low-frequency modes is included (a vibrational exciton or vibron). A review of the evidence thus far is in order. In $d_{14}$-durene a specific counterexample to the AO theory was noted where two isolated peaks collapsed toward each other with increasing temperatures. Also, the combination band spectra for

Figure 15. The Raman spectra of a mixed crystal of durene at various temperatures. For each isotopic species there are two modes clearly observable at lowered temperatures.

METHYL ROCK SPECTRA
IN 1:3 $d_{14}$: $h_{14}$ - DURENE

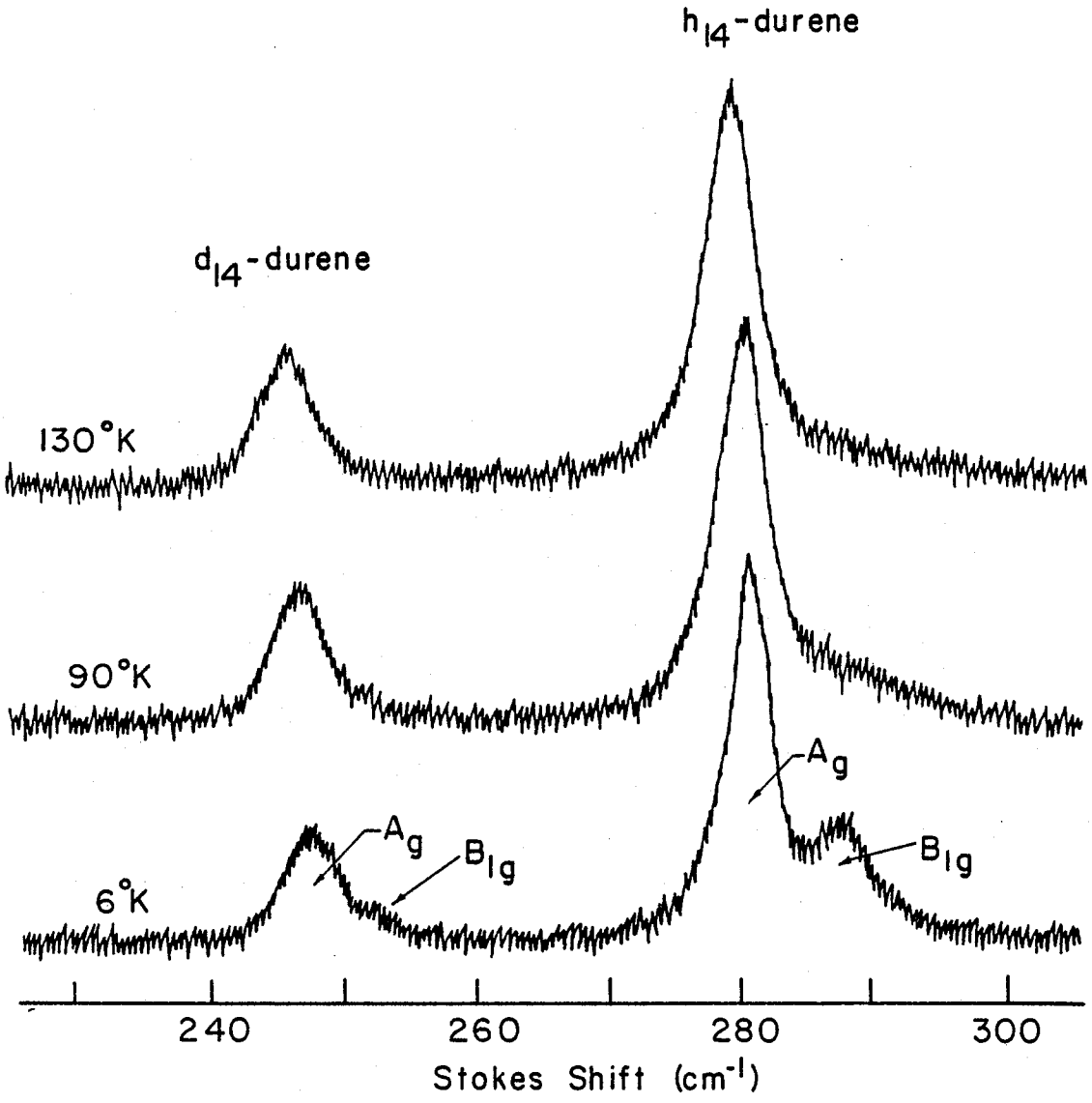


XBL 794-6108

Figure 16. The Raman in-plane methyl rocks in durene are illustrated. The modes which are coupled to the in-plane rock are pointed out. The predominance of this mode as a cause for a significant anharmonic shift is understood on the basis of steric interactions.

# RAMAN ACTIVE IN-PLANE METHYL ROCKING MODES IN DURENE

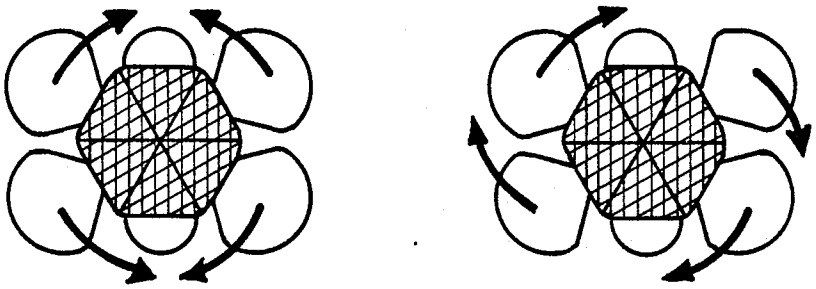

$A_g$ Symmetry $\qquad$ $B_{1g}$ Symmetry

Methyl Rock as Observed Dephasing Channel

| | PEAK ($cm^{-1}$) | $E_i$ ($cm^{-1}$) | $\tau$ (psec) | Symmetry of Methyl Rock |
|---|---|---|---|---|
| Pure $h_{14}$-durene | 2970.3 | 265±6 | 0.19 | $A_g$ |
| | 3027.5 | 263±19 | 0.36 | $B_{1g}$ |
| Pure $d_{14}$-durene | 2035.4 | 252±10 | 0.66 | $B_{1g}$ |
| | 2191.1 | 240±20 | 0.30 | $A_g$ |
| | 2225.9 | 240±15 | 0.36 | $A_g$ |

XBL794-6105

both forms of durene is qualitatively consistent with the hotband models-HSC or DC and inconsistent with the AO model. Therefore, it seems safe to eliminate the AO model from contention as a predominate dephasing mechanism in this system at least. A closer examination of the FTIR combination bands reveals that the couplings do have a negative anharmonic shift in some cases where it is predicted on the basis of the HSC theory- a result not expected on the basis of the DC model. The ratio of the linebroadening to frequency shift was very constant for most of the modes as a function of temperature, a result more consistent with either AO or HSC than with the DC model. There is an apparent inconsistency between the spectroscopic linewidths and the HSC extracted values of $\tau$. It was postulated that the low-frequency modes can act as excitons. As a check on this postulate and to check the validity of some DC mechanisms, isotopic dilution experiments are in order. Those experiments, results, and interpretations are the subject of the next section.

C. Mixed Molecular Solids-Exciton Model

The previous section dealt with results obtained on pure crystals. There, the idea was put forth that the low-frequency mode may exhibit excitonic or delocalized properties; this resolves the discrepancy between the lifetime that one obtains from HSC analysis and the (usually longer) spectroscopic lifetime of the low-frequency mode. Appendix II outlines some properties of vibrational excitons (vibrons) in molecular crystals, which are relevant to this study.

However, for this idea to be believed it must be subjected to a detailed experimental study. There are two spectroscopic regions which are appropriate to study. The low-frequency region as well as the high-frequency region may be monitored as functions of both temperature and concentration. The low-frequency part of the spectrum may contain evidence for excitonic effects directly, whereas the high-frequency modes would be expected to display effects indirectly through coupling to low-frequency modes - particularly in that $\tau$ is expected to be concentration dependent.

Figure 15 indicated that the Raman spectra was investigated for isotopically mixed crystals in the methyl rocking region. Table 8 lists some lineshape parameters associated with the predominate ($A_g$) methyl rock resonance for both forms of durene at various isotopic concentrations at 10°K. There are a variety of reasons for choosing the coldest temperature attainable for this study: the linewidths are smaller at colder temperatures resulting in an increased signal to noise ratio and less uncertainty as to the peak position, the $B_{1g}$ methyl rock is sufficiently separated from the $A_g$ methyl rock at colder temperatures, the frequency shift that the $A_g$ methyl rock experiences as a function of

Table 8. Concentration Dependence of $A_g$ Methyl Rock Lineshapes in $h_{14}$- and $d_{14}$-durene

| | Environment | | | |
|---|---|---|---|---|
| | 100% $d_{14}$-durene | 50% $d_{14}$-durene<br>50% $h_{14}$-durene | 25% $d_{14}$-durene<br>75% $h_{14}$-durene | 10% $d_{14}$-durene<br>90% $h_{14}$-durene |
| $d_{14}$-durene | | | | |
| peak position ($cm^{-1}$) | 249.2 | 248.4 | 247.6 | 246.6 |
| FWHM ($cm^{-1}$) | 4.0 | 5.2 | 5.0 | 4.0 |
| $h_{14}$-durene | | | | |
| peak position | | 278.4 | 280.4 | 280.8 |
| FWHM ($cm^{-1}$) | | 4.4 | 3.6 | 3.6 |

temperature (Fig. 15) is minimized at colder temperatures which results in smaller uncertainties associated with the methyl rock parameters introduced by an uncertainty associated with the temperature, and importantly the phase disrupting events induced by phonons are minimized at colder temperatures which increases the probability of observing some delocalized effects associated with the optical phonon/vibrational exciton (Appendix II). As Table 8 indicates there is a definite shift associated with the $A_g$ methyl rock for both forms of durene (about 3 $cm^{-1}$ over the concentration range) which is outside of experimental error (resolution better than 1 $cm^{-1}$ and fairly small FWHM on the order of 4 $cm^{-1}$).

There are two distinct explanations for a concentration dependent shift. We can call the first type of model for this behavior "static" which includes such phenomena as dielectric constant, and hydrogen bonding. The second model is based on coherent energy transfer resulting in the optical phonon/vibrational exciton band which should be concentration dependent. Examine the data of Table 8 in terms of the "static" model. Note that the frequency of the $d_{14}$-durene methyl rock increases with increasing concentration of $d_{14}$-durene. Thus in terms of the "static" model we would assign to $d_{14}$-durene a special value of some chemical property (for instance a larger value of hydrogen bonding or a smaller value of the dielectric constant than that possessed by $h_{14}$-durene). Thus we would expect that the $h_{14}$-durene peak would also increase to greater frequencies as the system becomes more plentiful in $d_{14}$-durene; however, this does not occur and the "static" model should be discarded. The exciton model would state that when a band forms, the spectroscopically allowed ($\vec{k} = 0$) state is displaced from the energy associated

with a "localized" state. A molecule which is surrounded entirely by its isotopic analog would vibrate at this localized value since the possibility of resonant interactions are non-existent. This discussion is confined to the so-called "separated band limit"[42] where the frequency difference between the bands for the two isotopic forms of durene exceeds the bandwidth. The lineshift data is consistent with this view. Examining the data related to $d_{14}$-durene leads to the interpretation that there is a positive value of J associated with the vibron (see Appendix II) since there is a steady increase of the frequency associated with the methyl rock with an increase in concentration. The data related to the $h_{14}$-durene methyl rock confirms this view,as the methyl rock frequency on $h_{14}$-durene also increases with an increase in concentration of $h_{14}$-durene. Thus, the evidence suggests that the exciton point of view has some validity.

Assuming that the $\vec{k} = 0$ state is an extreme state at an edge of the band then it appears that the bandwidth is on the order of 6 $cm^{-1}$. Additional evidence supporting this view comes from the temperature dependent linewidths. Table 9 lists the full width at half maximum for the $A_g$ methyl rock in pure $d_{14}$-durene as a function of temperature. Localization of this extended excitation might be expected in analogy to electronic excitons[58] due to scattering from phonons at higher temperatures. Another way to view this phenomena is that there is an "exchange" process where the various $\vec{k}$ states scatter into each other. This leads to the redistribution of Raman scattering cross-section to states other than $\vec{k} = 0$, which leads to the lineshape function reflecting the entire range of $\vec{k}$ states at elevated temperatures. Thus there is a consistency between the estimate of 6 $cm^{-1}$ for the exciton bandwidth and the observed

Table 9. Temperature Dependent Linewidth of $A_g$ Methyl Rock in $d_{14}$-durene (FWHM in $cm^{-1}$)

| 10°K | 90° | 130° | 170° | 225° | 250° | 275° |
|---|---|---|---|---|---|---|
| 4.0 | 4.6 | 4.8 | 6.0 | 6.1 | 6.1 | 6.2 |

broadening from 4.0 $cm^{-1}$ to 6.2 $cm^{-1}$ for the $A_g$ methyl rock in $d_{14}$-durene.

As mentioned in Chapter II, the effect of observing the change with concentration of HSC parameters (even in the event that one of the other theories is correct) can provide a very critical test of the relative validity of the various theories. So while the above (temperature and concentration dependence of the low-frequency spectral parameters) provides support of the model that we have developed; the effect of isotopic dilution on the high frequency modes will provide a very thorough examination of the theory. Let us consider the effect of isotopic dilution on $\tau$. Recall that $\tau$ is the time an excitation resides upon a given molecule and we expect two contributions to this resident lifetime; namely, the excitation can decay into the lattice or transfer its energy to a neighboring molecule. We can partition the decay rate into these two contributions:

$$1/\tau = 1/\tau_{res} + 1/\tau_{rel}. \tag{130}$$

Here we assume that the mechanisms which cause a rate for resonant energy transfer, $1/\tau_{res}$, are independent of the mechanisms responsible for relaxation into the lattice, $1/\tau_{rel}$, and that all the decay routes are indeed expressed as rates (i.e., exponentials). Let us consider the effect of isotopic dilution for each of these contributions. The model that we will take for relaxation into the lattice is that it depends on the density of states of lattice modes. This should be essentially independent of concentration in that the lattice modes are expected to obey the amalgamation limit which is that the trap depth (band separation) is less than the bandwidth. The idea is that the molecular weight of

$h_{14}$-durene is 134 amu, that of $d_{14}$-durene is 144 amu; thus a phonon mode which is derived from the translational degrees of freedom and displaces all the atoms equally will assume a frequency of oscillation in $d_{14}$-durene $(134/144)^{\frac{1}{2}} = .964$ of the frequency for the same phonon motion in $h_{14}$-durene. This should ensure that the density of states of the phonon modes and therefore the rate of decay of the vibron into the lattice should be a constant over the concentration range. The model for the methyl rock is best described in terms of a separated band limit because the rocks involve a greater displacement of the hydrogen or deuterium than the carbon and therefore a more significant isotopic splitting; as Figure 15 indicates the bands are well separated (244 and 280 $cm^{-1}$) by an amount which greatly exceeds our estimate for the exciton bandwidth (6 $cm^{-1}$). Therefore we expect that the time for transfer of energy to a nearest neighbor should be concentration dependent. If the molecule of interest is present in a mole fraction c, then the effective resident lifetime should obey the following functional form:

$$1/\tau_{res} = \alpha(c)1/\tau_{res,pure}. \tag{131}$$

Here the rate of resonant energy transfer in the pure crystal is given by $1/\tau_{res,pure}$. The function $\alpha(c)$ should obey the following functional form: its maximum value should be obtained in the pure crystal ($\alpha(c) = 1$ at $c = 1$) and monotonically decrease to zero at $c = 0$. The specific form for $\alpha(c)$ depends on whether the low-frequency mode is localized or extended. If the energy transfer takes place incoherently we expect to see a very smooth functional form for $\alpha(c)$. However, the situation for a delocalized excitation is very different. Based on the idea of percolation as described in Appendix II or on the related idea of Anderson localization,[59] it is expected that the rate of energy transfer will be

essentially a constant until some critical concentration is reached. Below this concentration localization is expected to occur into first finite clusters, then upon further dilution into isolated molecules. Therefore, a steady increase in the value of $\tau_{res}$ with increasing isotopic dilution is the hallmark of a non-excitonic, delocalized excitation; whereas the constancy of this value over a wide concentration range indicates a delocalized excitation - if it is also the case that the residence lifetime is less than the dephasing lifetime. The entire functional form of the residence lifetime, $\tau$, is derived by substituting Eqn. (131) into Eqn. (130):

$$1/\tau = 1/\tau_{rel} + \alpha(c)\left[\frac{1}{\tau_{res,pure}}\right] \qquad (132)$$

This analysis should be true regardless of the theory (HSC, AO, DC) which explains the dephasing of high-frequency modes; i.e., the residence lifetime should either remain a constant or increase upon isotopic dilution. However, as was pointed out in Chapter II, Section E different behaviors are expected for the HSC extracted value of $\tau$ depending on the relative validity of the various dephasing theories. If HSC theory is correct then the extracted value of $\tau$ represents its actual value and this theory can prove to be a powerful tool. If AO theory is correct then none of the extracted values should change because the dephasing is not sensitive to the residence lifetime. The DC situation is complicated, but for the alternative theory described by Equations (124,125) the HSC value of $\tau$ should decrease.

I analyzed three Raman peaks in the $d_{14}$-durene spectrum as a function of dilution with $h_{14}$-durene in terms of HSC theory. The same temperatures, slit widths, laser line and other variables were consistently

used to minimize errors, as described in Section A. Thus confidence can be achieved in the trends that are observed. The three peaks were all coupled to a methyl rock motion - two thought to be coupled to the excitonic $A_g$ mode and the other thought to be coupled to the localized $B_{1g}$ mode (see Fig. 16). Table 10 lists the results for two of these peaks, the other one will be discussed later. Note that the $A_g$ methyl rock which is coupled to the high-frequency mode at 2225 $cm^{-1}$ behaves as expected, in that for this concentration range $\tau$ remains a constant. That result is consistent with the other evidence that was obtained in favor of the exciton model for the low-frequency mode. Comparing this result with the other theories we find the following. It is consistent with the AO theory in that none of the HSC parameters change with concentration; however, other evidence, in particular, the combination region (Fig. 14b) seems to be more in line with the HSC scheme as discussed previously. The parameters $\delta\Omega$ (the excitonic shift associated with the high-frequency mode), as well as intermolecular contributions to $R_D$, $R_\nu^T$, and $R_\nu^A$ in the DC theory can not assume significant values and be consistent with the observed concentration behavior. Thus we conclude that these parameters are insignificant for this case. Also concentration dependent frequency shifts for the high-frequency mode at zero temperature like those observed for the $A_g$ low-frequency were not seen. This is additional evidence that the high-frequency mode does not behave as an exciton and $\delta\Omega$ is approximately zero. The alternative DC theory (Eqns. (124,125)) is consistent with the concentration behavior except that the combination band region provides a more consistent picture for the HSC picture (Section B).

Table 10. Concentration Dependence of Exchange Parameters of C-D Stretch Modes in $d_{14}$-durene

2225 $cm^{-1}$ Stretch

| Environment | ($cm^{-1}$) | $E_i$ ($cm^{-1}$) | (psec) |
|---|---|---|---|
| 100% $d_{14}$-durene | -16.1 ± .7 | 240 ± 10 (240) | .36 ± .07 |
| 50% $d_{14}$-durene 50% $h_{14}$-durene | -15.0 ± 1 | 250 ± 10 (240) | .35 ± .07 |
| 25% $d_{14}$-durene 75% $h_{14}$-durene | -14.1 ± 1 | 250 ± 10 (240) | .34 ± .07 |

2035 $cm^{-1}$ Stretch

| | | | |
|---|---|---|---|
| 100% $d_{14}$-durene | -12.0 ± .5 | 252 ± 15 (240) | .66 ± .05 |
| 50% $d_{14}$-durene 50% $h_{14}$-durene | -10.5 ± 1 | 211 ± 15 (240) | .90 ± .05 |
| 25% $d_{14}$-durene 75% $h_{14}$-durene | -11.0 ± 1 | 230 ± 15 (240) | 1.1 ± .08 |
| 10% $d_{14}$-durene 90% $h_{14}$-durene | -12.0 ± 1 | 235 ± 15 (240) | 1.2 ± .1 |

Evidence obtained from the concentration dependent behavior of the high-frequency 2035 $cm^{-1}$ C-D stretch is more definite and more convincing than the preceding example. A plot of the HSC extracted rate for the low-frequency excitation leaving the molecule is provided by Figure 17. Note that this is the $B_{1g}$ in-plane methyl rock and is expected to be a localized vibration, in which case the energy transfer takes place incoherently. In Equation (132) the function $\alpha(c)$ is replaced with the simplest function which obeys the boundary conditions, namely $\alpha(c) = c$. A least squares analysis yields for the relaxation time into the lattice for the $B_{1g}$ methyl rock a value of $1.4 \pm 0.1$ psec and the resonant energy transfer time of 1.2 psec. This result confirms our expectations concerning this mode, namely, that it is localized.

Recall that the $A_g$ mode was found to have a residence (HSC) lifetime of between 0.30 and 0.36 psec. Using the value of 0.33 psec and the same value for decay into the lattice as the $B_{1g}$ mode (1.4 psec) we can develop a picture which makes sense: 1) Using $1 = 5.3$ psec-$cm^{-1}$ and assuming that the resonant energy takes place coherently (optic phonon/vibrational exciton) and therefore does not contribute to the linewidth, the intrinsic (one $\vec{k}$ state and no inhomogeneous contribution) linewidth is $3.8 \pm .3$ $cm^{-1}$ which is in agreement with the value of 4.0 $cm^{-1}$ (Table 9); 2) Using these values and Equation (130) yields the value of .43 psec for the (coherent) energy transfer time of the $A_g$ mode; 3) It is this shorter value of the energy transfer time which allows at least a partial delocalization and band structure to occur. Thus we now see that a very consistent view emerges from a consideration of experimental results from a variety of places.

Figure 17. The HSC extracted value for the rate at which an excitation of a $B_{1g}$ in-plane methyl rock leaves a molecular site verses concentration. The intercept gives the value of 1.4 $\pm$ .1 psec as the time that is required for an excitation to decay in the lattice. The time for energy transfer to neighboring molecules in the pure crystal is 1.2 $\pm$ .1 psec (which is about 4 times slower than the excitonic $A_g$ rock). This result plus the broader peak suggest that this $B_{1g}$ mode is localized.

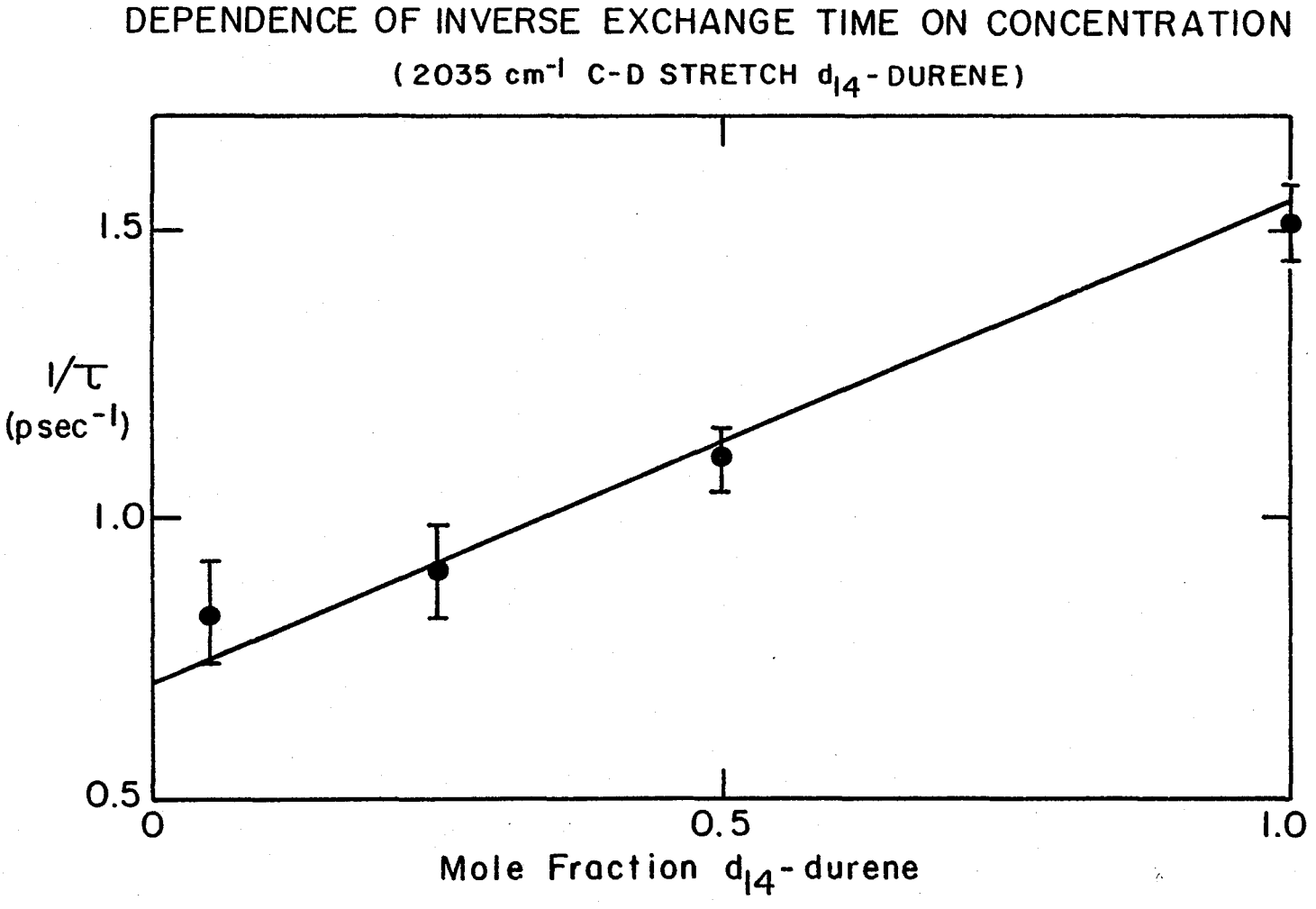
DEPENDENCE OF INVERSE EXCHANGE TIME ON CONCENTRATION
( 2035 cm-1 C-D STRETCH d14 - DURENE)
1.5
1.0
0.5
1/τ
(psec-1)
0
0.5
1.0
Mole Fraction d14 - durene

XBL794-6106

This concentration dependent behavior of the 2035 $cm^{-1}$ stretch is important not only because of the information which develops from it by the HSC viewpoint but also because it provides data which provides a discerning test of the two other theories. AO theory predicts that all the variables extracted out by HSC theory should remain invariant. However, Table 10 and Figure 17 clearly indicates that there is a factor of two change in the lifetime without changes in the other variables. In a similar fashion, the predictions of DC theory are inconsistent with the observed behavior. The intermolecular contributions to the parameters $\delta\Omega$, $R_D$, $R_\nu^T$, and $R_\nu^A$ must be neglected just as in the 2225 $cm^{-1}$ stretch case. Also the alternative DC theory (Eqns. (124,125)) predicts that the HSC '$\tau$' should get shorter with dilution if there is intermolecular energy transfer and the true lifetime is lengthening. Because the opposite behavior is seen we are forced to discard this mechanism for vibrational dephasing in this case.

The last mode which was analyzed as a function of concentration is the 2190 $cm^{-1}$ C-D stretch in $d_{14}$-durene. The parameters as a function of dilution as well as a possible (intermolecular) HSC mechanism are depicted on Figure 18. At first glance the data seems to be most consistent with some of the DC mechanisms in that all the parameters change and that there is a shortening of $\tau$. However, there are two facts which seem to imply an intermolecular coupling. First, the "activation energy" is 240 $cm^{-1}$ in pure $d_{14}$-durene which corresponds to the $A_g$ methyl rocking motion in $d_{14}$-durene and as the system becomes more concentrated in $h_{14}$-durene, the "activation energy" changes to the same methyl rock motion on an $h_{14}$-durene molecule. Secondly, there is no mode on $d_{14}$-durene at $285 \pm 10$ $cm^{-1}$. Therefore, we conclude that there is an

Figure 18. A possible intermolecular mechanism for dephasing based upon steric hindrance between adjacent molecules. This explains the observed changes in the exchange theory (HSC) parameters as a function of isotopic dilution.

# INTERMOLECULAR VIBRATIONAL DEPHASING IN DURENE

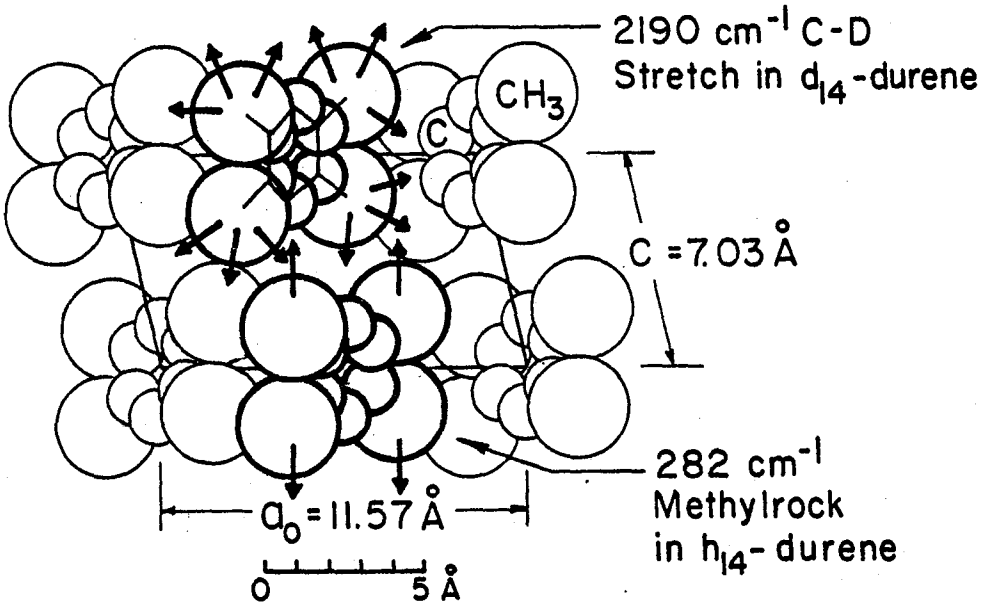


2190 $cm^{-1}$ C - D Stretch of $D_{14}$-Durene
[Methyl D's]

| Environment | $\delta w$ ($cm^{-1}$) | $E_i$ ($cm^{-1}$) | $\tau$ (psec) |
|---|---|---|---|
| 100% $d_{14}$-durene | 19.5 ± 1 | 240 ± 10 | 0.30 ± .05 |
| 50% $d_{14}$-durene<br>50% $h_{14}$-durene | 21.1 ± .5 | 260 ± 10 | 0.24 ± .03 |
| 25% $d_{14}$-durene<br>75% $h_{14}$-durene | 22.4 ± .5 | 280 ± 10 | 0.21 ± .03 |
| 10% $d_{14}$-durene<br>90% $h_{14}$-durene | 21.6 ± .3 | 285 ± 10 | 0.19 ± .03 |

XBL 7811-6183 A

intermolecular dephasing mechanism. If this is the case then all three theories may be suitably modified so as to accommodate the observed behavior. It also becomes more difficult to test the three theories because the situation becomes more complex, particularly at intermediate concentrations. We definitely predict a case of inhomogeneous broadening at those concentrations because there exists a distribution of neighbors which exert slightly different anharmonic shifts and different degrees of exchange. As Figure 18 indicates, we expect that the motion of the methyl rock can perturb more than one neighboring molecule. Also the methyl rock is thought to be delocalized which adds another degree of complexity. With the data at hand it is not possible to address the details of this case and to definitely eliminate one theory in favor of another. However, there does exist one collaborative fact in favor of the HSC model. Based on this model and the data of Figure 18, we would state that resident lifetime of the 282 $cm^{-1}$ mode on $h_{14}$-durene is 0.19 psec. This number agrees with the value obtained by monitoring the 2970 $cm^{-1}$ stretch in pure $h_{14}$-durene (Table 6) where the methyl rock is coupled to this motion and the extracted lifetime is also 0.19 psec.

D. Conclusion

The subject of Chapter II was three differing approaches to vibrational dephasing in solids. All three of these theories are mathematically correct, in that given certain parameters a certain lineshape will result. Because the qualitative temperature behavior of the lineshape function is similar in all three cases (and fortunately to observed lineshape functions), the assessment of the relative validity of the three theories involves a more quantitative approach to this problem. It should be pointed out that these three theories do not represent the totality of theoretical effort concerning vibrational dephasing in condensed media (see, for example, Refs. 57-59). However, all three of these theories claim relevance to the results presented in References 13 and 14 with widely differing physical assumptions which result in similar lineshapes. Section E of Chapter II discussed what features should be studied to determine this relative validity.

The results of Chapter III give strong evidence in favor of the HSC model which has been extended to include the possibility of energy transfer. That is, the HSC value of $\tau$ should be less than the lifetime of the low-frequency excitation. To summarize the evidence in favor of the HSC model we should include: 1) There exists an excellent match between the activation energies of both the shift and broadening and an observed low-frequency mode of the molecule. 2) The combination bands which are predicted by the extracted exchange parameters have been observed. 3) There exists some evidence that the low-frequency mode can be described in terms of a delocalized excitation.

The evidence in favor of the other models is not as strong. For at least some of the modes the observed behavior is in contradiction with

some of the predictions. In other cases the behavior could be justified in terms of these models, as well as the HSC model.

One advantage of the HSC model is the ability to extract out of the data a meaningful interpretation of the dynamics of the system. With corroborative evidence such as the combination bands and mixed crystals studies, the picture of the molecular solid can become rather detailed.

# Chapter IV

## SOME RESULTS AND DISCUSSION ON LIQUIDS

### A. A Model of Inhomogeneous Broadening

In this chapter the subject changes. Here I would like to present results which by themselves do not present a very convincing case but provides evidence more of a corroborative nature. S. M. George and H. Auweter[60] undertook an investigation of a series of eleven room temperature liquids which varied in parameters such as dipole moment, molecular weight, and hydrogen bonding but all possessing a methyl ($CH_3$) group.

The interested reader should consult Reference 60 for the details, but a brief synopsis follows. By means of a picosecond pulse-and-probe technique explained in Reference 1, the homogeneous portion of a line-shape can be extracted from those resonances which display a suitably large non-linear stimulated Raman cross-section. One such resonance is the $A_1$ symmetric stretch of a methyl group. The homogeneous portion of this symmetric methyl stretch for the liquids was determined. By assuming that the lineshape for spontaneous Raman scattering, $I(\omega)$, is a convolution of a Lorentzian homogeneous function, $L(\omega)$, and an inhomogeneous lineshape having a Gaussian form, $G(\omega)$, i.e.,

$$I(\omega) = \int_{-\infty}^{\infty} L(\omega')G(\omega-\omega')d\omega' \qquad (133)$$

the inhomogeneous lineshape may be determined. The width of this Gaussian inhomogeneous function varied from 0.9 $cm^{-1}$ in 1,1,1-Trichloethane to 16.3 $cm^{-1}$ in methanol. Various models were tried by George et al.[60] to

correlate this inhomogenity with some physical parameter. No correlation was observed for the following models: an intermolecular attraction parameter associated with each liquid (the boiling point divided by the molecular weight), the dipole moment of the molecule, hydrogen bonding, and structural associativity (the ultrasonic absorption). A positive correlation does exist with the free volume (which is the (volume associated with the liquid/volume associated with the solid at the melting point)-1) and the inhomogeneous broadening. This can be understood because the presence of free volume establishes the possibility that there is a distribution of environmental sites (some molecules have greater or lesser amount of free volume surrounding them than other molecules) which in turn leads to an inhomogeneous distribution. Following this idea further, the authors determined that the distribution width in the local number density is proportional to density times the square root of the isothermal compressibility:

$$\sigma\rho \propto \bar{\rho}(kTK_T)^{1/2}$$

$$\propto \bar{\rho}\sqrt{K_T} \qquad (134)$$

The appropriate parameters are listed in Table 11 for molecules which will be important in this Chapter. They form a representative sample of the 11 liquids which were studied in Reference 60. The main importance of Reference 60 is that it clearly shows the amount of inhomogeneity associated with vibrational linewidths in liquids. The inhomogeneous contribution may indeed be the dominant mechanism for line-broadening. Therefore, experimental linewidth studies should rightfully consider this factor. Unfortunately, the majority of experimental studies have interpreted Raman linewidth experiments on liquids in terms

Table 11. Parameters of Organic Liquids, Symmetric $CH_3$-stretch (from Reference 60)

| Molecule | $\omega(cm^{-1})$ | Calculated Homogeneous $\Delta\omega(cm^{-1})$ | Isotropic Spontaneous Raman $\Delta\omega(cm^{-1})$ | Gaussian Inhomogeneous $\Delta\omega(cm^{-1})$ | % Free Volume | $\sigma_\rho$ (Arbitrary Units) |
|---|---|---|---|---|---|---|
| 1,1,1-Trichloroethane | 2938.5 | 4.1 | 4.3 | 0.9 | 5.7 | 294 |
| Acetonitrite | 2945 | 2.8 | 6.6 | 5.5 | 8.7 | 453 |
| Dimethylsulfoxide | 2914.5 | 7.6 | 11.8 | 6.9 | 0.6 | 314 |
| Acetone | 2925 | 3.5 | 16.5 | 14.6 | 16.2 | 484 |
| Pentane | 2877 | 3.9 | ≃17 | ≃14.8 | 18.5 | 456 |

of "dynamics" and not inhomogeneous "statics" (see, for example, Refs. 61-65).

B. Raman Studies of Solutions

The observant reader should have noted that in Table 11 dimethylsulfoxide (DMSO) does not seem to fit the trends relating free volume or the distribution width in the local number density to inhomogeneous broadening. This molecular liquid possesses nearly the same density in a liquid state at room temperature as it does as a solid at the melting point. However, it appears to possess nearly the same inhomogeneous component as its homogeneous component. One study which I undertook to see if the linewidths do indeed correlate with the free volume was to cool down the samples and take the Raman spectrum as a function of temperature. The idea is that as the sample approaches (or crosses) the freezing point the free volume should approach zero and so should the inhomogeneous linewidth. Figure 19 illustrates the temperature dependent spectra of DMSO- note that the peak in the region of the symmetric methyl stretch "splits" into two components at lower temperatures. It seems as though there is an anomalously large value of the apparent inhomogeneous width, due to the fact that the two underlying components merge together at elevated temperatures. One reason for this is that DMSO has two methyl groups which can interact. The proper description of the normal modes must at least include the possibility for allowing the $CH_3$ symmetric stretches on both carbons to vibrate in a coordinated fashion, i.e., either in or out of phase with respect to each other. Thus, two peaks should be present and lead to an overestimate of the inhomogeneous broadening in the liquid.

Figure 19. The temperature dependent spectrum of the $CH_3$ symmetric stretch. The solid phase clearly exhibits a splitting which is obscured in the liquid, resulting in larger apparent values of both the homogeneous and inhomogeneous linewidths.

RAMAN SPECTRA OF THE SYMMETRIC $CH_3$ STRETCH IN DMSO (SOLID)

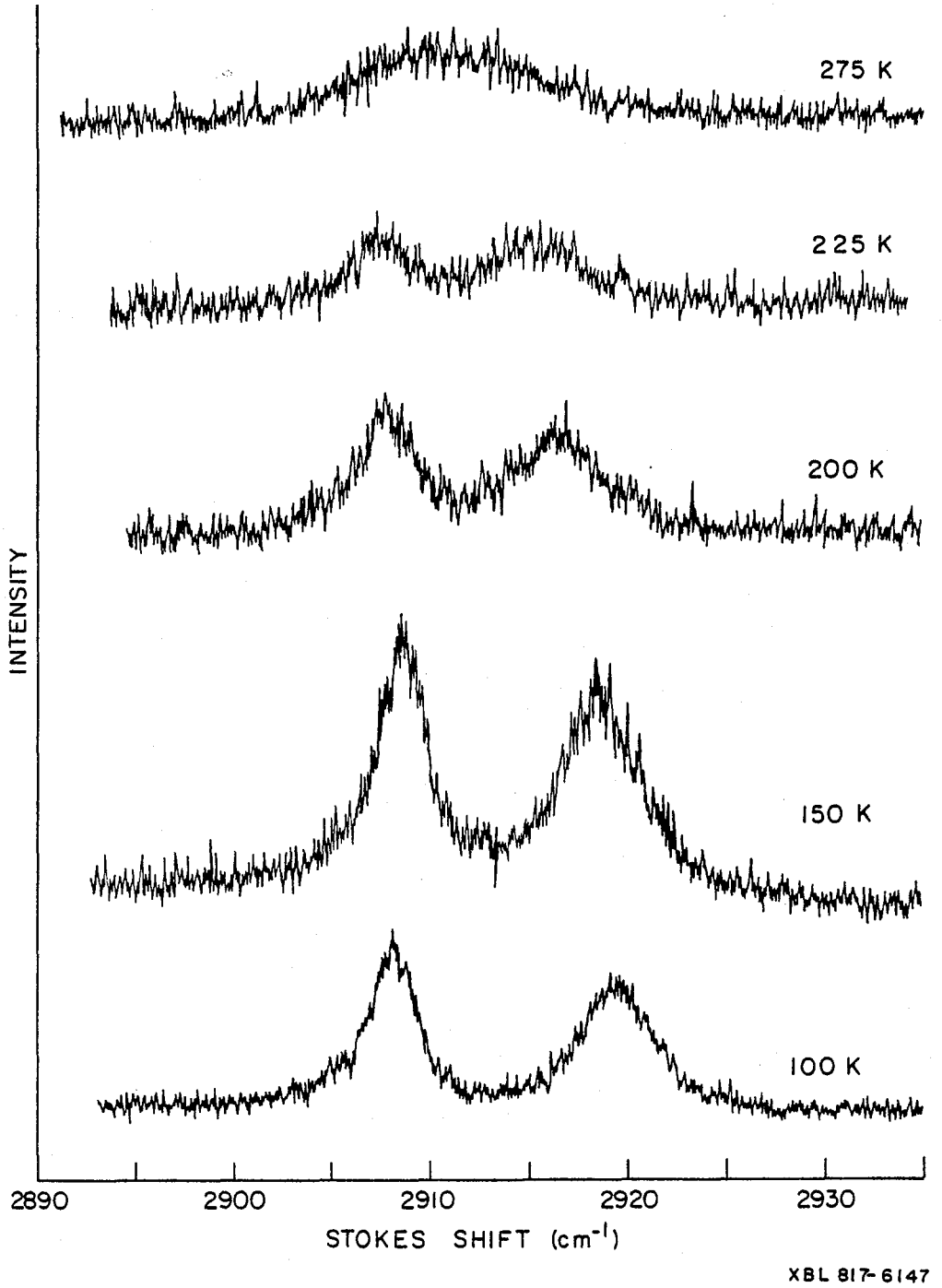

As an aside, we can observe that this example of the temperature dependence in the solid provides another counterexample to the AO model similar to the case analyzed in Figure 12. Here we have an "isolated doublet" which should provide a test of the AO model. The peak at 2909 $cm^{-1}$ is the lowest frequency peak in the Raman spectrum for hundreds of wavenumbers yet it shifts to lower frequencies with increasing temperature. The AO model would predict that it should shift toward higher frequencies.

Because acetone and DMSO have similar structures ($O=C-(CH_3)_2$ vs $O=S-(CH_3)_2$) it seems reasonable to believe that the symmetric methyl stretch in acetone would have a similar underlying splitting as in DMSO. The spectrum of the solid phase of acetone as a function of temperature does reveal a slightly discernible (0.5 $cm^{-1}$) splitting at 10°K which is not significant enough to affect the results listed in Table 11 at room temperature. Therefore, unlike DMSO, we can have confidence in the homogeneous and inhomogeneous widths listed in Table 11 for acetone.

The values for the homogeneous (3.5 $cm^{-1}$) and inhomogeneous (14.6 $cm^{-1}$) widths in acetone give rise to an experimental check of these values. It would seem that if the origin of the inhomogeneous width is a quasi-static distribution of environmental sites then there should be no effect exerted by isotopic dilution on this linewidth. However, there probably is a dynamic intermolecular effect on the homogeneous linewidth. The origin of this can come about directly through resonant energy transfer of the high-frequency stretching mode being considered, or indirectly through energy exchange of the low-frequency modes which are in turn coupled to the high-frequency mode (i.e., the HSC process described in Chapter II). Thus we expect, within the context of the

density distribution model for inhomogeneous broadening, that the width of the Raman line should decrease upon isotopic dilution from 16.5 $cm^{-1}$ to a value which is not less than 14.6 $cm^{-1}$ (see Table 11). Table 12 indicates the results of such an experiment. Because of the extreme broadness of the peak and the fact that signal to noise decreases with concentration, it was necessary to increase the spectral width of the monochromator. Even so, Table 12 implies that with dilution the width does not decrease more than the homogeneous width, but only about 1 $cm^{-1}$ of the 3.5 $cm^{-1}$ available homogeneous spectral width. It is important to realize that this in itself only constitutes a check (not a test) of the values assigned to the homogeneous and inhomogeneous linewidths. It would only be a test if the results were inconsistent with the picosecond experiments of George et al. However, additional information can be obtained by combining both experiments together. If we would believe that the entire linewidth is homogeneous in origin then it seems that only 6% or so of that linewidth is due to dynamic intermolecular effects. We interpret the above results as implying that about 30% of the homogeneous linewidth is accounted by intermolecular energy transfer effects. Note that the narrowing of the $d_6$-acetone resonance can be accounted by the same model and leads to more consistency in the picture that we are developing.

Table 13 indicates some temperature dependent values for the width of the symmetric stretch. The results above the freezing point need to be reconciled with temperature dependent picosecond results. Experiments of this nature are in progress in our laboratory. It is possible that the widths may increase as the temperature decreases, as indicated by Eqn. (134), if other factors such as the density and the isothermal

Table 12. Raman Spectral Widths of the Symmetric Methyl Stretch (FWHM) in Isotopically Mixed Acetone Liquid Solutions at Room Temperature. (Spectral Resolution ~1.2 $cm^{-1}$)

| | % Volume of $h_6$-Acetone | | | | | | | |
|---|---|---|---|---|---|---|---|---|
| | 100 | 90 | 80 | 67 | 50 | 25 | 10 | 0 |
| $h_6$-Acetone FWHM ($cm^{-1}$) | 17.3* | 17.0 | 16.8 | 16.8 | 16.6 | 16.5 | 16.4 | x |
| $d_6$-Acetone FWHM ($cm^{-1}$) | x | 10.3 ± .3 | 10.5 | 10.5 | 11.0 | 11.2 | 11.3 | 11.5 |
| | 0 | 10 | 20 | 33 | 50 | 75 | 90 | 100 |
| | % Volume of $d_6$-Acetone | | | | | | | |

* Under 0.25 $cm^{-1}$ Resolution this is 16.5 $cm^{-1}$.

Table 13. Full Width Half Maximum of the Symmetric $CH_3$ Stretch in Acetone as a Function of Temperature (Spectral Resolution = 0.25 $cm^{-1}$); (Freezing Point = 177.8°K)

| Temperature (°K) | 10 | 175 | 179 | 185 | 295 |
|---|---|---|---|---|---|
| Width ($cm^{-1}$) | 12.3 | 16.8 | 16.9 | 17.0 | 16.5 |

compressibility change more rapidly than the temperature. What I found interesting about the spontaneous Raman spectrum of acetone is the results obtained as a function of how fast it is frozen. If cooled down very rapidly the widths can actually increase drastically (to about 50 $cm^{-1}$). The value of 12.3 $cm^{-1}$ represents the smallest value obtained when the sample was cooled down very slowly (holding the temperature for about an hour a degree above the freezing point, and then an hour one to five degrees below the freezing point). It becomes difficult to realize what this means; however, an attempt to explain it is as follows. The value of 50 $cm^{-1}$ could be the 'true' inhomogeneous width caused by differing environmental sites. However, it could be the case that in the liquid the sites are not as stable (quasi-static) as previously thought. Thus, an environmental exchange process could narrow the inhomogeneous width. A second explanation (which is more consistent with the model of density distributions causing inhomogeneous broadening) is obtained by simply changing the time scale of the environmental exchanging process. If an acetone molecule in the liquid experiences collisions which severely change the frequency associated with the stretch as a function of collision coordinate (see, for example, Ref. 3), then when the sample is frozen hard enough molecules can perhaps be amorphously "frozen in" various degrees of the collision coordinate and, therefore, vibrate in an inhomogeneous distribution. In contrast, the molecules in a liquid experience a collisional event over a time period of very short duration and are thereby able to "exchange average" the various frequencies associated with the collision.

It is this second explanation which is most consistent with the hypothesis currently adopted by members of our research group. Namely, a

molecule in a liquid is surrounded by a "quasi-static" cage. The different cage environments results in different frequencies on an inhomogeneous profile. "Rattling" inside the cage or experiencing rapid (but small) fluctuations of the cage results in homogeneous linebroadening.

With this idea in mind, let us consider the effect of solutions. This is a subject that can become complicated very easily. The level of approach here is qualitative. Unless there are some very large competing processes (e.g., incommensurant sizes or microscopic concentration inhomogeneities, such as clusters) then a molecule placed in dilute solution should experience the density fluctuations (and the inhomogeneous broadening) of the solvent. Table 14 reports the results of mixing trichloroethane and $d_6$-acetone. The reason for using the deuterated form of acetone is to prevent overlapping (and thus obscuring) spectral bands. Recall (Table 11) that trichloroethane is characterized by small values of both free volume density fluctuations and inhomogeneous broadening; whereas acetone is characterized by larger values of these quantities. The qualitative features of this mixture is as expected. The trichloroethane peak when diluted in acetone broadens, and the acetone peak narrows when placed in the highly compactly spaced trichloroethane. However, the magnitude of the spectral change is not as great as would be expected if the "cage" composed of the solvent molecules is unaffected by the solute molecule. It seems reasonable to assume that there is an interaction between the molecule and the solvent such that the molecule can affect the order/disorder locally (i.e., density fluctuations). Speculating on the trichloroethane/acetone system, we can say that the inhomogeneous broadening seems to assume a compromise that is somewhere between the molecule having complete local control and the solvent exerting complete control.

Table 14. FWHM ($cm^{-1}$) of the Methyl Symmetric Stretches in Binary Mixtures of 1,1,1-trichloroethane and $d_6$-acetone. (~1.2 $cm^{-1}$ Spectral Resolution)

| | % by Volume Trichloroethane | | | | | | | | | | |
|---|---|---|---|---|---|---|---|---|---|---|---|
| | 100 | 97.5 | 95 | 90 | 75 | 67 | 50 | 33 | 25 | 10 | 0 |
| Trichloroethane ($\pm$.1 $cm^{-1}$) | 4.7* | 4.9 | 4.9 | 5.1 | 5.4 | 5.4 | 5.65 | 5.8 | 5.9 | 6.2 $\pm$ .2 | x |
| $d_6$-Acetone ($\pm$.1 $cm^{-1}$) | x | 10.2 $\pm$ .5 | 10.2 $\pm$ .4 | 10.0 $\pm$ .3 | 10.0 | 10.2 | 10.9 | 11.0 | 11.2 | 11.4 | 11.5 |

* This peak has a width of 4.1 $cm^{-1}$ under 0.25 $cm^{-1}$ resolution.

## C. Conclusion

In this chapter, evidence has been presented which qualitatively supports a model of inhomogeneous broadening in liquids based on the statistical distribution of local number density. Systems possessing a greater "free volume" have a greater isothermal compressibility and greater amounts of variety in environmental sites and therefore greater inhomogeneous broadening than more compact systems. The results shown here do not represent an exhaustive study, but instead show the type of areas that can now be explored utilizing the knowledge that certain vibrational transitions are characterized by a large amount of inhomogeneous broadening.

# Chapter V

## SUMMARY AND FUTURE PROSPECTS

The central feature of this work has been the utilization of the Raman spectra of molecular condensed phase matter in order to understand some properties of that matter. We have seen in detail three theories which attempt to explain the temperature dependence of spectral lines in molecular solids. Data was presented on the durene system which required the rendezvous of data from various sources (temperature and concentration dependence of both the high and low-frequency modes and combination band spectra) before a definite attack on the problem could be made.

The result of this study is the conclusion that the exchange theory model holds up nicely when the possibility of delocalization of the low-frequency modes is included. Allowing for this possibility, we can learn a great deal about the vibrational dynamics of our molecular solid. The exchange theory formalism and ideas needs to be tested further and hopefully will find itself put to good service in other areas. References 17 and 18 indicate that it may be applicable to excitons in molecular crystals. It was recently told to the author that exchange theory may be applied to the tunneling of hydrogen in metal-hydrides.[66] The generalization of this approach most likely needs to be established for each type of case.

The results in liquids presented in Chapter IV suggest that the data gathered by spontaneous Raman spectroscopy can support a model developed by picosecond stimulated Raman spectroscopy, as well as being able to add refinements. The establishment of the inhomogeneity of vibrational

transitions in liquids (Ref. 60) opens up virgin territory for exploration and development by physical chemists. I fully expect that the near future will see fruitful progress in this area, particularly in the area of solutions.

# Appendix I

## THE EFFECT OF COUPLING TO MORE THAN ONE MODE ON THE HSC THEORY

There is nothing a priori to suggest that within the context of HSC theory that more than one mode may be involved in a coupling scheme to the high-frequency mode of interest. One particular piece of evidence to suggest that the low-frequency mode(s) which couple to the high-frequency mode at least do not possess different energies is a constant value of the broadening divided by the shift over a wide temperature range (Figs. 14a and 14b). But what will be the effect of multiple coupling to a high-frequency mode when the (more than one) low-frequency modes have very similar energies?

Figure A1 shows an extreme case in durene. There are four in-plane methyl rocks each possessing similar energies (within 5-10%), and it seems reasonable to assume that if one of these motions is coupled to a particular stretch then one or more of the remaining low-frequency motions may also be coupled to that same stretch.

Figure A2 depicts a special situation where two different low-frequency modes, possessing similar energies, are coupled to the same high-frequency mode resulting in different exchange times and anharmonic shifts. Note that relaxation occurs between a state possessing one quantum of excitation in a low-frequency mode and the ground state; but the multi-quantum exchange process $|0,0,1\rangle \rightarrow |0,1,0\rangle$ (even though it is nearly resonant) is ignored. One could generalize the discussion of Section B in Chapter 1, utilizing a 3 x 3 matrix approach to derive the resulting lineshape function. It is easier in the low-temperature limit to make use of the DC formalism of Section D in Chapter II. The

Figure A1. Four different modes possessing similar energies in the durene molecule as well as similar steric changes upon excitation. Thus it might be expected that if one low-frequency mode is anharmonically coupled to a particular stretching high-frequency then the others may be also coupled.

# METHYL ROCKING MODES IN DURENE

| RAMAN ACTIVE | INFRARED ACTIVE |
| --- | --- |
| 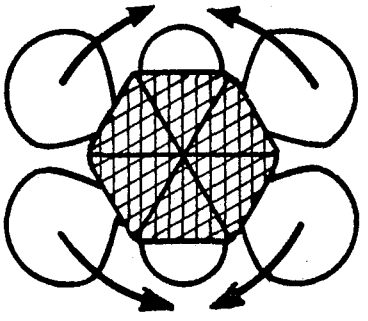 | 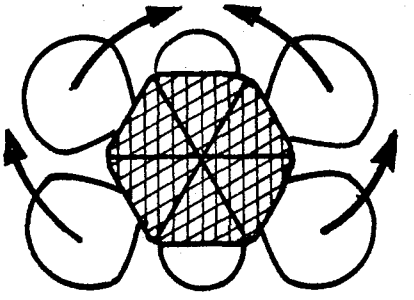 |
| $A_g$ Symmetry | $B_{2U}$ Symmetry |
| 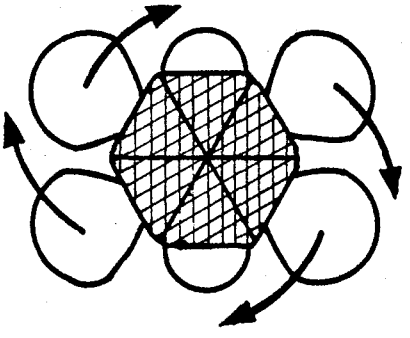 | 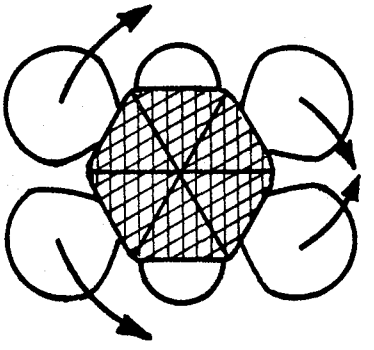 |
| $B_{1g}$ Symmetry | $B_{3U}$ Symmetry |

XBL 816-5937

Figure A2. The model that we take in this appendix for coupling to two modes with similar energies.

# MULTIPLE MODE INTERMOLECULAR ENERGY EXCHANGE THEORY

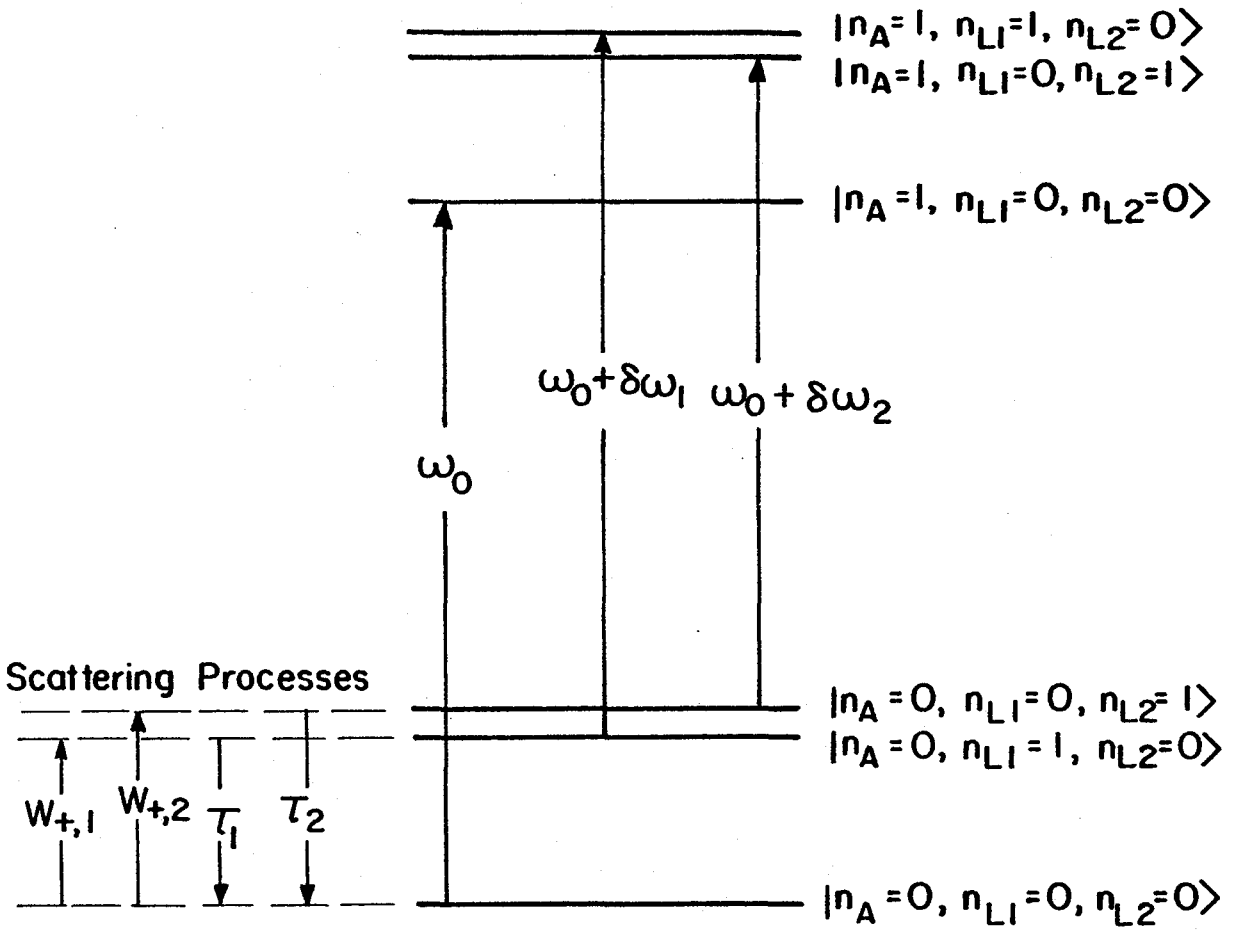


XBL 816-5932

application of that formalism where cross-correlations have been ignored yields the following parameters for a Lorentzian lineshape approximation in the low-temperature ($k_BT > E_{L1}, E_{L2}$) limit:

$$\omega_{eff} = \omega_o + \frac{\delta\omega_1[\exp(-E_1/kT)]}{1+(\delta\omega_1)^2\tau_1^2} + \frac{\delta\omega_2[\exp(-E_2/kT)]}{1+(\delta\omega_2)^2\tau_2^2} \tag{A1}$$

$$(T_2^{eff})^{-1} = (T_2')^{-1} + \frac{(\delta\omega_1)^2\tau_1[\exp(-E_1/kT)]}{1+(\delta\omega_1)^2\tau_1^2} + \frac{(\delta\omega_2)^2\tau_2[\exp(-E_2/kT)]}{1+(\delta\omega_2)^2\tau_2^2} \tag{A2}$$

We are looking for a situation where the simple application of HSC - <u>selectively coupled</u> theory would appear correct. This situation occurs when $(E_1 \approx E_2) = E_L$. HSC theory (Eqns. 42,43) would predict the following form for the effective parameters.

$$\omega_{eff} = \omega_o + \frac{'\delta\omega'[\exp(-E_L/kT)]}{1+('\delta\omega')^2('\tau')^2} \tag{A3}$$

$$(T_2^{eff})^{-1} = (T_2')^{-1} + \frac{('\delta\omega')^2'\tau'[\exp(-E_L/kT)]}{1+('\delta\omega')^2('\tau')^2} \tag{A4}$$

Substituting $E_L$ for $E_1$ and $E_2$ and comparing Eqns. (A1-4) results in the following relationships:

$$\frac{'\delta\omega'}{1+('\delta\omega')^2('\tau')^2} = \frac{\delta\omega_1[1+(\delta\omega_2)^2\tau_2^2]+(\delta\omega_2)[1+(\delta\omega_1)^2\tau_1^2]}{[1+(\delta\omega_1)^2\tau_1^2][1+(\delta\omega_2)^2\tau_2^2]} \tag{A5}$$

$$\frac{('\delta\omega')^2,\tau'}{1+('\delta\omega')^2('\tau')^2} \quad \frac{(\delta\omega_1)^2\tau_1[1+(\delta\omega_2)^2\tau_2^2]+(\delta\omega_2)^2\tau_2[1+(\delta\omega_1)^2\tau_1^2]}{[1+(\delta\omega_1)^2\tau_1^2][1+(\delta\omega_2)^2\tau_2^2]} \tag{A6}$$

After some manipulation this yields involved relationships for '$\delta\omega$' and '$\tau$' in terms of $\tau_1$, $\tau_2$, $\delta\omega_1$, and $\delta\omega_2$ which does not shed light on what

is occurring and will not be reproduced here. A special case will be considered which demonstrates the effect of multiple coupling in a simple way. Consider the case where $(\delta\omega_1)^2(\tau_1)^2 = (\delta\omega_2)^2(\tau_2)^2$. In this limit (which could occur if both modes are in intermediate exchange) we obtain when $\delta\omega_1$ and $\delta\omega_2$ are of the same sign:

$$'\delta\omega' = \delta\omega_1 + \delta\omega_2 \tag{A7}$$

$$1/'\tau' = 1/\tau_1 + 1/\tau_2. \tag{A8}$$

Thus we immediately see that the HSC extracted value for the resident lifetime, $\tau$, is shorter than the 'true' values of $\tau_1$ or $\tau_2$. Thus in this case the application of HSC- selectively coupled theory would provide a good fit at lower temperatures but would extract out larger anharmonic shifts and shorter times than what is occurring.

When $\delta\omega_1$ and $\delta\omega_2$ are of opposite signs the algebraic expression becomes messy. In the interest of physical insight let us consider the case of intermediate exchange: $(\delta\omega_1\tau_1) = -(\delta\omega_2\tau_2) = 1$. Now we would extract out the following parameters:

$$'\delta\omega' = \frac{(\delta\omega_1 - |\delta\omega_2|)^2 + (\delta\omega_1 + |\delta\omega_2|^2)}{2(\delta\omega_1 - |\delta\omega_2|)} \tag{A9}$$

$$'\tau' = \frac{2(\delta\omega_1 + |\delta\omega_2|)}{(\delta\omega_1 - |\delta\omega_2|)^2 + (\delta\omega_1 + |\delta\omega_2|)^2} \tag{A10}$$

As a numerical example consider $\delta\omega_1 = 10\ cm^{-1}$ ($\tau_1 = .1/cm^{-1}$) and $\delta\omega_2 = 5\ cm^{-1}$ ($\tau_2 = .2/cm^{-1}$). In this example we obtain for '$\delta\omega$' 25 $cm^{-1}$ and for '$\tau$' the value of $.12/cm^{-1}$.

To summarize this appendix we can say that one should be cautious in utilizing HSC selectively coupled model when the 'activation' energy of the low-frequency mode corresponds to more than one mode. In this case it becomes possible to obtain erroneous values for the exchange parameters. A check such as the spectroscopic observation of the combination levels to obtain the value of the anharmonic shift should prove fruitful.

# Appendix II

## VIBRATIONAL EXCITONS

It is the purpose of this Appendix to give the reader a basic understanding of vibrons in molecular crystals, particularly those aspects which are important to understanding the results obtained in the durene system. The idea of molecular vibrations being delocalized in a crystal dates back to the early 1930's with the pioneering work of Frenkel.[44] Frenkel developed the idea of "molecular" excitation waves represented by the functions

$$\chi_k = \sum_{\ell} \frac{1}{n^{\frac{1}{2}}} \exp(ik\ell)\ \phi_{\ell} \qquad \text{(A11)}$$

where $\phi_{\ell}$ is the product of molecular vibrational wavefunctions each in its ground state with the exception of the $\ell^{th}$ molecule which is in the vibrational excited state under consideration. This approach is analogous to the LCAO or tight binding approximations to determine the electronic state in covalently bonded solids.[45,46] Frenkel's work led to the idea of the conservation of energy and momentum (in particular crystal momentum), and group velocity. Davydov[47] did research in the late 1940's and early 1950's on electronic excitons in molecular crystals (where the electron and hole most likely reside on the same molecule), resulting in the Davydov splittings which occur when there is more than one molecule occupying a primitive unit cell. In that case, it is expedient to utilize unit cell wavefunctions[48]

$$\gamma^{\alpha,\beta} = (2)^{-\frac{1}{2}} (\phi_p \pm \phi_{p+1}) \qquad \text{(A12)}$$

in place of the $\phi$ in Equation (A11), where in Equation (A12) molecules p and p+1 share the same (bimolecular) unit cell. This yields an expression analogous to Equation (A11)

$$\phi^{\alpha,\beta}(k_a,k_b,k_c) = \left(\frac{2}{N}\right)^{\frac{1}{2}} \sum_{\mu,\nu,\omega} \exp[i(k_a \cdot a_\mu + k_b \cdot b_\nu + k_c \cdot c_\omega)] \times \gamma^{\alpha,\beta}(\mu,\nu,\omega) \quad \text{(A13)}$$

where there are (N/2) unit cells specified by the indices $\mu$, $\nu$, $\omega$.

A model for excitons that is assumed in a variety of places[49-51] is a Hamiltonian which takes the following form

$$H_{ex} = \sum_n E_o a_n^\dagger a_n + \sum_{n-n'} J_{n-n'} a_n^\dagger a_{n'} \quad \text{(A14)}$$

for Frenkel excitons in a perfect, non-vibrating crystal. The J terms correspond to resonant energy transfer from site n' to site n. As an example, consider a one-dimensional crystal which is either infinite in extent or a closed finite ring, where the only transfer terms of importance are nearest neighbor interactions. Now the Hamiltonian becomes:

$$H_{ex} + \sum_n E_o a_n^\dagger a_n + \sum_n J(a_n^\dagger a_{n-1} + a_{n-1}^\dagger a_n). \quad \text{(A15)}$$

The application of this Hamiltonian on the Bloch-function (Eqn. (A11)) yields the dispersion relation

$$E(k) = E_o + 2J\cos(ka). \quad \text{(A16)}$$

Figure A3 depicts the relationship between two extremum excitons in (fictional) one-dimensional durene.

The origin of the J terms can arise from the mechanical intermolecular forces of which the dipole mechanism is one such force. The usual idea associated with (electronic) excitons is that a dipole moment

Figure A3. Optic phonons which can be approximated as excitons occur in molecular crystals (see text). This figure shows two limits on a hypothetical one-dimensional aromatic system for an excitonic state composed of $A_g$ methyl rock motions on individual molecules. Note that none of the molecular motions results in a dipole. Analogous behavior is expected in real (3-dimensional) systems.

# EXCITONS IN DURENE

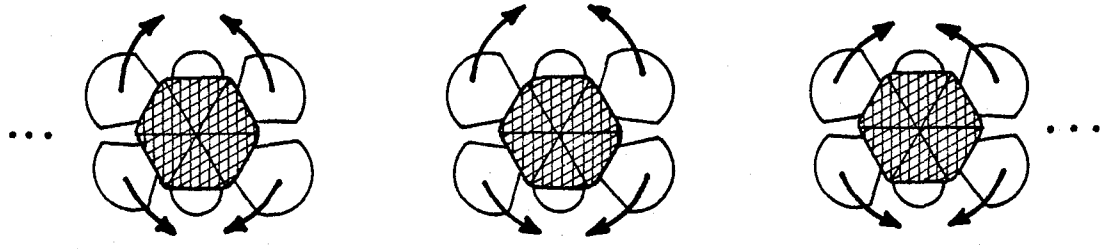

$k = 0$, $A_g$ Methyl Rock Exciton

$E = E_0 + 2J$

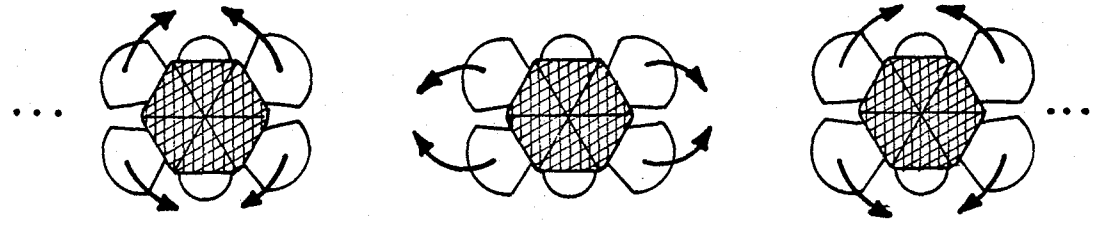

$k = \pi/a$, $A_g$ Methyl Rock Exciton

$E = E_0 - 2J$

XBL817-6042

associated with an excitation localized on a given molecule will induce dipole moments on other molecules which surround it; these dipoles oscillate at precisely the right frequency to "pump" the same excited state - hence energy is transferred and the state is delocalized.

Precisely the same formulation can be used if the only forces between molecules are van der Waals forces. The excitation of an oscillator will disturb its environment through the van der Waals force, that disturbance is at precisely the right frequency to induce the transfer of energy to identical molecules. Usually we would call such an entity a phonon if the forces which mediate the transfer of energy and give rise to a dispersion relation are intermolecular bonds. In this case, since $E(k=0) > 0$ the state would be called an optical phonon. Interestingly enough under certain circumstances an optical phonon and an exciton will have virtually identical dispersion relations. Consider the one-dimensional diatomic lattice depicted in Figure A4, where there are two types of bonds - a strong intramolecular and a weaker intermolecular. For that case the equation of motion for two atoms in a unit cell reads

$$M\ddot{x}_N = K'(x_{N-1} - x_N) + K(x_{N+1} - x_N)$$

$$M\ddot{x}_{N+1} = K(x_N - x_{N+1}) + K'(x_{N+2} - x_{N+1}). \qquad \text{(A17)}$$

Requiring that all the atoms oscillate with the same frequency ($x_j = x_j(t=0)\exp(i\omega t)$) and in Bloch states ($x_{j+2} = x_j \exp(ika)$) results in the following simple set of coupled algebraic equations

$$X_N(\omega^2 M - (K'+K)) + X_{N+1}(K'e^{-ik_a} + K) = 0$$

$$X_N(K + K'e^{-ik_a}) + X_{N+1}(\omega^2 M - (K+K')) = 0 \qquad \text{(A18)}$$

Figure A4. The model system used for calculations. This ideal system is an infinite one-dimensional system composed of diatomic molecules where there exist two types of force constants; an intermolecular constant (K') and an intramolecular constant (K).

# PHONONS IN A ONE-DIMENSIONAL HOMODIATOMIC LATTICE

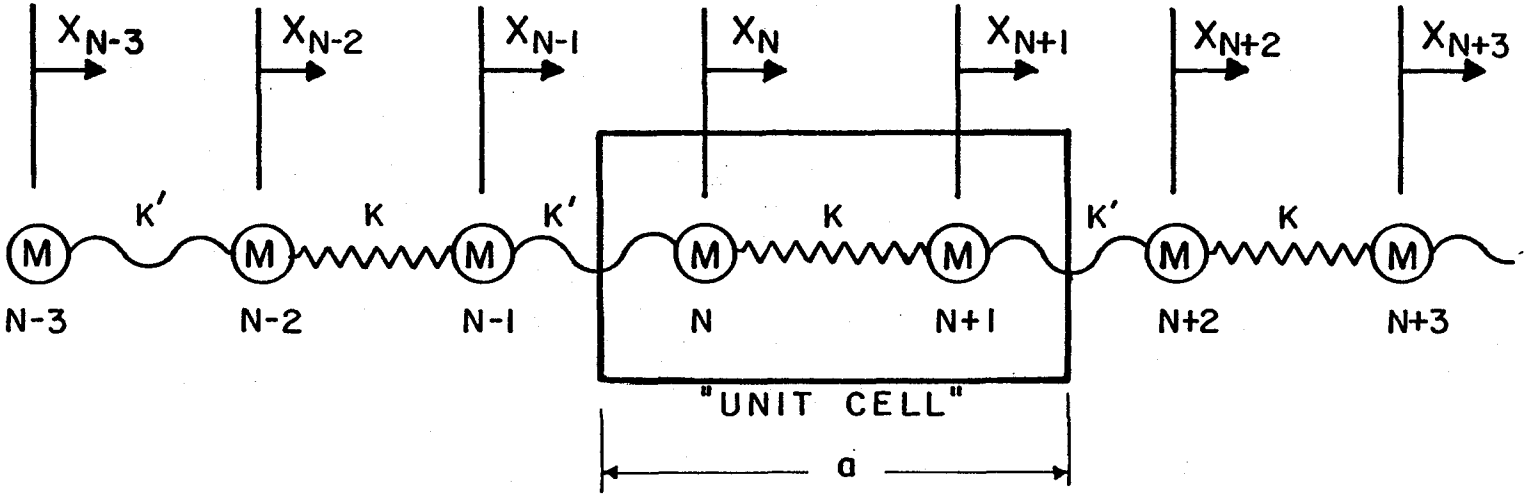


XBL 817-6040

which has non-trivial solutions if the determinate of the matrix of coefficients is zero. This results in the following expression for the frequency

$$\omega^2 = \frac{(K'+K)}{M}\left\{1 \pm \sqrt{1 - \frac{2KK'(1-\cos(ka))}{(K'+K)^2}}\right\} \tag{A19}$$

The "+" sign corresponds to the optic branch and the "-" sign to the acoustic branch. Thus we will consider only the "+" sign. To make this dispersion relation resemble that of an exciton requires application of the same approximation twice, namely

$$2KK'/(K'+K)^2 << 1. \tag{A20}$$

This approximation is the same as stating that the intramolecular forces are so much greater than intermolecular forces. Assuming the validity of Equation (A20) or expanding about k=0 yields

$$\omega^2 = \frac{2(K'+K)}{M}\left\{1 - \frac{KK'(1-\cos(ka))}{2(K'+K)^2}\right\} \tag{A21}$$

Taking the square root of Equation (A21) and again applying the approximation of Equation (A20) yields for the frequency

$$\omega = \sqrt{\frac{2(K'+K)}{M}}\left\{1 - \frac{KK'}{4(K'+K)^2}(1-\cos(ka))\right\} \tag{A22}$$

Comparing Equation (A22) to Equation (A16) results in the following "excitonic" parameters for the optic phonon in a molecular crystal

$$E_o = \hbar\sqrt{\frac{2(K'+K)}{M}}\left\{1 - \frac{1-KK'}{4(K'+K)^2}\right\} \tag{A23}$$

and

$$J = \hbar\sqrt{\frac{2(K'+K)}{M}}\left\{\frac{KK'}{8(K'+K)^2}\right\}. \qquad \text{(A24)}$$

We can rewrite Equation (A24) again in the regime where Equation (A20) is valid in the following form

$$J \simeq \omega_o\left(\frac{K'}{8K}\right). \qquad \text{(A25)}$$

Thus, looking at an optic phonon as an exciton in molecular crystals is a valid approach and allows the utilization of the body of knowledge related to excitons to be applied to this situation. For example, Reference 50 indicates that the rate of energy transfer goes as 2J between neighboring molecules. Thus a "wave packet" containing a spread of wave vectors localizing the packet to a molecule would cause that molecule to oscillate 4K/K' times before it donated its energy to a neighbor. Also the ideas of incoherence and mixed crystals can best be considered in the exciton context. Again it is important to emphasize that this is not valid in a covalent crystal where the "intermolecular" and "intramolecular" bonds are the same, but only in the case of a molecular crystal. Also keep in mind that the ratio of the intermolecular to intramolecular force constants has to be within certain definite limits; if it is too large the expansions that were used are invalid, if it is zero or very small the vibrational mode will be localized upon a single molecule.

Kopelman and others have made great theoretical and experimental progress in understanding vibrational excitons in aromatic molecular solids.[42,43,52-54a,b] Their calculations for various vibrations in solid benzene yield an exciton bandwidth typically 5 to 10 $cm^{-1}$ wide (the actual FWHM is smaller because of a "spike" in the exciton band

around various singularities). One of the largest vibron bandwidths (40 $cm^{-1}$) yet seen is the $A_{2u}$ (umbrella) mode in benzene. Remarkably enough this mode retains its excitonic identity upon melting.[52] Studies of mixed $C_6H_6/C_6D_6$ liquid samples yield interesting results. There is a monotonic decrease in the FWHM in the infrared spectrum of the $A_{2u}$ mode in benzene from 40 $cm^{-1}$ in pure benzene to 4 $cm^{-1}$ in an extrapolation to zero concentration in perdeuterobenzene. The residual bandwidth of 4 $cm^{-1}$ the authors attribute to homogeneous and/or inhomogeneous effects unrelated to the exciton width. The decrease in the spectral widths is smooth except for a discontinuity (15 $cm^{-1}$ to 10 $cm^{-1}$) at a molar concentration of 0.34- a result the authors cannot entirely explain. A suggested explanation is that this concentration (in the liquid) may represent a break from extended excitons to localized excitons which have different broadening mechanisms. In solids, a break is expected in the exciton properties at a critical concentration. This is based on the idea of percolation. Kopelman[54a] distinguishes between four different types of percolation: classical, lattice, static, dynamic. The basic ideas of percolation may be understood in the case of classical percolation. The situation to which this theory is often applied is electrical conduction[55] in randomly distributed alloy. The idea is that a site in the alloy may be occupied by one of the constituents with a probability equal to that constituents molar concentration. If only one of the constituents conducts electricity then upon dilution electrons have to find a pathway of atoms which are nearest neighbors composed of that conducting constituent. Below a certain critical concentration the conducting atoms are isolated into finite clusters and unable to conduct macroscopic distances. This

critical concentration is the cutoff point of the metal-insulator transition. The same ideas may be applied to energy and excitation transfer in molecular crystals. Lattice percolation is mainly concerned with the cluster states below the critical concentration. Static percolation is concerned with the transition with concentration from localized to extended states and is appropriate with excitons which are long-lived and interact with nearest neighbors only. If the lifetime of the exciton becomes shorter, then the idea of dynamic percolation must be used which results in a smaller critical concentration. In general the critical concentration decreases with increasing coordination number, dimensionality and range of interaction. It is this latter model of dynamic coupling which seems to be most appropriate for the optical phonons/vibrons in durene where it appears that the excitation travels 5 to 10 sites before decaying into the lattice. Thus we need "clusters" of less than 5 to 10 $d_{14}$- durene in an $h_{14}$-durene host crystal. Based on three-dimensional energy transfer and a coordination number of 6 as well as nearest neighbor interactions, the critical concentration is below 10%. If thermalized hopping is allowed where the excitation can go from the 245 $cm^{-1}$ methyl rock in $d_{14}$-durene to the methyl rock at 280 $cm^{-1}$ in $h_{14}$-durene, then there would be no percolation at all.

Another concept which is related to this discussion is Anderson localization. In a mixed crystal the idea is that each component introduces a randomness in the potential function which now can be decomposed into a periodic part and a random part. A transition from extended states to localized states will happen when the ratio of the random part of the potential, $V_o$, to the bandwidth B exceeds a certain critical value on the order of 2 for a coordination number of 6.[56,57] In a 50/50%

mixture of isotopically mixed durene the random part of the potential is approximately half the difference between the energies of the methyl rock (18 $cm^{-1}$), so a bandwidth exceeding 9 $cm^{-1}$ would likely insure that Anderson localization does not play a predominate role.

Finally, for dispersive excitations which are delocalized there is a selection rule, namely that the state which is observed is approximately at $\vec{k} = 0$. Figure A5 shows how this comes about by the conservation of momentum and energy.

Figure A5. Raman spectroscopy of excitons observes only a state which has almost zero wavevector. The total exciton bandwidth is not observed. L and S corresponds to the laser and Stokes photons respectively.

# RAMAN SPECTROSCOPY OF DISPERSIVE EXCITATIONS

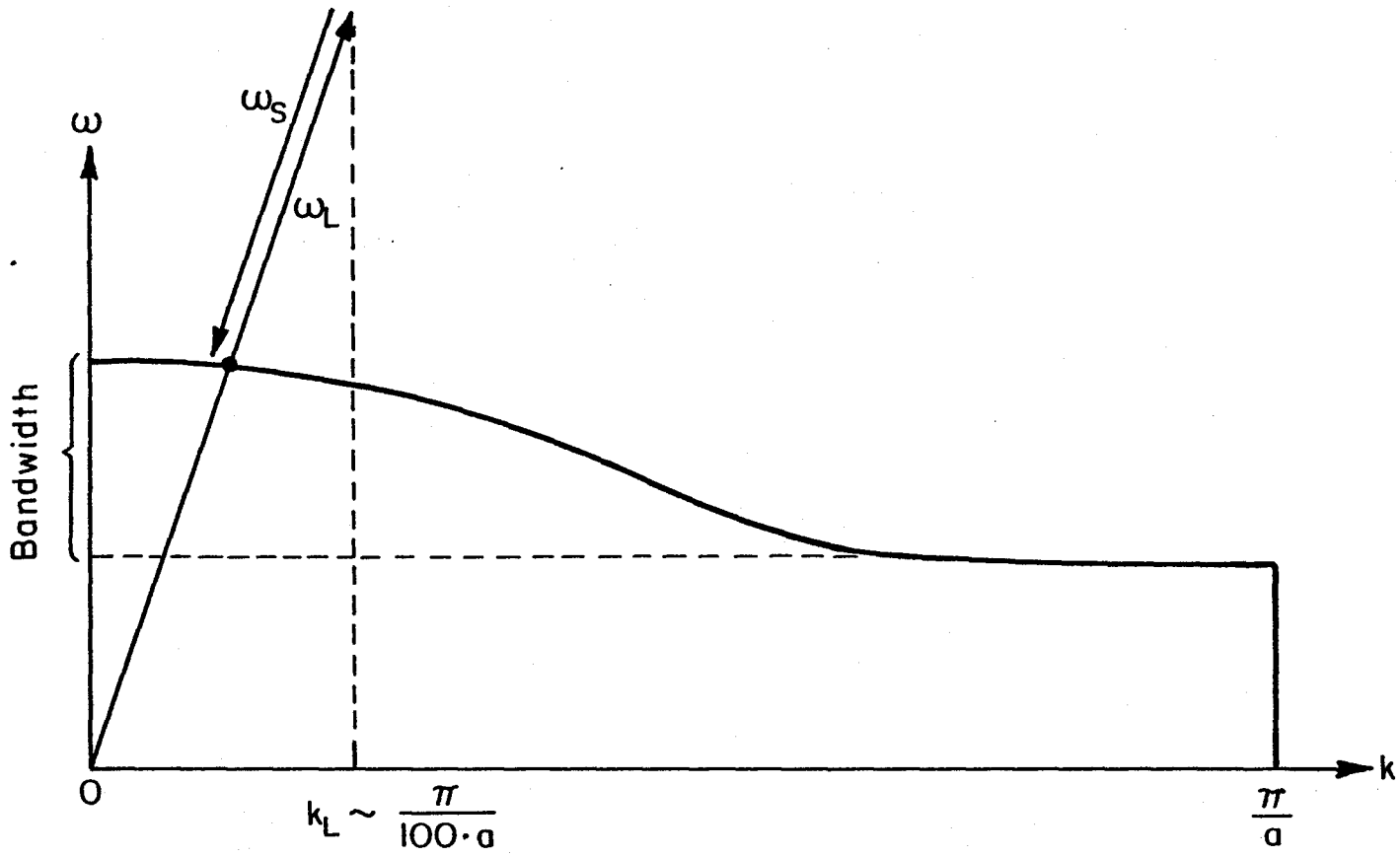


XBL 817-6039

## REFERENCES


1a. A. Lauberau, D. Von der Linde and W. Kaiser, Phys. Rev. Lett. 28, 1162 (1972).
b. A. Lauberau and W. Kaiser, Rev. Mod. Phys. 50, 607 (1978).

2. D. Richard and J. Ducuing, J. Chem. Phys. 62, 3616 (1975).

3. S. F. Fischer and A. Lauberau, Chem. Phys. Lett. 35, 6 (1976).

4. Ref. 3; and K. Tanabe, Chem. Phys. 38, 125 (1979).

5. D. W. Oxtoby, J. Chem. Phys. 70, 2605 (1979).

6. R. G. Gordon, J. Chem. Phys. 40, 1973 (1964); 43, 1307 (1975).

7. L. A. Nafie and W. L. Peticolas, J. Chem. Phys. 57, 3145 (1972).

8. Handbook of Chemistry and Physics, Chemical Rubber Company, Cleveland (1971).

9. Paul A. Cornelius, Ph.D. Thesis, University of California (Berkeley) (1980).

10a. P. W. Anderson and P. R. Weiss, Rev. Mod. Phys. 25, 269 (1953).
b. P. W. Anderson, J. Phys. Soc. Jap. 9, 888 (1954).

11. Robert M. Shelby, Ph.D. Thesis, University of California (Berkeley) (1978).

12. William H. Louisell, Quantum Statistical Properties of Radiation, John Wiley and Sons, New York (1973).

13. C. B. Harris, R. M. Shelby, and P. A. Cornelius, Phys. Rev. Lett. 38, 1415 (1977); Chem. Phys. Lett. 57, 8 (1978).

14. R. M. Shelby, C. B. Harris, and P. A. Cornelius, J. Chem. Phys. 70, 34 (1979).

15. T. J. Swift and R. E. Connick, J. Chem. Phys. 37, 307 (1962).

16. R. A. MacPhail, R. G. Snyder, and H. L. Strauss, J. Am. Chem. Soc. 102, 3976 (1980).

17. James L. Chao, Ph.D. Thesis, University of California (Berkeley), (1980).

18a. C. B. Harris, J. Chem. Phys. 67, 5607 (1977).
b. C. B. Harris, Chem. Phys. Lett. 52, 5 (1977).

19. M. Sargent III, M. O. Scully, and W. E. Lamb, Jr., Laser Physics, Addison-Wesley, Reading, MA (1974), Chapter 16.

20. I. Oppenheim, K. E. Shuler, and G. H. Weiss, Stochastic Processes in Chemical Physics: The Master Equation, MIT Press, Cambridge (1977), Chapter 3.

21. J. I. Steinfeld, Molecules and Radiation, Harper and Row, New York (1974), p. 25.

22. A. Yariv, Quantum Electronics, John Wiley and Sons, New York (1975), Chapter 8.

23. G. F. D. Duff and D. Naylor, Differential Equations of Applied Mathematics, John Wiley and Sons, New York (1966).

24. R. J. Abbott and D. W. Oxtoby, J. Chem. Phys. 70, 4703 (1979).

25. References 13, 14, 9, and 11.

26. D. Robert and L. Galaty, J. Chem. Phys. 64, 2721 (1976).

27. R. Kubo, J. Phys. Soc. Jap. 17, 1100 (1962).

28. A. Nitzan and R. Silbey, J. Chem. Phys. 60, 4070 (1974).

29. Reference 20, Section 2.4.

30. A. H. W. Beck, Statistical Mechanics, Fluctuations and Noise, John Wiley and Sons, New York (1976), Chapter 6.

31. R. K. Wertheimer, Mol. Phys. 35, 257 (1978).

32. R. K. Wertheimer, Mol. Phys. 36, 1631 (1978).

33. R. K. Wertheimer, Mol. Phys. 38, 797 (1979).

34. R. K. Wertheimer, Chem. Phys. 41, 229 (1979).

35. R. K. Wertheimer, Chem. Phys. 45, 415 (1980).

36. R. K. Wertheimer, Chem. Phys. Lett., 52, 224 (1977).

37. R. K. Wertheimer, Private Communications.

38. H. Mori, Prog. Theor. Phys. 34, 423 (1965).

39. Reference 9, Appendix 2.

40. H. Mori, Prog. Theor. Phys. 34, 399 (1965).

41. R. Zwanzig, Phys. Rev. 124, 983 (1961).

42. P. N. Prasad and R. Kopelman, J. Chem. Phys. 58, 126 (1973).

43. P. N. Prasad and R. Kopelman, J. Chem. Phys. 58, 5031 (1973).

44. J. Frenkel, Phys. Rev. 37, 1276 (1931).

45. W. A. Harrison, Electronic Structure and the Properties of Solids, W. H. Freeman, San Francisco (1980), p. 71-80.

46. C. Kittel, Quantum Theory of Solids, John Wiley and Sons, New York (1963), p. 270.

47. A. S. Davydov, JETP, 18, 210 (1948).

48. R. M. Hexter, J. Chem. Phys. 33, 1833 (1960).

49. S. Fischer and S. A. Rice, J. Chem. Phys. 52, 2089 (1970).

50. C. B. Harris and D. A. Zwemer, Ann. Rev. Phys. Chem. 29, 473 (1978).

51. P. Reineker and R. Kühne, Phys. Rev. B 21, 2448 (1980).

52. J. C. Laufer and R. Kopelman, J. Chem. Phys. 53, 3674 (1970).

53. R. LeSar and R. Kopelman, J. Chem. Phys. 66, 5035 (1977).

54ab E. M. Monberg and R. Kopelman, Chem. Phys. Lett. 58, 492 and 497 (1978).

55. B. J. Last and D. J. Thouless, Phys. Rev. Lett. 49, 410 (1977).

56. N. F. Mott, Metal-Insulator Transitions, Barnes and Noble, New York (1974).

57. S. Mukamel, Chem. Phys. 31, 327 (1978).

58. S. Mukamel, Chem. Phys. 37, 33 (1979).

59. D. E. McCumber, Phys. Rev. 133A, 163 (1964).

60. S. M. George, H. Auweter, and C. B. Harris, J. Chem. Phys. 73, 5573 (1980).

61. M. N. Neuman and G. C. Tabisz, Chem. Phys. 15, 195 (1976).

62. H. S. Goldberg and P. S. Pershan, J. Chem. Phys. 58, 3816 (1972).

63. K. Tanabe, Chem. Phys. Lett. 63, 43 (1979).

64. W. Schindler and H. A. Posch, Chem. Phys. 43, 9 (1979).

65. K. Tanabe and J. Jonas, Chem. Phys. 38, 131 (1979).

66. G. Lucazeau, Private Communication (1981).